Nelson North Wastewater Treatment Plant (NWWTP) dispersion modelling

Report prepared for Nelson City Council

July 2023

MetOcean SOLUTIONS

Document History

Versions

Version	Revision Date	Summary	Reviewed by
0.0	20/09/2021	Initial document created	Tran
0.1	14/11/2021	Draft for internal review	Cussioli
0.2	26/11/2021	Draft for internal review	Cussioli/Weppe
0.3	26/11/2021	Draft for Internal review	Berthot
0.4	05/12/2021	Draft for Internal review	Cussioli
0.5	19/09/2022	Revised draft with client's comments	Cussioli/Weppe
0.6	23/09/2022	Draft for Internal review	Cussioli/Weppe
0.7	29/07/2023	Updated draft for client review	Weppe/Cussioli

Distribution

Version	Date	Distribution
1.0		

Document ID: P0526

Contents

List of Figures

List of Tables

1.Introduction

Nelson City Council (NCC) is interested in understanding the dilution and discharge characteristics of contaminant discharged from the Nelson North Wastewater Treatment Plant (NWWTP), and how the dilution characteristics may affect nearby beaches. The wastewater treatment plant is located at the northern end of The Haven (Figure 1-1).

The NWWTP which treats on average approximately 7,200 m^3 of wastewater every day (2013-2021, data provided by Nelson City Council); was upgraded in 2007-2009 and is designed to comply with the requirements of the 2004 resource consent. The design of the new plant has allowed for better management of variable inflows and allows adjustments in operation to be made to reduce the negative effects of winter conditions on the pond operation.

The council now require a renewal of the Resource Consent, which will require an understanding of how the wastewater is expected to dilute within the environment by applying a numerical modelling approach.

The NWWTP serves the northern catchment of Nelson City, comprising mainly domestic residences, and a small percentage of industrial discharges from the Port and Vanguard Street industrial areas. Wastewater is collected by a reticulation system that is then pumped from the Neale Park Pump Station to the wastewater treatment plant located at the northern end of the Nelson Haven (Figure 1-1).

The treatment concept for the wastewater treatment plant is based on:

- Removing gross solids through the inlet works
- Pre-treating the wastewater flow to remove organics and solids using a trickling filter and clarifier (as required depending on pond conditions)
- Pond based treatment for the removal of organics, solids, and pathogens
- Natural disinfection using the maturation pond and wetlands

The main components of the NWWTP, includes:

- Flow Buffer (1) – attenuates peak flows during periods of high rainfall
- Screening and Grit Removal (2) –removes gross solids and non-organic material, which is disposed off-site
- Clarifier (3) – when on-line, removes readily settleable solids (sludge)
- Sludge Tanks (4) – sludge from the clarifier is either discharged into the facultative pond or mechanically thickened, stored in tanks and periodically trucked off-site to Bell Island WWTP

- Trickling Filter (5) – when on-line, removes organic material via a fixed film growth process
- Oxidation Ponds (6) – Two ponds, a facultative pond and a maturation pond, operate in series to collectively remove organics, solids and pathogens
- Wetlands (7) – Two wetlands operate in parallel to further treat (or polish) the wastewater
- Bio-Filter (8) – Foul air extracted from selected, covered elements of NWWTP is treated by a bark 'biofilter'
- Outfall (9) – The outfall pipe goes 350m into Tasman Bay

The relative orientation of the infrastructure listed above are illustrated in Figure 1-2.

Figure 1-1 Location of the NWWTP, including approximate location of the outfall/diffuser and the buoy deployment.

Figure 1-2 NWWTP infrastructure layout.

2.Methodology

2.1. Buoy Data

A buoy deployment was undertaken by Cawthron Institute to assist with the characterisation of the hydrodynamic regime in the vicinity of the treated wastewater discharge point (Figure 1-1). The measurement period extended from 5 August 2020 to 26 November 2020, and included measurement of currents, salinity, temperature, oxygen, chlorophyll, turbidity, and wave parameters. The deployment included a range of instruments as provided in Table 2-1.

The buoy provides current velocity data for the near-field model setup and for the calibration and validation of the hydrodynamic model.

Table 2-1 Wakapuaka buoy - Instruments deployed at -41.1986, 173.3215.

Measurement	Instrument	Instrument name
Currents	ADCP	RDI Sentinel V50 ADP and RDI Sentinel V20 ADP
Salinity	CT Sensor	WETLabs WQM
Temperature	ADCP and CT Sensor	RDI Sentinel V50 ADP, RDI Sentinel V20 ADP, and WETLabs WQM
Oxygen	DO sensor	WETLabs WQM
Chlorophyll	Fluorometer	WETLabs WQM
Turbidity	Turbidity sensor	WETLabs WQM
Wave	Wave sensor	Seaview SVS-603

2.2. Near-field modelling

Near-field modelling of the initial turbulent mixing was undertaken using CORMIX[1]. CORMIX is a USEPA-supported mixing zone model and decision support system for environmental impact assessment of regulatory mixing zones resulting from continuous point source discharges. The system emphasizes the role of boundary interaction to

[1] http://www.cormix.info/

predict steady-state mixing behaviour and plume geometry. CORMIX was used to define the near-field plume characteristics (plume extent, initial dilution) under a range of representative conditions of current velocities and discharge characteristics. The nearfield plume extent and initial dilution was used as input into the far-field model.

The nearfield is the region of a receiving water where the initial jet characteristic of momentum flux, buoyancy flux and outfall geometry influence the jet trajectory and mixing of a wastewater discharge.

2.2.1. Simulations

Details of the outlet pipe design were provided by NCC and show in Figure 2-1.

The concrete pipe is perpendicular to the shoreline and extends approximately 430 m from the manhole (located at the treatment plant) to the offshore outlet hole. There are a total of 10 outlet holes, 9 of them located on the top half of the pipe and 1 hole located at the end of the pipe.

The holes on the top half of the pipe are equally spaced at 1.93 m along 20 m from the offshore outlet tip. Each hole is 0.3 m by 0.3 m with alternating opening angles. The hole located at the end of the pipe is parallel to the seabed and fitted with a conical reducer with a diameter of 0.3 m.

In CORMIX, it is not possible to simulate the alternating holes together with the conical reducer hole located at the end of the pipe. Therefore, we considered the conical reducer hole to be at the same height and angle as the other 9 alternating holes, totalling 10 alternating holes in our simulations. The pipe is located at the seabed and holes are approximately 1.2 m above the seabed.

The ambient temperature and salinity were assumed to be 14 °C and 34 psu respectively, based on the data measured by sensors attached to the buoy deployment described in the previous section. The wastewater temperature and salinity were calculated as the average of measurements provided by NCC and set to 17.3 °C and 1.2 psu, respectively. The measurements were carried out approximately 1-2 times a month from 13-Aug-2020 to 13-Jan-2021.

Timeseries of wastewater discharge for the past 9 years were provided by NCC. We plotted it to compare the discharge flow between each year (Figure 2-2) and the 2020-2021 period was adopted at the 'current year' scenario for this modelling assessment. Note that 2019-2020 (red line) has a significant peak, but 2020-2021 (black line) have some significant peaks at or above 20,000 m^3/day and it is the most recent year. The average flow for the 2020-2021 period is 8,119 m^3/day.

The consent flow (year 2059) was calculated based on an expected ratio of population increase (Table 2-2). The population increase ratio from 2021 to 2059 is 1.3. Therefore, we multiplied the 2020-2021 daily flow data by 1.3 to scale up the flows for the year 2059, resulting in an average flow of 10,555 m^3/day. We combined flow rates of 2021 and 2059 to bracket all possible flow rates to be simulated, and calculated the 10^{th}, 50^{th} (median) and 90^{th} percentiles of the flow rates (hereafter p10, p50, and p90, respectively).

Note that the calculation of the population increase ratio assumes population growth is uniformly distributed. Also, no allowance for climate change impacts (e.g., change in frequency, intensity and duration of storm events) were considered in the calculation.

Based on the analysis of current velocity timeseries data from Wakapuaka buoy, a range of velocities were selected for the simulations, from near stagnant (0.05 m/s), increasing with intervals of 0.10 m/s, to the maximum velocity of 0.40 m/s (Figure 2-8). While typical spring tide current at the bottom where the pipe is located is in the order of 0.11 m/s, an extreme case of 0.40 m/s was also considered. Wind velocities were kept at 0 m/s to provide a conservative, lower, estimate of the near-field dilution rates.

A total of 15 CORMIX near-field simulation where undertaken, considering p10, p50, and p90 of discharge flow under 5 different ambient current velocities: 0.05, 0.10, 0.20, 0.30, 0.40 m/s (Table 2-3).

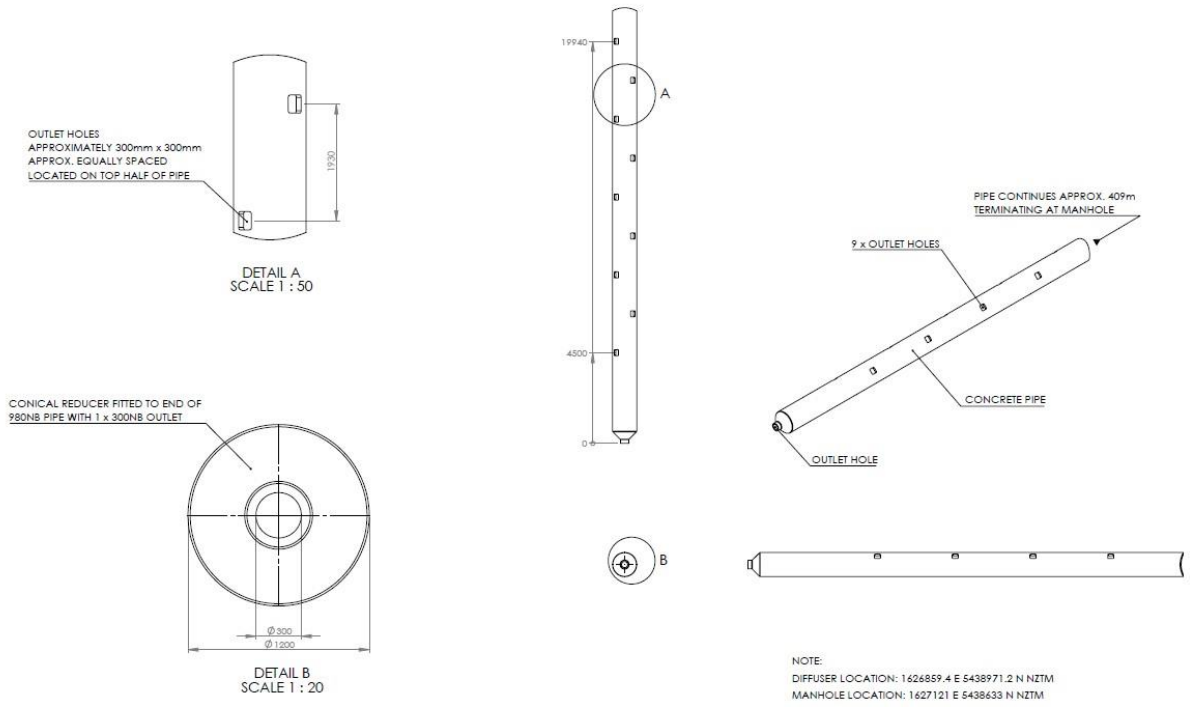

Figure 2-1 Pipe design and dimensions (Source: Nelson City Council).

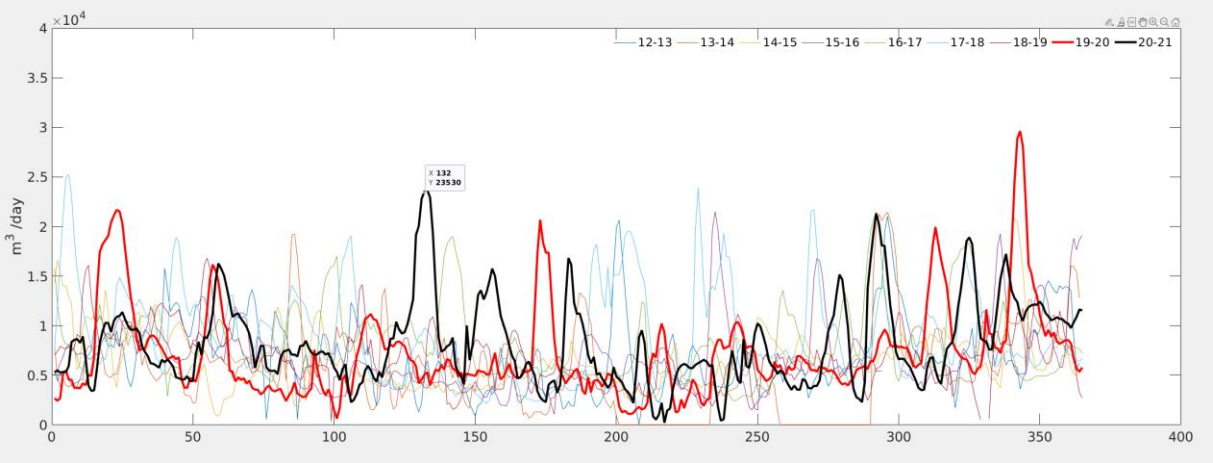

Figure 2-2 Wastewater discharge for the past 9 years provided by NCC. Different years represented by line colours indicated at the top of figure.

Table 2-2 Nelson North WWTP previous and projected population. Data provided by Stantec.

Year	NNWWTP Population
2019	26,219
2020	26,641
2021	26,655
2050	32,518
2059	34,897

Table 2-3 CORMIX near-field list of simulations.

Scenarios	Ambient current (m/s)	Flow rate (m^3/s)
p10	0.05	0.048
	0.10	
	0.20	
	0.30	
	0.40	
p50	0.05	0.094
	0.10	
	0.20	
	0.30	
	0.40	
p90	0.05	0.185
	0.10	
	0.20	
	0.30	
	0.40	

2.3. Hydrodynamic modelling

The simulation of wastewater far-field dispersion within a complex coastal system requires high resolution hydrodynamic fields. For the present study, high-resolution 3D modelling of the tidal/river/stream discharge hydrodynamics undertaken for other studies within the region would be utilised. These simulations cover a range of climatic conditions (i.e., La Niña/ El Niño complete years) and provide a sound statistical basis to examine the dispersion of contaminants within the receiving environs. The simulations are based on the open-source model SCHISM[2] [3].

Open-source science models allow full transparency of the code, numeric, boundary conditions and outputs. Further, it allows other consultants and researchers to replicate or enhance any previous modelling efforts for a given environment.

SCHISM is a prognostic finite-element unstructured-grid model designed to simulate 3D baroclinic, 3D barotropic or 2D barotropic circulation. The barotropic mode equations employ a semi-implicit finite-element Eulerian-Lagrangian algorithm to solve the shallow water equations, forced by relevant physical processes (atmospheric, oceanic and fluvial forcing). A detailed description of the SCHISM model formulation, governing equations and numerics can be found in Zhang & Baptista (2008).

The finite-element grid structure (i.e., triangles) used by SCHISM has resolution and scale benefits over other regular or curvilinear based hydrodynamic models. SCHISM is computationally efficiently in the way resolves the shape and complex bathymetry associated with estuaries, while the governing equations are similar to other open-source models such as Delft3D. SCHISM has been used extensively within the scientific community[4], and forms the backbone to operational systems used to predict nowcast and forecast estuarine water levels, currents, water temperature and salinity[5].

2.3.1. Computational grid

The model resolution has been optimised to ensure the salient hydrodynamic processes are accurately captured, with offshore resolution of the order 10s-100s m, and inside the rivers and estuaries at 5-10 m, depending on the bathymetry gradients. The model domain includes the main river systems which discharge into Tasman Bay (Figure 2-3).

[2] http://ccrm.vims.edu/schism/

[3] http://www.ccrm.vims.edu/w/index.php/Main_Page#SCHISM_WIKI

[4] http://ccrm.vims.edu/schism/schism_pubs.html

[5] https://tidesandcurrents.noaa.gov/ofs/creofs/creofs_info.html

The original hydrodynamic model domain was established for the Bell Island WWTP treated wastewater discharge modelling and its grid was extended for the Nelson Port modelling work scopes (MetOcean Solutions Ltd, 2017 and MetOcean Solutions, 2020).

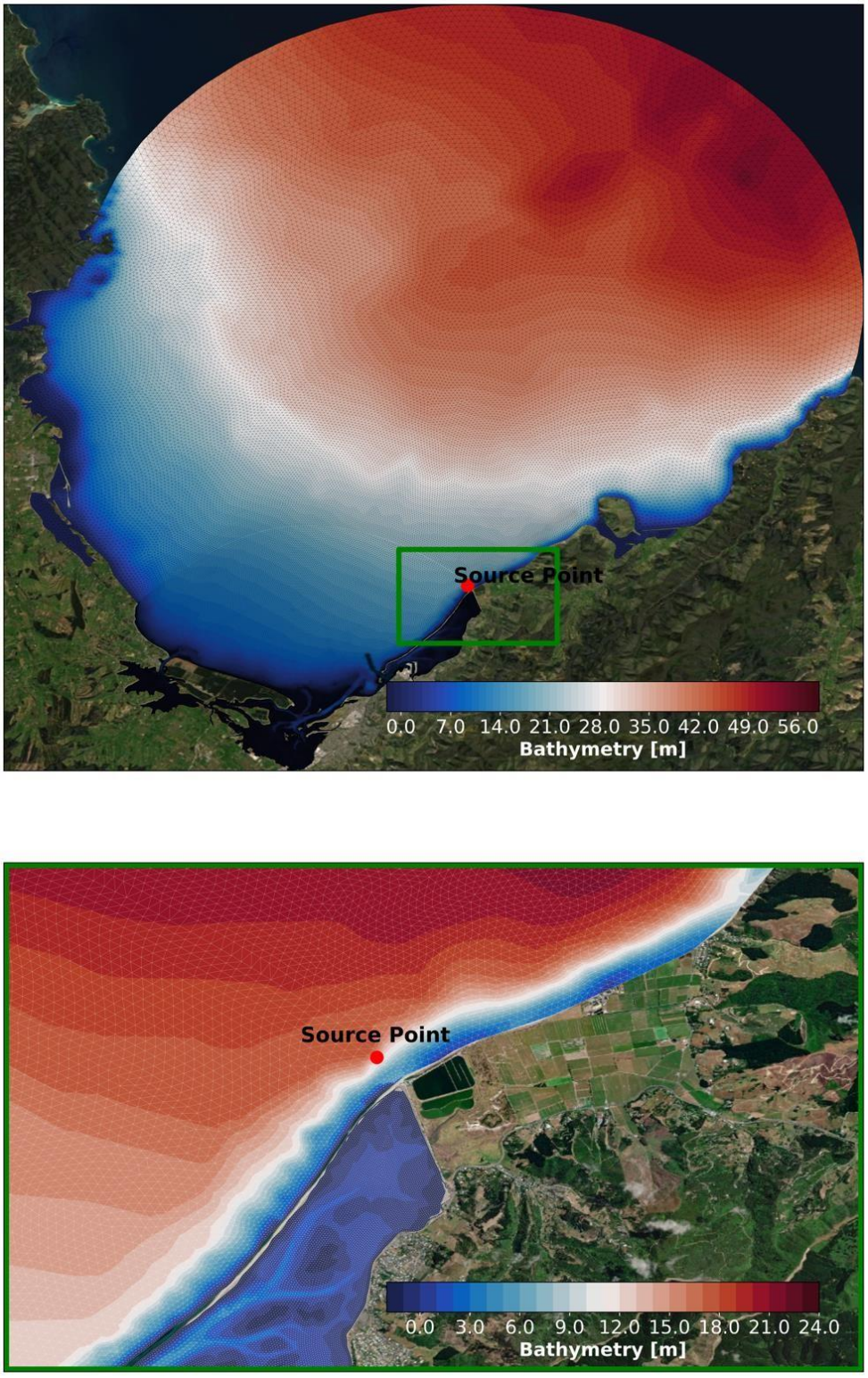

Figure 2-3 Map showing the SCHISM model domain, bathymetry and discharge location from the NWWTP.

2.3.2. Vertical grid

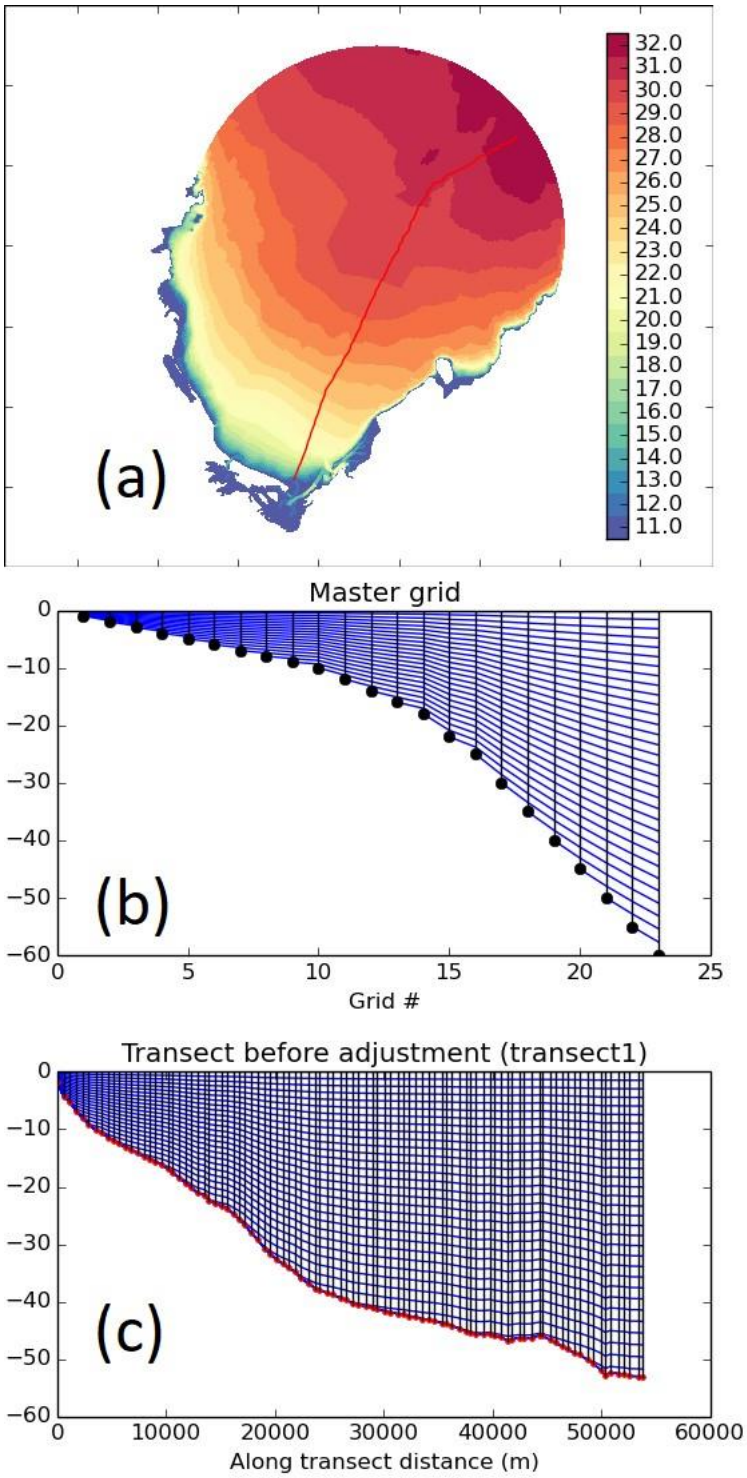

Figure 2-4 Vertical grid used in the present study: (a) - a map showing number of vertical layers across the computational domain with an transect; (b) & (c) – master grid and vertical grid along the transect.

2.3.3. Model forcing and boundary conditions

In this study we applied similar model setup and forcing than the previous work for Bell Island (MetOcean Solutions Ltd, 2017).

2.3.3.1. Tidal forcing

The widely used tidal constituents sourced to force regional and coastal domains in hydrodynamic models - the Oregon State University Tidal Inverse Solution (OTIS, Egbert & Erofeeva, 2002) – was rather coarse for direct use in New Zealand coastal domains. Therefore, tidal constituents from the harmonic analysis of a long term 2D Princeton Ocean Model (POM, Mellor, 1998) tidal simulation with 5 km horizontal resolution were used to derive tidal boundaries.

The NZ-POM domain was forced at the open boundaries by tidal elevation and current harmonic constituents derived from the OTIS Pacific Ocean solution[6] . The SCHISM domain was forced at the open boundary by elevation and current constituents derived from the POM 2D simulation.

2.3.3.2. Offshore residual current forcing

Open boundary non-tidal inflows and outflows were provided by 3-dimensional velocity, temperature and salinity fields and spatially variable sea surface height derived from a nationwide implementation of the Regional Ocean Modelling System (NZ-ROMS) nested within the global Climate Forecast System Reanalysis (Saha et al., 2010).

Velocity boundary conditions were interpolated to each node and sigma level, along the offshore model boundary for each model time-step. Residual elevations were interpolated to each boundary node and each model time-step.

2.3.3.3. Atmospheric forcing

MetOcean Solutions maintains an up-to-date atmospheric hindcast reanalysis from 1979 to 2016 at 12 km resolution for the entire New Zealand and approximately 4 km over central New Zealand (including Nelson). This atmospheric hindcast was produced using the Weather and Research Forecasting (WRF) model forced with boundary conditions from the global CFSR product.

The improvement in resolution from the 35 km of CFSR adds accuracy and variability to the atmospheric fields that force the SCHISM model, especially over coastal margins where topography is known to substantially change the large-scale wind patterns and

[6] http://volkov.oce.orst.edu/tides/PO.html

local responses. WRF variables such as winds, atmospheric pressure, relative humidity, surface temperature, long and short-wave radiation, and precipitation rate were used at hourly intervals to provide air-sea fluxes to force the Bell Island SCHISM model.

The wind speed from this hindcast has been validated at numerous sites around New Zealand; shown in Figure 2-5 are time series data from Auckland Airport in January 2007 and a quantile-quantile plot from a full year (2007) at Brother's Island in the Cook Strait.

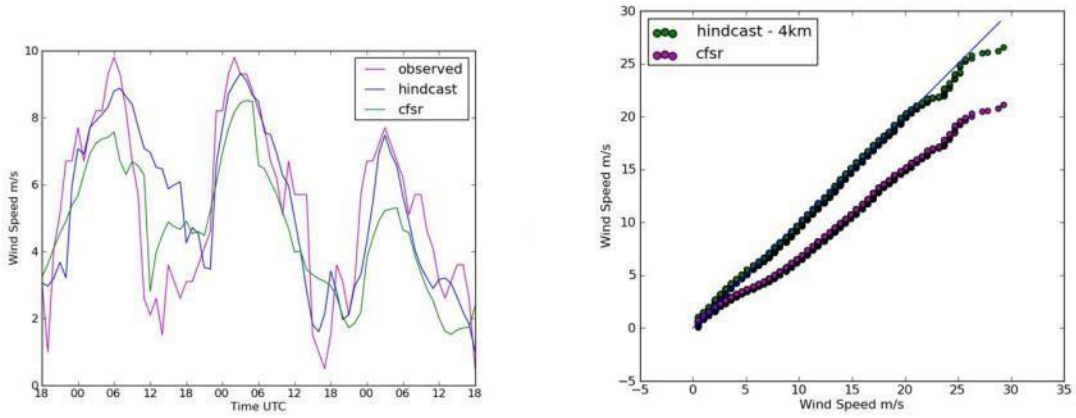

Figure 2-5 Comparison of both CFSR data and a high-resolution WRF hindcast for Auckland Airport during a few days in January 2007 (left) and quantile-quantile plot of both CFSR (magenta) and the WRF hindcast (green) against the observations from Brother's Island in the Cook Strait during 2007.

2.3.3.4. Fluvial discharges

Time-varying open boundary fluvial inputs were prescribed for the Waimea River, Neimann Creek, Jenkins Creek and the Maitai River (Figure 2-6) supplied by both Tasman District Council and Nelson City Council. An example of the measured time-series of discharges for the Waimea River is given in Figure 2-7.

Figure 2-6 Open fluvial boundaries at which time-varying discharges were defined

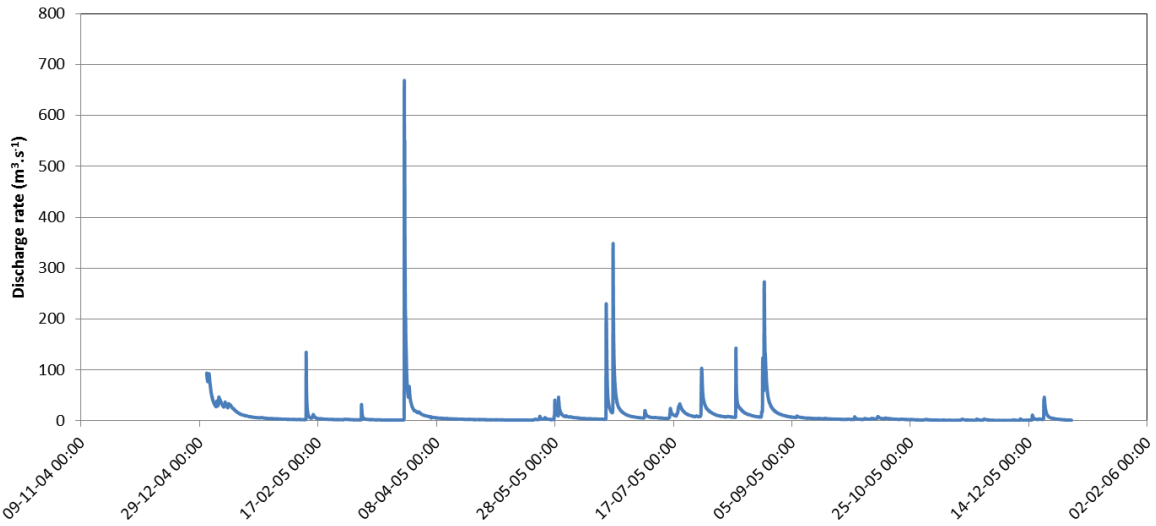

Figure 2-7 Example of the temporal variability in Waimea River discharge rates used at the open boundary of the SCHISM model.

2.3.3.5. Temperature and Salinity

Salinity and temperature boundary conditions were interpolated to each node and sigma level, along the offshore model boundary for each model time-step. Residual elevations were interpolated to each boundary node and each model time-step. Temperature and salinity were treated as passive tracers in the 2D depth averaged baroclinic model.

2.3.4. Model calibration and validation

The governing fluvial and tidal flow dynamics have been calibrated and validated against available measured data collected as part of the Bell Island field data deployment, and data maintained by the Port.

However, further model validation against measured data available was also taken in the present study. The measured data were taken from Wakapuaka buoy located offshore near NWWTP (Figure 1-1).

Comparison of the modelled water elevation against the NIWA predicted tide and the modelled current speed and direction against the field data at middle water depth (~8.68 m below the surface) shows a good agreement between the two datasets (Figure 2-8).

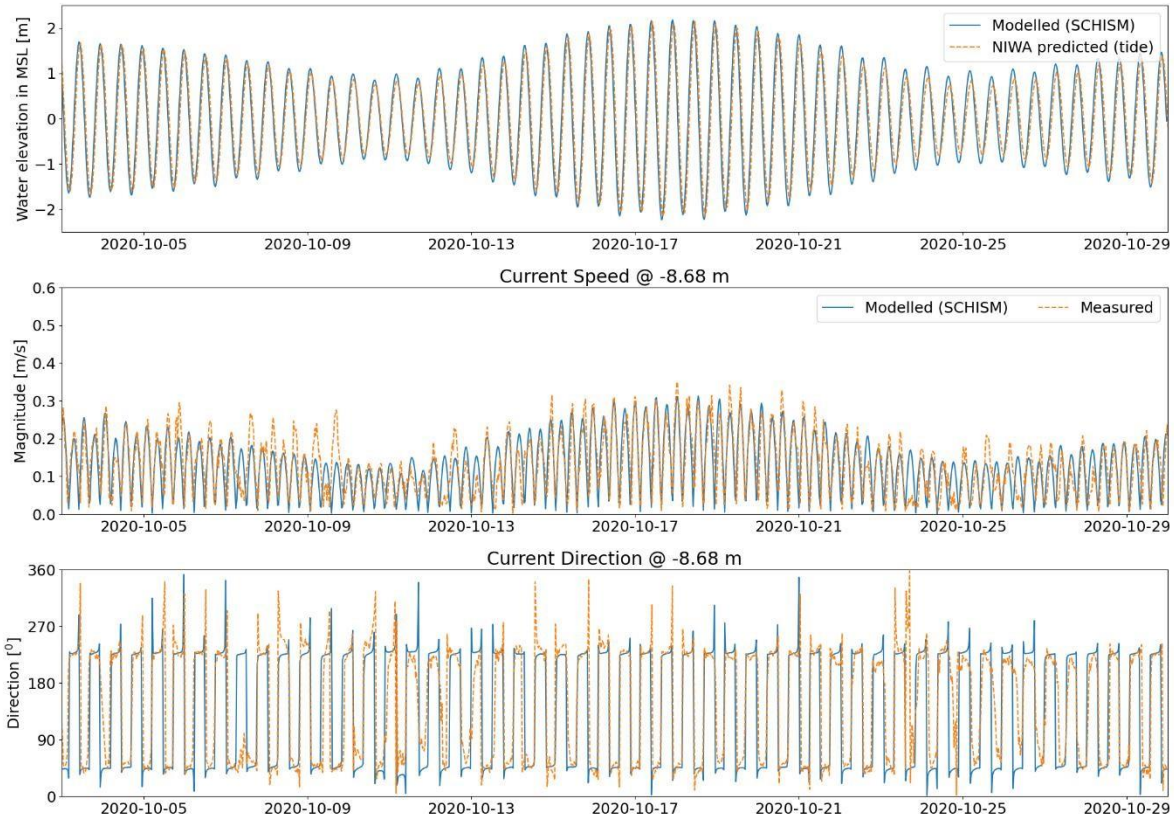

Figure 2-8 Model validation: Top panel – modelled surface elevation against NIWA predicted tide; Middle and Bottom panels – modelled current speed and direction against field data at buoy provided by the client.

2.4. Far-field modelling

2.4.1. Modelling Approach

The release of pollutants in the oceanic or estuarine environment through an outfall is a process that is generally either continuous over time, or at prescribed times (e.g., specific tidal stage and amplitudes). These discharges are often subject to significant fluctuations in released quantities. The outcome of such releases is inherently non-deterministic and is governed, in part, by random variables such as currents, turbulences, wastewater network use and precipitation, it is therefore difficult to accurately predict.

However, the expected hydrodynamic regime can be assessed from the historical conditions, thereby allowing estimations of the general geographical dispersion. In the present study, the approach consisted of running two year-long simulations within contrasting historical contexts: La Niña and El Niño episodes (April 2010-April 2011, and April 2015-April 2016, respectively).

During El Niño conditions, New Zealand typically experiences stronger or more frequent westerly winds during summer. This leads to a greater risk of drier-than-normal conditions in east coast areas and more rain than normal in the west. In winter, colder southerly winds tend to prevail, while in spring and autumn, south-westerlies tend to be stronger or more frequent, bringing a mix of the summer and winter effects.

During La Niña conditions more north–easterly winds are characteristic, which tend to bring moist, rainy conditions to the north–east of the North Island, and reduced rainfall to the south and south–west of the South Island.

Considering both La Niña /El Niño episodes aims to produce robust probabilistic estimate of the plume dispersion and dilution and thus provide guidance on expected concentration levels associated within the outfall region for existing and proposed consent flow accounting for increasing population.

The general dispersion model employed and considered scenarios are described below.

2.4.2. Opendrift Model description

The dispersion of contaminant discharged in the ocean at the outfall was simulated using the ocean trajectory modelling framework OpenDrift[7] (Dagestad K.F et al., 2018).

[7] https://github.com/OpenDrift/opendrift

OpenDrift is an open-source Python-based framework for Lagrangian particle tracking developed by the Norwegian Meteorological Institute, where it is notably used operationally for emergency response for oil spill and search and rescue events. The framework is highly modular and can be used for any type of drift calculations in the ocean or atmosphere. A number of modules have already been developed, including an oil drift module (see Röhrs et al., 2019), a stochastic search-and-rescue module, a pelagic egg module, a plastic drift module.

The contaminant dispersion simulations described in the study were undertaken using the OceanDrift[8] module that assumes passive particles with no settling velocities, subject to horizontal and vertical advection and mixing.

The dispersion modelling consists of a trajectory tracking scheme applied to discrete particles in time and space-varying 3D oceanic currents.

$$\frac{dx_p}{dt} = \tilde{u}(x,y,z,t) + u_t$$

$$\frac{dy_p}{dt} = \tilde{v}(x,y,z,t) + v_t$$

$$\frac{dz_p}{dt} = w_t + w_s$$

Equation 2-1 (a, b, c)

where (x_p, y_p, z_p) are particle 3D coordinates, $\tilde{u}_{(x,y,z,t)}$, $\tilde{v}_{(x,y,z,t)}$ are horizontal ocean currents, (u_t, v_t, w_t) are the diffusion components representing turbulent motions, and w_s is the sediment settling velocity (here equals to zero).

In the horizontal plane, particles were advected by ocean currents using a 4th order Runge-Kutta tracking scheme, and subject to additional displacement by horizontal diffusion.

In the OpenDrift framework, the horizontal diffusion is included by applying an uncertainty to the horizontal current magnitudes. The magnitude of the current uncertainty was estimated using the general diffusion Equation 2-1.

$$\int_t^{t+\Delta t} u_t . dt = \sqrt{2 . K_{u,v} . \Delta t} \; . \theta(-1,1)$$

Equation 2.2

[8] https://github.com/OpenDrift/opendrift/blob/master/opendrift/models/oceandrift.py

where $\theta(-1,1)$ is a random number from a uniform distribution between -1 and 1, Δt is the time-step of the model in seconds (900 sec. used here) and $K_{u,v}$ is the *horizontal* eddy diffusivity coefficient in $m^2 \cdot s^{-1}$.

In the vertical plane, particles are subject to both vertical settling (w_s) (here w_s=0) and diffusive displacement (w_t) due to vertical turbulent motion through the water column. In OpenDrift, the vertical mixing process is parameterised in using a numerical scheme described in Visser (1997) which is similar to equation 2.2 when using a constant vertical diffusion coefficient K_z (as employed here).

The horizontal and vertical diffusion are included in the dispersion modelling account for the mixing and diffusion caused by sub grid scale turbulent processes, such as eddies, that are not explicitly resolved by the hydrodynamic models.

For dispersion at oceanic scales, (Okubo, 1974; Okubo, 1971) proposed that $k_{u,v}$ varies approximately as Equation 2.3, which is close to the general 4/3 power law often considered for atmospheric (Richardson, 1962) and oceanic diffusions (Batchelor, 1952; Stommel, 1949) (Equation 2.4).

$$k_{u,v} = 0.103.L^{1.15}$$

Equation 2.3

$$k_{u,v} = \alpha.L^{\frac{4}{3}}$$

Equation 2.4

where L is the horizontal scale of the mixing phenomena and α indicates proportionality.

These equations relate the magnitude of the eddy diffusivity $k_{u,v}$ to the length scale of the phenomena and this 4/3 power relationship was found to be relevant over a large range of scale (10m to 1000km) (Okubo, 1974; Okubo, 1971). A similar relationship was found by List et al. (1990) in coastal waters.

In the present study, since high resolution flows are available (Section 2.3), the amount of added diffusion should be limited. A generic horizontal coefficient of 0.025 m^2/s was applied which is consistent with a length scale of order 70 m. The spatial scales of the vertical turbulent motions within the water column are one or several orders of magnitude smaller than horizontal ones. The vertical diffusion coefficient was set to a generic value of 5 cm^2/s.

In the present model implementation, any particle reaching the shoreline, the seabed or sea surface was re-suspended to continue its dispersion (i.e., non-sticky boundaries).

Particles reaching the edges of the model domain (see Figure 2-3) were removed from the simulations.

2.4.3. Discharge scenarios

The approach employed in the present study consisted in running 1 year-long simulations of wastewater discharges from the outfall location (Figure 2-9, and Table 2-4), within two contrasting historical contexts El Niño / La Niña episodes (April 2015- April 2016, and April 2010- April 2011 respectively).

To reproduce the expected variation of discharge rates over time, an annual time series of daily discharge volumes measured through the calendar years 2020-2021 at the wastewater plant was used as a reference for both El Niño / La Niña scenarios. Simulations were reproduced with projected discharge flow rate increase i.e., consent flow (year 2059). A factor of 1.3 was applied to the current daily discharge flow timeseries (see section 2.2.1).

The nearfield plume dynamics vary over time in response to ambient flow speed and direction and effective outfall discharge rate. This was included in the (far-field) model by releasing particles within time-varying triangular footprints, describing the nearfield range NFR. The dimensions of the release footprints (NFR length, NFR half width, NFR thickness) were defined by interpolation from the look-up table generated from the nearfield modelling results (see section 3.1), accounting for ambient hydrodynamic flow speed at the outfall location, and outfall discharge rate. The triangular release footprints were then aligned with instantaneous flow direction (Figure 2-11). Note the particles were released in the surface layer of the water column within a thickness defined by the NFR thickness as the plume is expected to be buoyant. This will also delay particle interaction with the seabed and thus produce conservative trajectories in terms of how far they could travel.

The number of particles released each day was scaled according to the effective daily discharge rate (i.e., more particles released for large discharge flow rates). Maximum particle age was set to 40 days after which they were removed from the simulation. This was defined from the maximum T90 considered of 32 days Using a maximum particle age prevents saturation of the particle-tracking model with “old” particles and allows keeping a very large number of active particles in the model at all times to correctly represent the plumes.

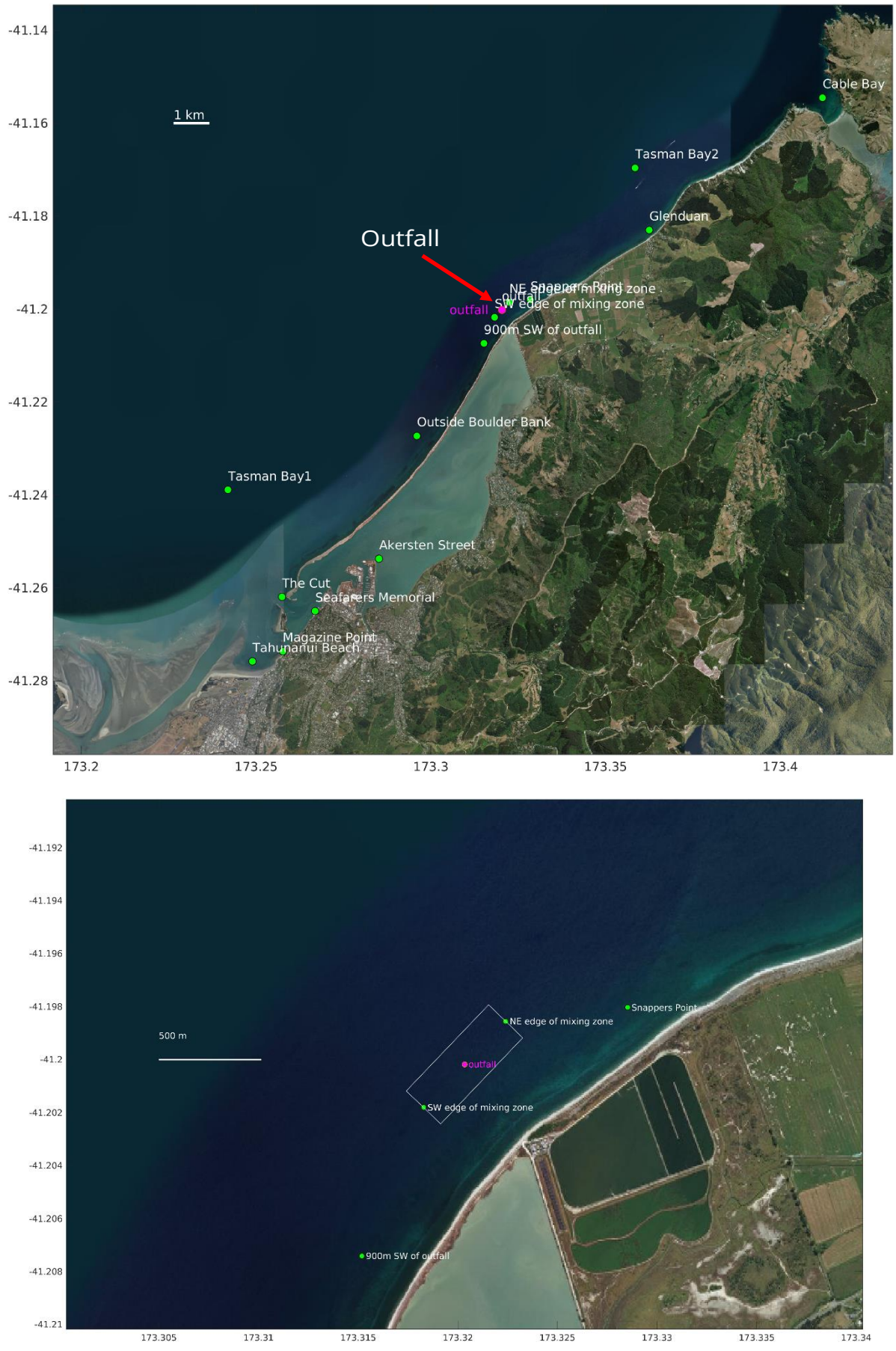

Figure 2-9 Location of outfall (red dot) and extraction sites (white).

Table 2-4 Site locations (see Figure 2-9).

Site Names	Lon	Lat	Depth
'outfall'	173.3203	-41.2002	12.0
'Cable Bay'	173.4121	-41.1545	3.6
'Glenduan'	173.3625	-41.1830	3.8
'Snappers Point'	173.3285	-41.1980	5.0
'900m SW of outfall'	173.3152	-41.2074	5.8
'Outside Boulder Bank'	173.2960	-41.2273	9.8
'Tasman Bay1'	173.2420	-41.2389	11.7
'Akersten Street'	173.2852	-41.2538	1.3
'The Cut'	173.2574	-41.2620	6.5
'Seafarers Memorial '	173.2669	-41.2650	1.7
'Magazine Point '	173.2577	-41.2737	0.6
'Tahunanui Beach'	173.2490	-41.2758	3.3
'Tasman Bay2'	173.3585	-41.1696	22.4
'SW edge of mixing zone'	173.3183	-41.2018	13.0
'NE edge of mixing zone'	173.3224	-41.1986	11.9

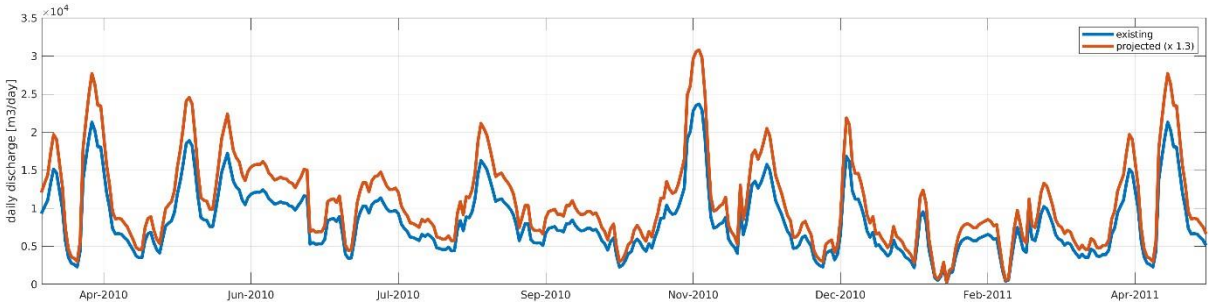

Figure 2-10 Timeseries of daily flow discharge over an annual period for the existing and projected future scenarios.

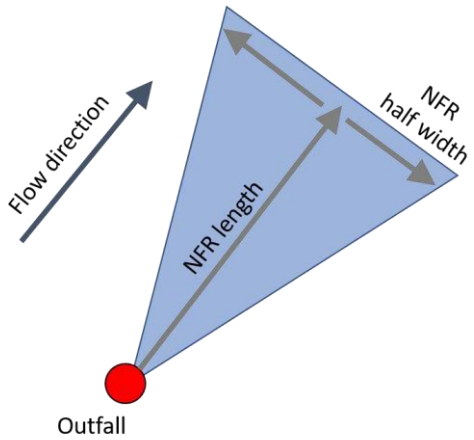

Figure 2-11 Sketch showing the triangular release footprint defined from the nearfield dynamics metrics NFR length and mid width. Particles were released on the surface layer within a thickness defined by the NFR thickness.

2.4.4. Post-processing

2.4.4.1. General approach

The dispersion model outputs a set of particle positions that change over time, thus describing their trajectories. Here, particles can describe any contaminant considered to be passive i.e., freely moved under influence of currents and mixing. Particle trajectories can be useful to assess general transport pathways in a qualitative sense, but it is often needed to reconstruct particle concentration fields, which is a more quantitative metric to assess actual contaminant concentration. The "concentration" of particles at a given point (x,y,z) is related to the particle "density" in the region surrounding this point, which can be estimated by counting particles within each cell of a user-defined grid.

To outline general dispersion pathways, the contaminant concentration fields were reconstructed from the particles clouds on 17 by 14 km frame centred on the outfall location, with a grid resolution of 100 m. Concentrations were computed at three levels in the water column, i.e. surface, mid depth and near bed. Snapshots of particle clouds are shown in Figure 2-12.

Gridded field of contaminant concentrations were reconstructed from the particle clouds using two different techniques, (a) 2D histogram (standard box-counting approach), and (b) kernel density estimator (Silverman, 1986).

For the 2D histogram approach, time-varying contaminant concentration C(t,x,y,z) were obtained by counting the number of particles, each carrying a given contaminant *load*, in each grid cell, for each water column band considered. The total contaminant *load* per cell was then normalized by the cell surface area [m^2], and vertical depth band [m] to obtain contaminant concentration in [load/m^3].

In the kernel density approach, individual particles are assumed to represent the centre of mass of a "cloud"; the density profile of the cloud is described by the *kernel function*, while the spreading of the particle's equivalent mass is defined by the *bandwidths* associated with a given particle or receptor (Bellasio, et al., 2017; Vitali et al., 2006). These two components are then used to derive a *particle density field*, also referred to as a *probability density function*. Here, the kernel density estimation is undertaken following the approach proposed by Botev, et al. (2010). The proposed method uses an adaptive kernel density estimation method based on the smoothing properties of linear diffusion processes. The key idea is to view the kernel from which the estimator is constructed as the transition density of a diffusion process (Botev, et al., 2010). This method limits the amount of guessing, notably to defining bandwidths, as well as possible excessive smoothing of the density fields (e.g., as obtained with Gaussian kernel density estimators).

Based on a given cloud of particles (X_{part},Y_{part}), the method yields a *probability density function PDF(x,y)*, derived from the *kernel density estimator* describing the density of particles throughout the domain. The spatial integration of the *probability density function PDF(x,y)* over the entire domain equals one.

The *PDF(x,y)* values can be converted to particle density when multiplied by the total number of particles in the domain i.e., with units [particles.m^{-2}]. The particle density can in turn be converted to *load* density, or *load* distribution, based on the equivalent *load* carried by individual particles i.e., with units [load.m^{-2}]. Contaminant load concentration is obtained by dividing the load density by the correct vertical depth band i.e., with units [load.m^{-3}].

In order to provide dilution fields (dimensionless), a generic contaminant concentration of Co = 1g/m^3 (or 1 mg/L) was assumed for the raw wastewater discharged at the outfall.

Dilution was then obtained as D = Co/C(t,x,y,z).

The reconstruction of contaminant concentration fields was undertaken using both the 2D histogram and kernel density approaches to obtain conservative concentration/dilution estimates for both high and low concentrations levels.

This 2D histogram approach is typically more conservative for larger concentration levels at sites near the release and as it will attribute the sum of all particle's load within a given grid cell to that cell. However, for areas with a smaller number of particles (e.g., further from release, or less exposed), concentration may possibly become zero if no particles are within a given cell. In contrast, the kernel density approach spatially smoothes individual particle loads, before doing the box-counting. This typically results in smaller concentrations peaks (e.g., a cell that included 10 particles load in the 2D histogram may now include only 8.5), however this allows better resolving lower concentrations levels at sites less exposed to the contaminants (e.g., a cell that included zero load with the 2D histogram method may now include 0.8 load, from nearby particles). The kernel density approach is similar that occur in Eulerian advection-diffusion models that can also be used to track contaminant dispersion.

Spatial statistics were derived from the obtained time-varying contaminant fields. In addition to the spatial statistics, dilution timeseries were extracted at a range of sites (Table 2-4) for further assessment such as QMRA (Quantitative microbial risk assessment). To ensure conservative estimates of contaminant concentrations at sites of interest, timeseries provided for the Quantitative Microbial Risk Assessment merged the results of both approaches, by taking the maximum of predicted concentrations with the kernel or 2D histogram techniques at each timestep.

2.4.4.2. Inclusion of contaminant inactivation

To account for the decay/inactivation of released contaminant, results were postprocessed accounting for a progressive decay of the contaminant load carried by each particle. Note a conservative scenario with no inactivation was also considered.

The decay rate can be simulated using the relationship below (e.g., Eregno et al., 2018) :

$$C = C_0 e^{-kt}$$

Equation 2.5

where t = time [days], Co = concentration at time zero [load/m^3], C = concentration [load/m^3] at time t, k = inactivation constant [$days^{-1}$].

Based on Boehm et al. (2019) who carried out a systemic review of virus decay rates in surface waters, two generic inactivation constants were considered to model average and rapid decay (notably for norovirus):

- Average decay K= 0.0708 [$days^{-1}$], T50 = 10 [days], T90 = 32 [days]
- Rapid decay K= 1.0715 [$days^{-1}$], T50 = 0.7 [days], T90 = 2 [days]

T50 and T90 are duration after which 50% and 90% of the virus have decayed.

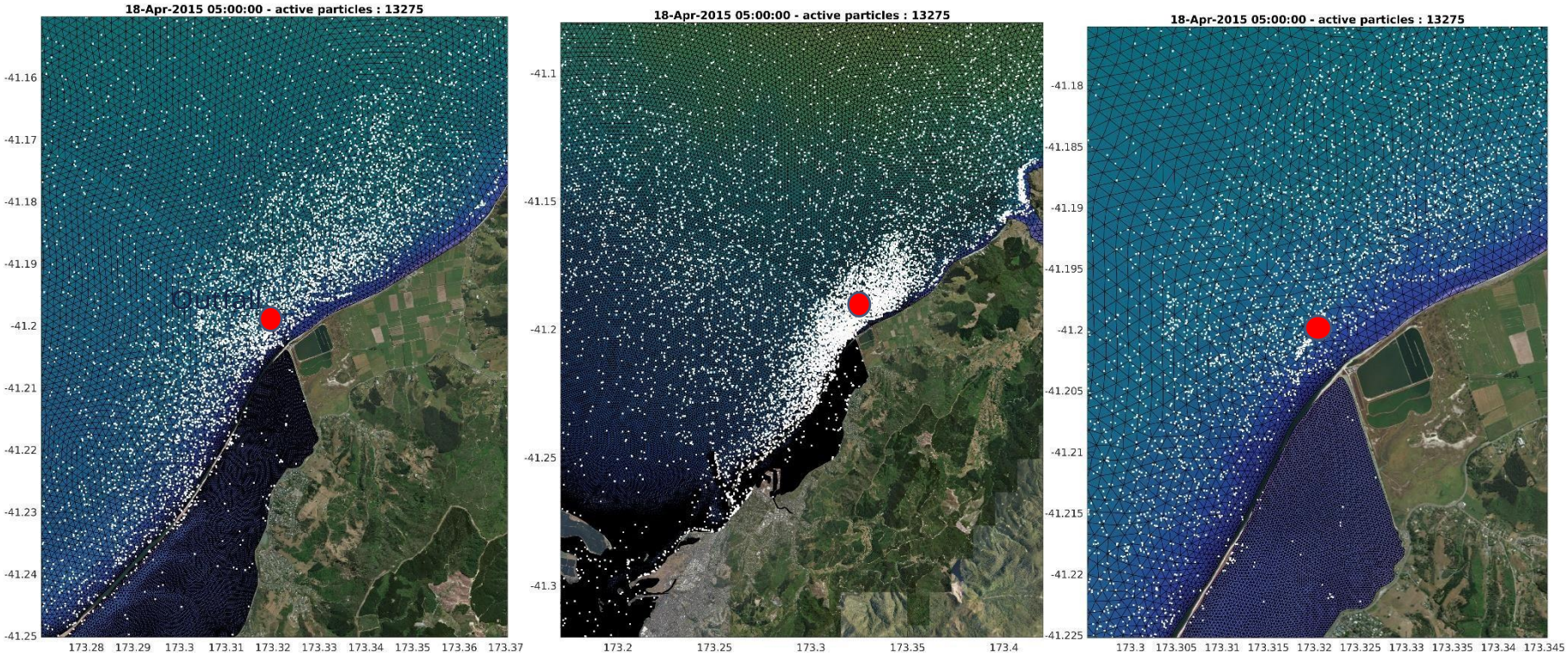

Figure 2-12 Snapshots of particle clouds at several zoom levels. The outfall is shown in red.

3. Results

3.1. Near field modelling

A range of simulations were undertaken in order to estimate the near field plume characteristics. It is noted that the discharge is occurring via 10 outlets that are holes on the pipe with no diffuser or complex structure. The nearfield plume shape is first represented by 10 point-sources release which are subsequently merged into one positive buoyant plume, represented by the diagram in Figure 3-1.

The nearfield region (NFR) describes the zone of strong initial mixing where the so-called nearfield processes occur (i.e., the initial jet characteristic of momentum flux, buoyancy flux and outfall geometry influence the jet trajectory and mixing of a wastewater discharge). It is the region of the receiving water where outfall design conditions are most likely to have an impact on in-stream concentrations. Beyond that is the far field region where physical mixing mechanisms are dominating with spreading motions and passive diffusion controlling the trajectory and dilution of the wastewater discharge plume.

A dilution factor of 'n' times at some distance from the discharge indicates a reduction in pollutant level by 'n' times (e.g., with a discharge concentration above background of a nominated value of 1 g/m^3 and dilution factor of 5 times, the expected concentration above background will be 1/5=0.2 g/m^3).

Results show that the dilution factor at the edge of the near field varies from 220.5 to 2871.4 (Table 3-1). Two examples of dilution along the plume centreline are shown in Figure 3.2 for simulations of p10 of discharge flow and ambient current speed of 0.05 m/s and p90 of discharge flow and ambient current speed of 0.4 m/s. The dilution in the first case (top panel, Figure 3-2) shows an approximately linear increase in dilution and a much higher increase rate further away from the source. The marked changes on the line in the plot are located at distances where CORMIX begins and end specific modules, in accordance with CORMIX hydrodynamic classification (MU1H – description in Appendix A) based on the characteristics of the jet flow and the ambient flow and illustrated in the diagram presented in Figure 3-1.

The second case (bottom panel, Figure 3-2), the hydrodynamic classification is MU8 (description in Appendix A), and different modules are then selected by CORMIX to model this plume, resulting in a different dilution behaviour. The difference is because the crossflowing discharge gets rapidly deflected by the strong ambient current.

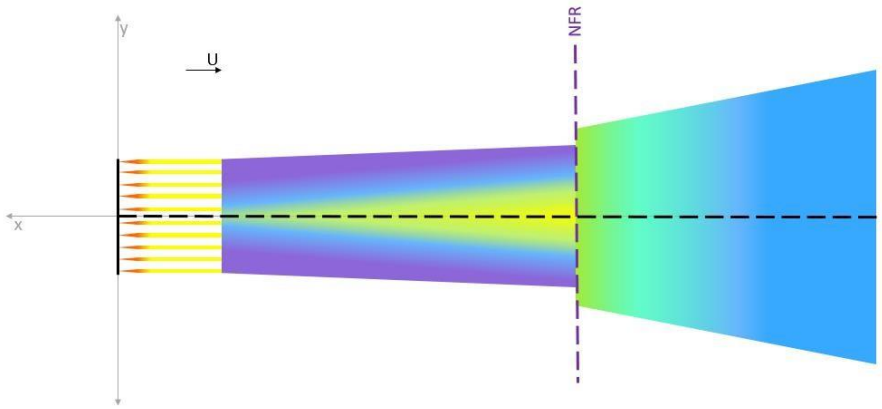

Figure 3-1 Diagram representing the different modules in CORMIX simulations of near-field plume. U = current direction, NFR = Near-field range. From left to right, individual jet/plumes before merging, merging of individual jet/plumes, begin of layer/boundary/terminal layer approach, end of near-field region (NFR). Beyond the NFR is the far-field region which is illustrated here but will be simulated using the particle tracking model (OpenDrift).

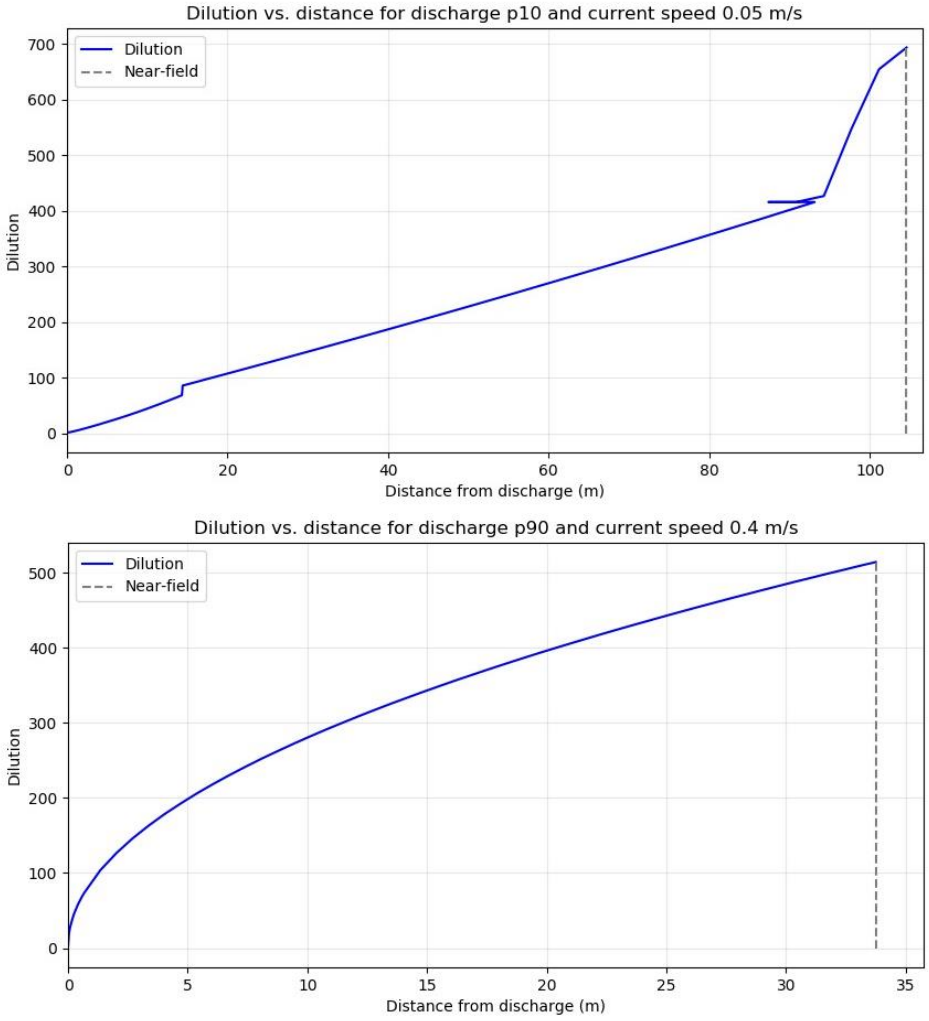

Figure 3-2 Dilution at distance from the discharge for simulations considering p10 of flow and 0.05 m/s ambient current speed (top) and p90 of flow and 0.40 m/s ambient current speed (bottom).

Dilution tends to be higher in faster ambient current velocities although variations to this trend can occur depending on the ambient currents compared to the discharge velocity (i.e., the velocity the discharge exit the pipe).

Results show that plume behave differently in terms of plume shape and length of nearfield zone under different flow rate scenarios (i.e., p10, p50 and p90). For flow rates representing p10 and p50 (0.048 m^3/s and 0.094 m^3/s) have near-field length increasing with increased ambient current velocity, reaching a distance of up to 1907.3 m from the discharge point. This distance is calculated based on the processes that define what is a near-field zone, as previously described. In terms of dilution, high values are predicted by the model at the edge of the near-field for these scenarios, e.g., for p10 flow rate and ambient velocity of 0.4 m/s dilution is 2871.4 at the edge of near-field which corresponds to 0.035% of the initial concentration (Table 3-1).

In all scenarios, plume is wider in near stagnant water and the plume is extends downstream (x-direction – flow direction) while reducing in extent in the across the flow direction (y-direction) under faster current flow (Table 3-1). The edge of the near field is located before the plume attaches to the shoreline in all simulations (for the conditions simulated in this study). For example, maximum predicted half-width of plume (distance from the centreline to the edge of plume) is 185.9 m while outlets are at least 400 m from the shore, therefore, plume does not contact the shoreline within the near-field zone.

The time when the plume transitions from near-field to far-field ranges from 3 minutes (p90, 0.4 m/s) to 77.8 minutes (1.3 hour, p10, 0.4 m/s). The far-field plume dispersion was modelled using the OpenDrift particle tracking model and results are presented in the next section.

Table 3-1 CORMIX scenarios. NFR = Near-field range.

Scenarios	Ambient current (m/s)	Flow rate (m^3/s)	Discharge velocity (m/s)	NFR length (m)	NFR half-width (m)	NFR thickness (m)	Concentration at NFR edge (%)	Dilution at NFR edge	Cumulative travel time (minutes)	CORMIX Hydrodynamic Classification
p10	0.05	0.048	0.07	104.6	24.7	13.5	0.144	693.4	18.5	MU1H
	0.10		0.07	220.1	21.1	11.8	0.096	1037.4	29.3	MU1H
	0.20		0.07	613.7	20.2	10.1	0.059	1702.5	48.7	MU1H
	0.30		0.07	1182.4	19.3	9.6	0.043	2308.5	63.6	MU1H
	0.40		0.07	1907.3	18.7	9.2	0.035	2871.4	77.8	MU1H
p50	0.05	0.094	0.13	121.7	92.4	3.5	0.292	342.6	24.8	MU1V
	0.10		0.13	167.5	21.1	12.9	0.173	577.4	20.0	MU1H
	0.20		0.13	433.3	20.6	10.5	0.108	922.6	33.2	MU1H
	0.30		0.13	825.0	19.8	9.9	0.081	1242.3	44.4	MU1H
	0.40		0.13	1333.9	19.1	9.5	0.065	1535.4	54.3	MU1H
p90	0.05	0.185	0.26	154.7	185.9	2.2	0.454	220.5	37.0	MU1V
	0.10		0.26	131.7	22.2	13.5	0.309	324.1	13.8	MU1H
	0.20		0.26	310.6	21.0	11.1	0.199	502.7	22.5	MU1H
	0.30		0.26	33.75	8.9	13.5	0.256	390.2	3.7	MU8
	0.40		0.26	33.75	8.8	13.5	0.194	514.5	2.8	MU8

3.2. Farfield modelling

The time-varying gridded contaminant concentration fields over the two annual El Niña and La Niña periods can be used to derive statistical maps informing on contaminant concentration levels, and dilution, throughout the study site.

General dispersion characteristics of contaminant discharged at the outfall are illustrated in Figure 3-5 to Figure 3-8. The figures show specific dilution contours (1/1000, 1/2000, 1/5000) for different scenarios included *El Niño* versus *La Niña* period, *existing* versus *future* discharge flow rate, and *average* versus *rapid* contaminant inactivation. Results for scenarios with no contaminant inactivation (i.e., worst-case) are provided in Figure 3-9 and Figure 3-10.

The dilution maps were obtained by normalizing the 90th percentile contaminant concentration (i.e., concentration exceeded only 10% of the time), found in top 4 m of the water column, by the initial outfall concentration Co i.e., Dilution = Co / C(t,x,y,z).

The dispersion footprints are clearly elongated in southwest-northeast axis which is driven by the local hydrodynamics (Figure 3-3 and Figure 3-4). Some smaller patches of 1/2000 dilution contour (grey) can be seen closer to the coast, especially in the vicinity of the outfall, and towards the north. We also note some possible small 1/5000 dilution patches on the estuary side of the spit. These are due to some particles entering the estuary by its entrance at the southern end of the spit and moving northwards with tidal flows (e.g., see Figure 2-12). These particles eventually become relatively static once in the inner estuary due to low flows and intermittent wetting drying thus generating some *relatively* higher concentration areas.

Dispersion patterns are very similar for La Niña and El Niño periods (Figure 3-5 and Figure 3-6 left panels), as the hydrodynamic regimes. We can note the 1/5000 dilution contour footprint during La Niña year is slightly wider to the northeast of the outfall, and it also extends further south relative to the El Niño scenario.

The increase of discharge flows (factor 1.3) due to the projected population increase results in similar footprint shapes but with larger spatial excursions, as expected (Figure 3-5 and Figure 3-6 right panels).

The inclusion of contaminant deactivation has a significant impact on the spatial extents of the plume footprints (Figure 3-7 and Figure 3-8). We note maximum excursions of the 1/5000 dilution of order 2-3 km from outfall assuming a virus T90= 2 days (time after which 90% of viral load has decayed), while it is ~ 7-8 km for a longer T90 = 32 days. As

expected, the extents of the plume footprints are the largest when no contaminant inactivation is considered (see Figure 3-9 and Figure 3-10).

Timeseries of contaminant concentration were extracted at several sites (see Figure 2-9) to provide a basis for further assessment such as QMRA (Quantitative microbial risk assessment). Plots of concentration timeseries for La Niña, with no inactivation, are presented in Figure 3-11 and Figure 3-12. El Niño results are shown in Figure 3-13 and Figure 3-14. Note the presented concentrations assume an initial undiluted concentration at the outfall Co = $1 g.m^{-3}$. Dilution factor can be obtained as Co/C(t).

As expected, concentrations are the largest at the outfall and we note a progressive reduction of concentrations levels moving away from its location both northeast-ward (i.e., Snapper's Point, Glenduan), and southwest-ward (i.e., 900m SW of outfall, Outside Boulder Bank).

Concentrations at sites located further south from the outfall, in the vicinity of the estuary entrance, and north (Tasman Bay 2) are further reduced though some peaks are still noticeable at times. It is interesting to note that peaks are not always synchronised with peaks near the outfall, due to local recirculation processes. Inspection of concentration fields suggests these peaks at sites relatively far south from the outfall can be due to contaminant accumulation in some lower current areas or with eddies. This is visible in Figure 3-9 and Figure 3-10 which shows some local patches of the $1/5000^{th}$ dilution contours south of the domain. It is reminded that the results shown do not included die-off, which is a worst-case assumption. In reality, it is likely progressive inactivation may reduce the contaminant load in these secondary accumulation zones.

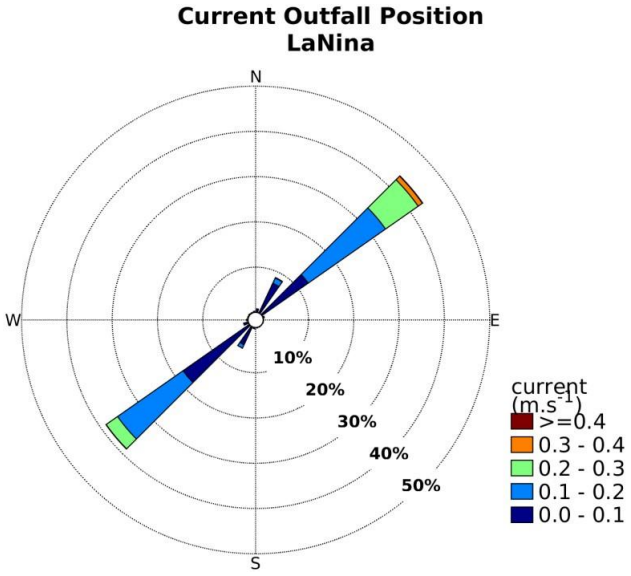

Figure 3-3 Rose of depth-averaged current at the outfall location during La Nina annual period.

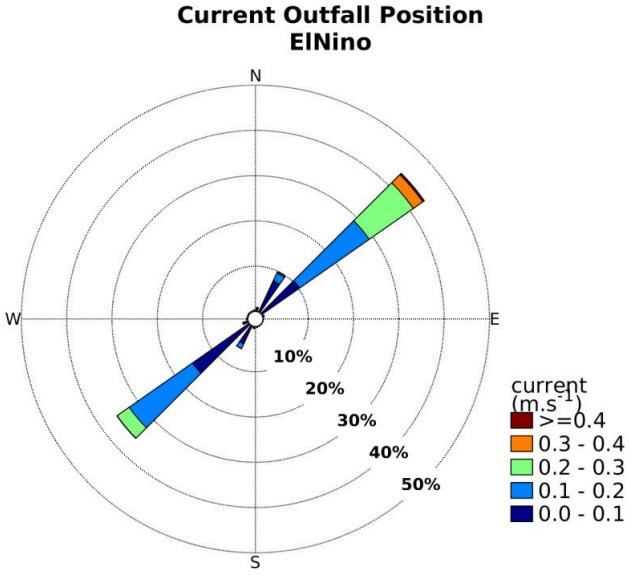

Figure 3-4 Rose of depth-averaged current at the outfall location during El Nino annual period.

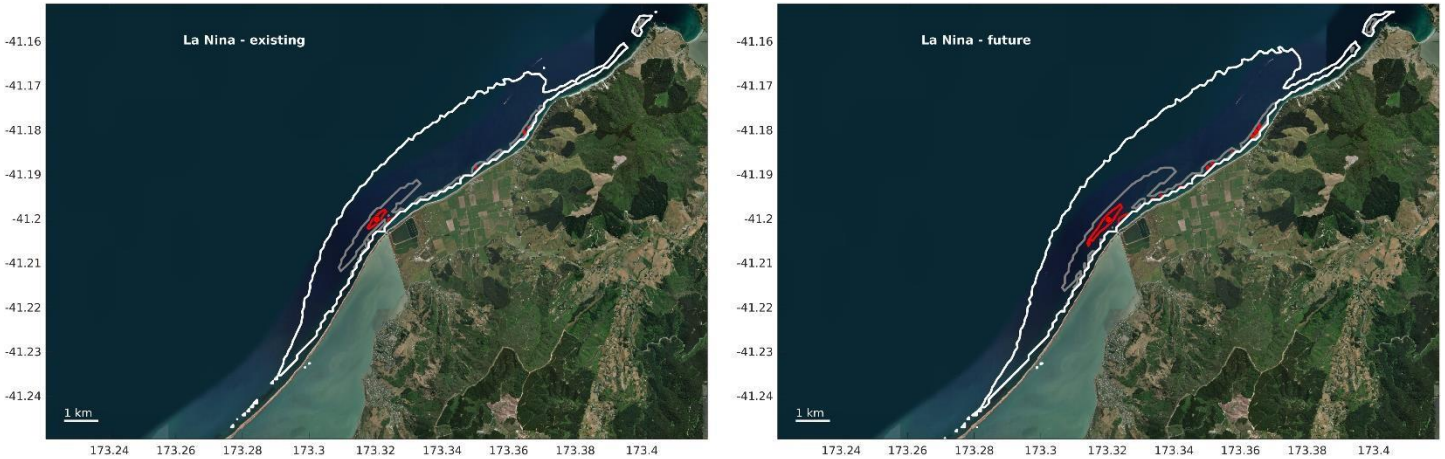

*Figure 3-5 Dilution contours 1/1000, 1/2000, 1/5000 (red, grey, white) in surface waters for the **La Niña annual period** for **existing** and **future** discharge flows (T90=32 days). The outfall location is show as a red dot.*

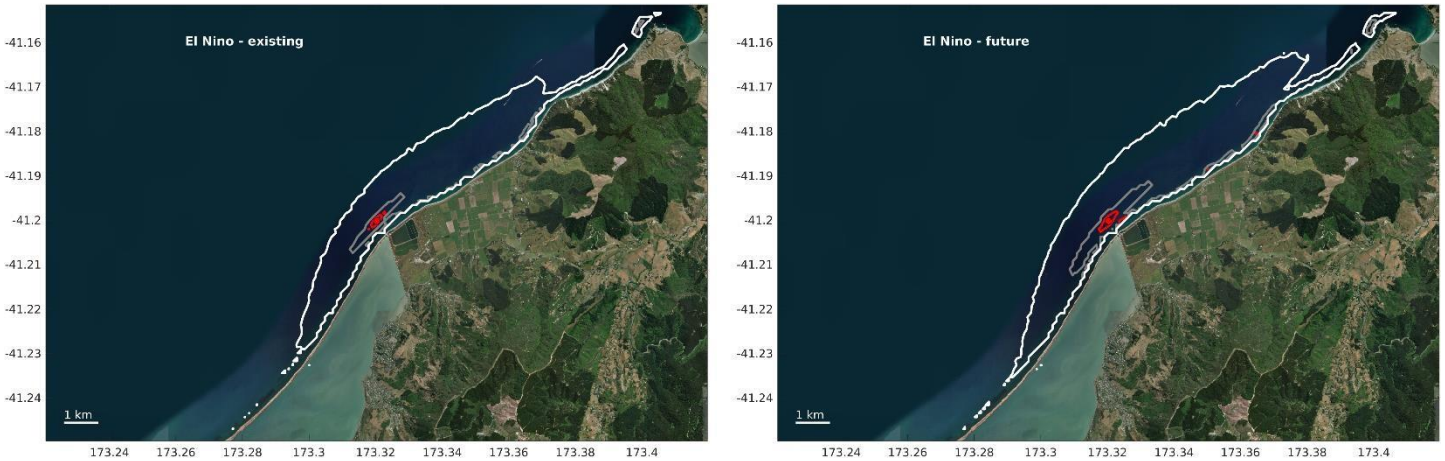

*Figure 3-6 Dilution contours 1/1000, 1/2000, 1/5000 (red, grey, white) in surface waters for the **El Niño annual period** for **existing** and **future** discharge flows (T90=32 days). The outfall location is show as a red dot.*

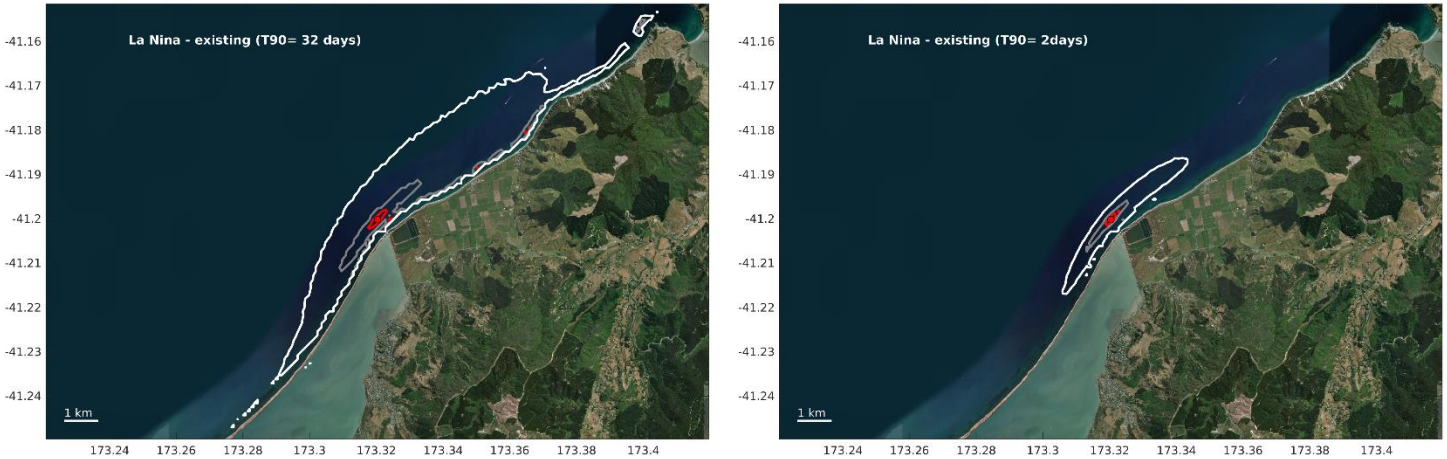

*Figure 3-7 Dilution contours 1/1000, 1/2000, 1/5000 (red, grey, white) in surface waters for the **La Niña annual period** for **existing** discharge flows for **different inactivation coefficients**. The outfall location is show as a red dot.*

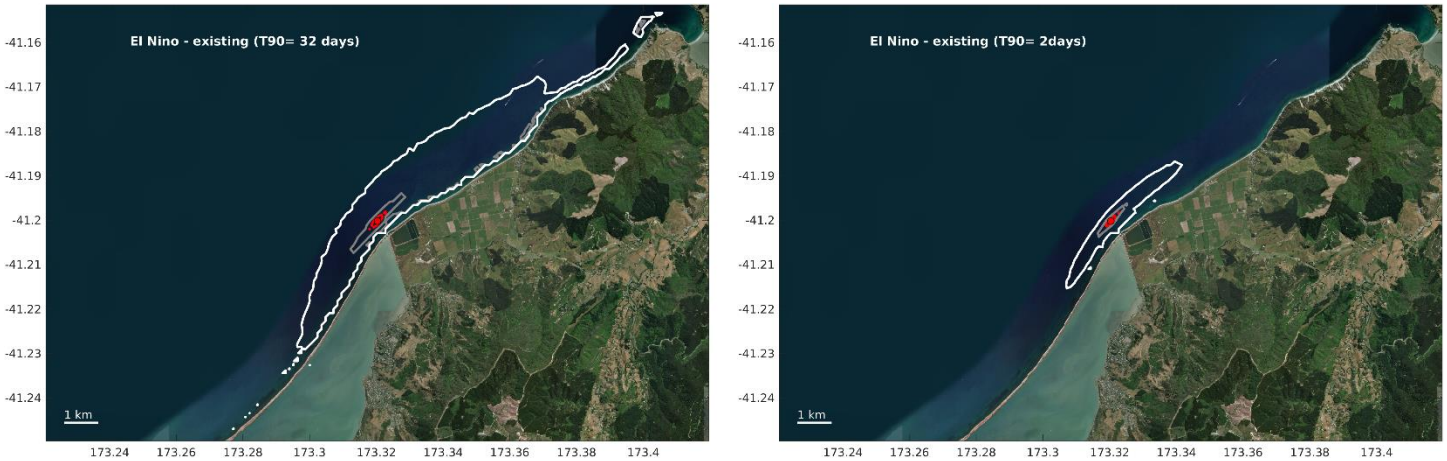

*Figure 3-8 Dilution contours 1/1000, 1/2000, 1/5000 (red, grey, white) in surface waters for the **El Niño annual period** for **existing** discharge flows for **different inactivation coefficients**. The outfall location is show as a red dot.*

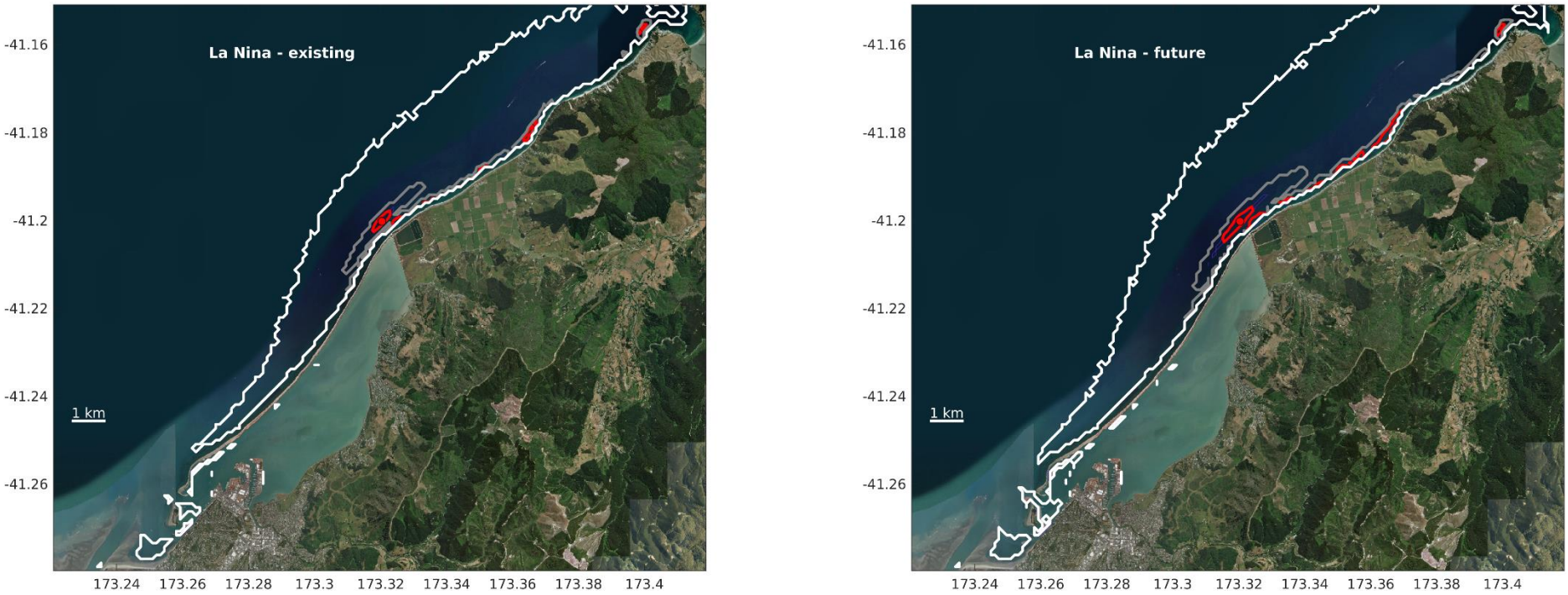

*Figure 3-9 Dilution contours 1/1000, 1/2000, 1/5000 (red, grey, white) in surface waters for the **La Niña annual period** for **existing** and **future** discharge flows (no inactivation). The outfall location is show as a red dot.*

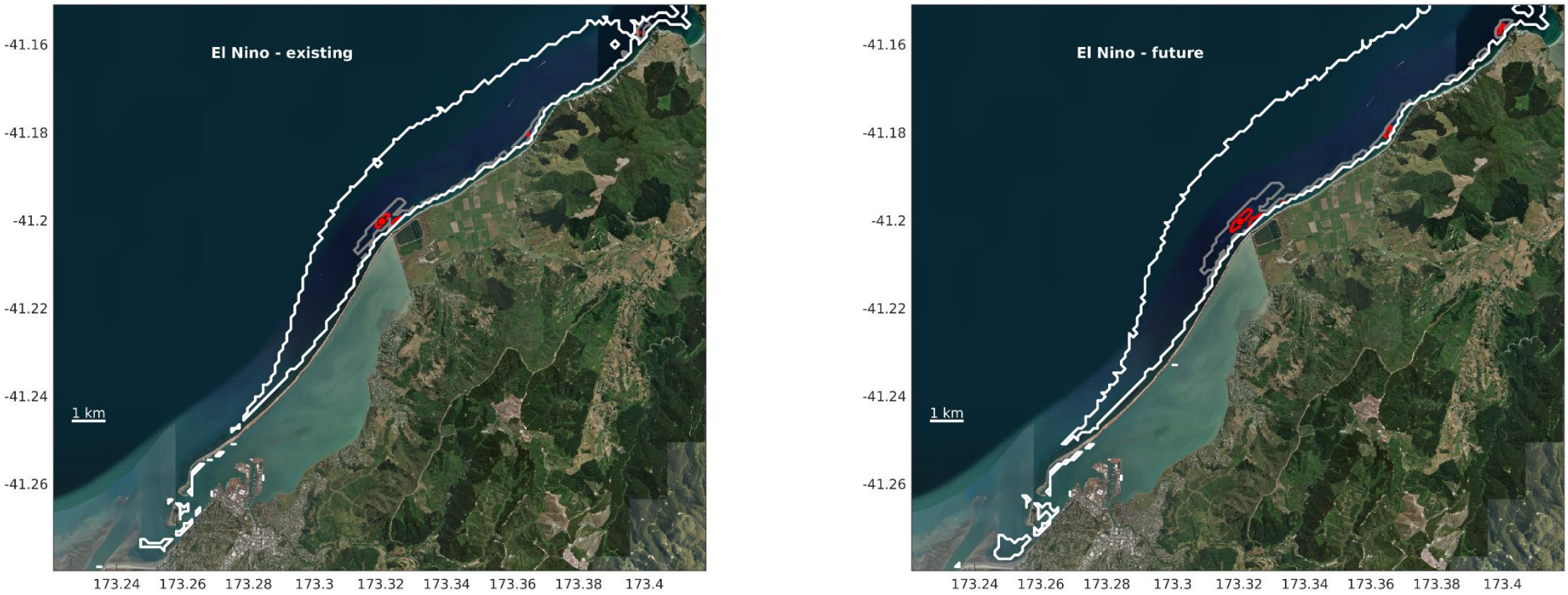

*Figure 3-10 Dilution contours 1/1000, 1/2000, 1/5000 (red, grey, white) in surface waters for the **El Niño annual period** for **existing** and **future** discharge flows (no inactivation). The outfall location is show as a red dot.*

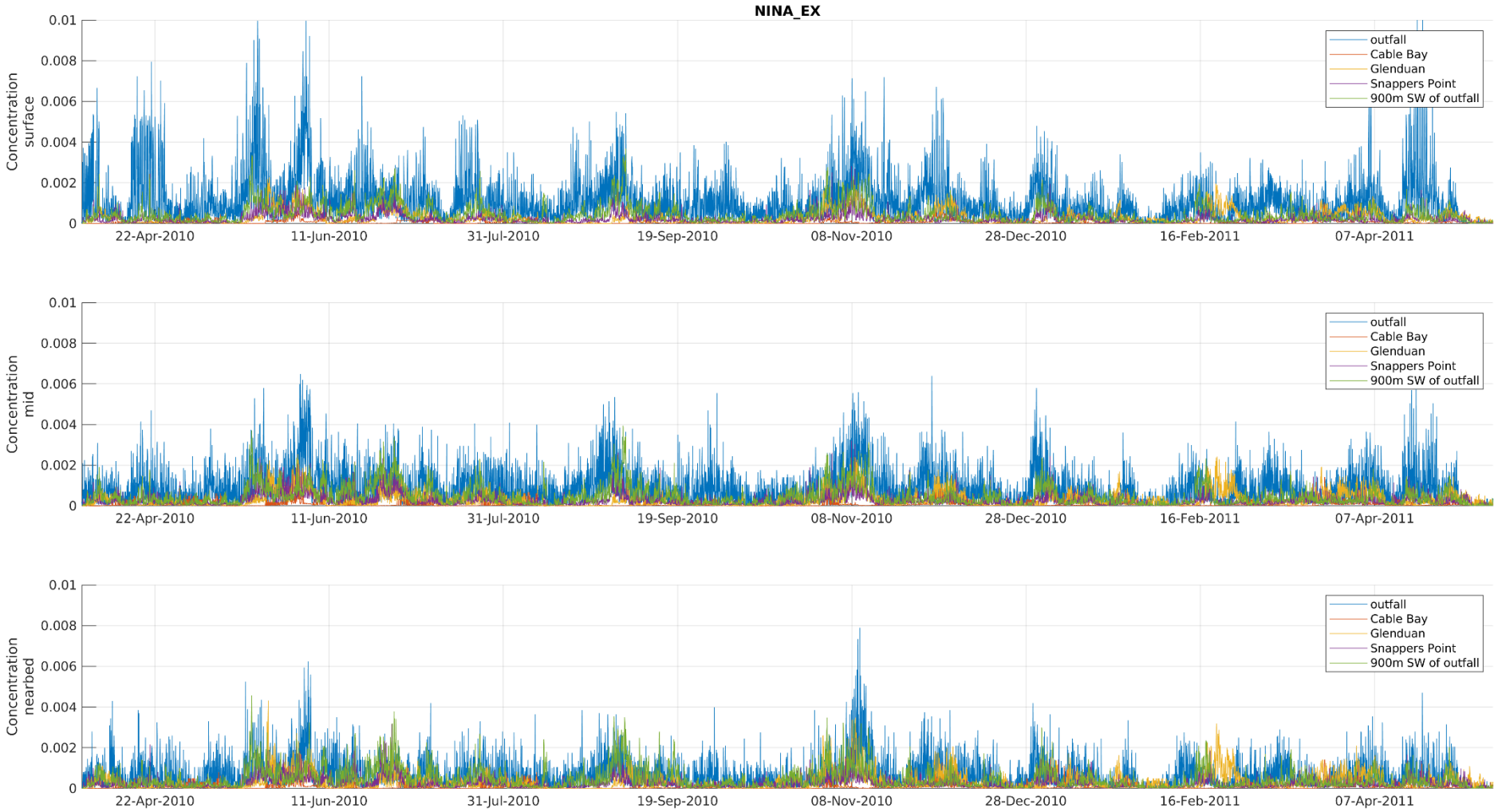
NINA_EX
Concentration surface
Concentration mid
Concentration nearbed
0.01
0.008
0.006
0.004
0.002
0
22-Apr-2010
11-Jun-2010
31-Jul-2010
19-Sep-2010
08-Nov-2010
28-Dec-2010
16-Feb-2011
07-Apr-2011
outfall
Cable Bay
Glenduan
Snappers Point
900m SW of outfall

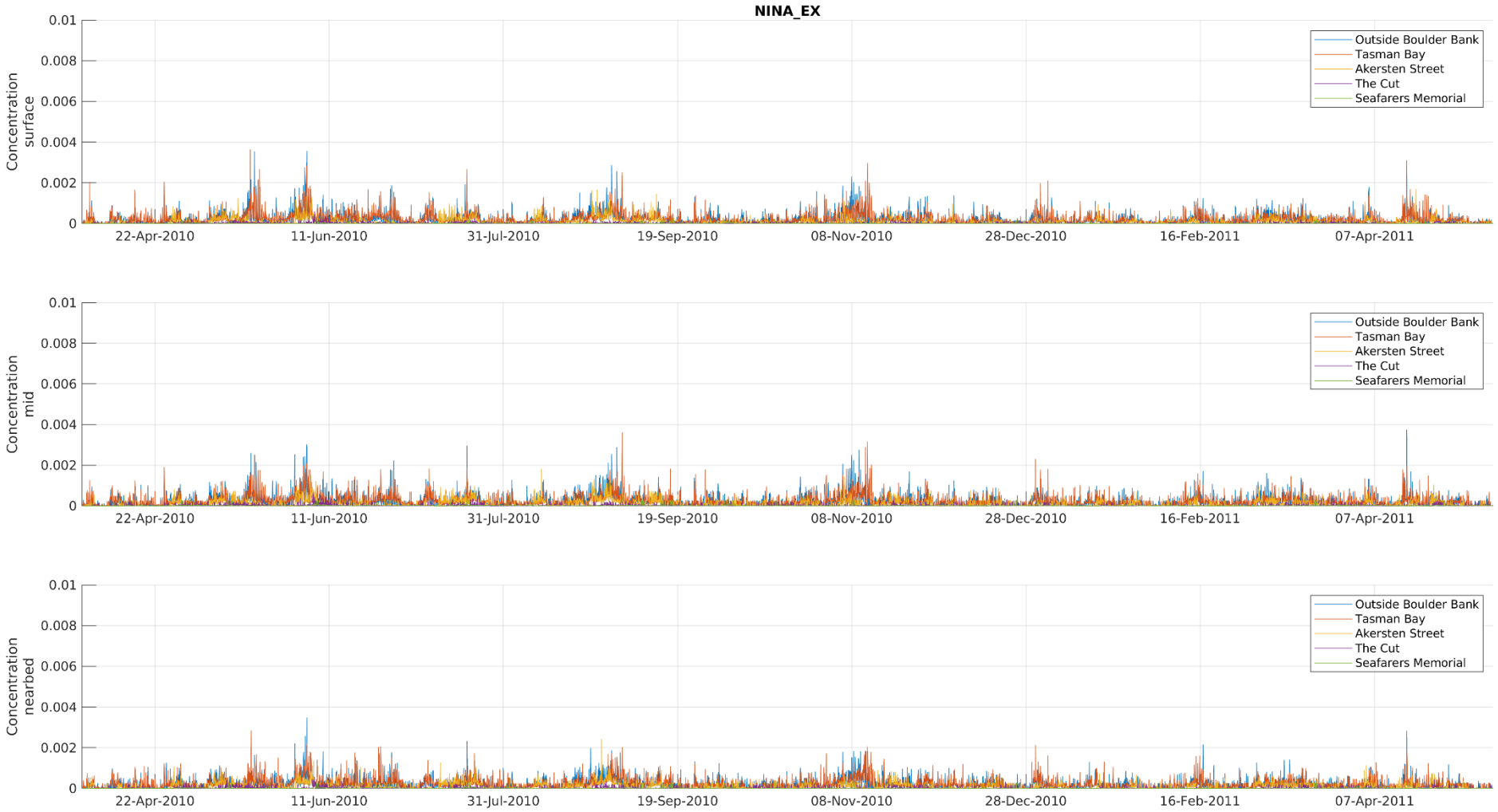
NINA_EX
Concentration surface
Concentration mid
Concentration nearbed
0.01
0.008
0.006
0.004
0.002
0
22-Apr-2010
11-Jun-2010
31-Jul-2010
19-Sep-2010
08-Nov-2010
28-Dec-2010
16-Feb-2011
07-Apr-2011
Outside Boulder Bank
Tasman Bay
Akersten Street
The Cut
Seafarers Memorial

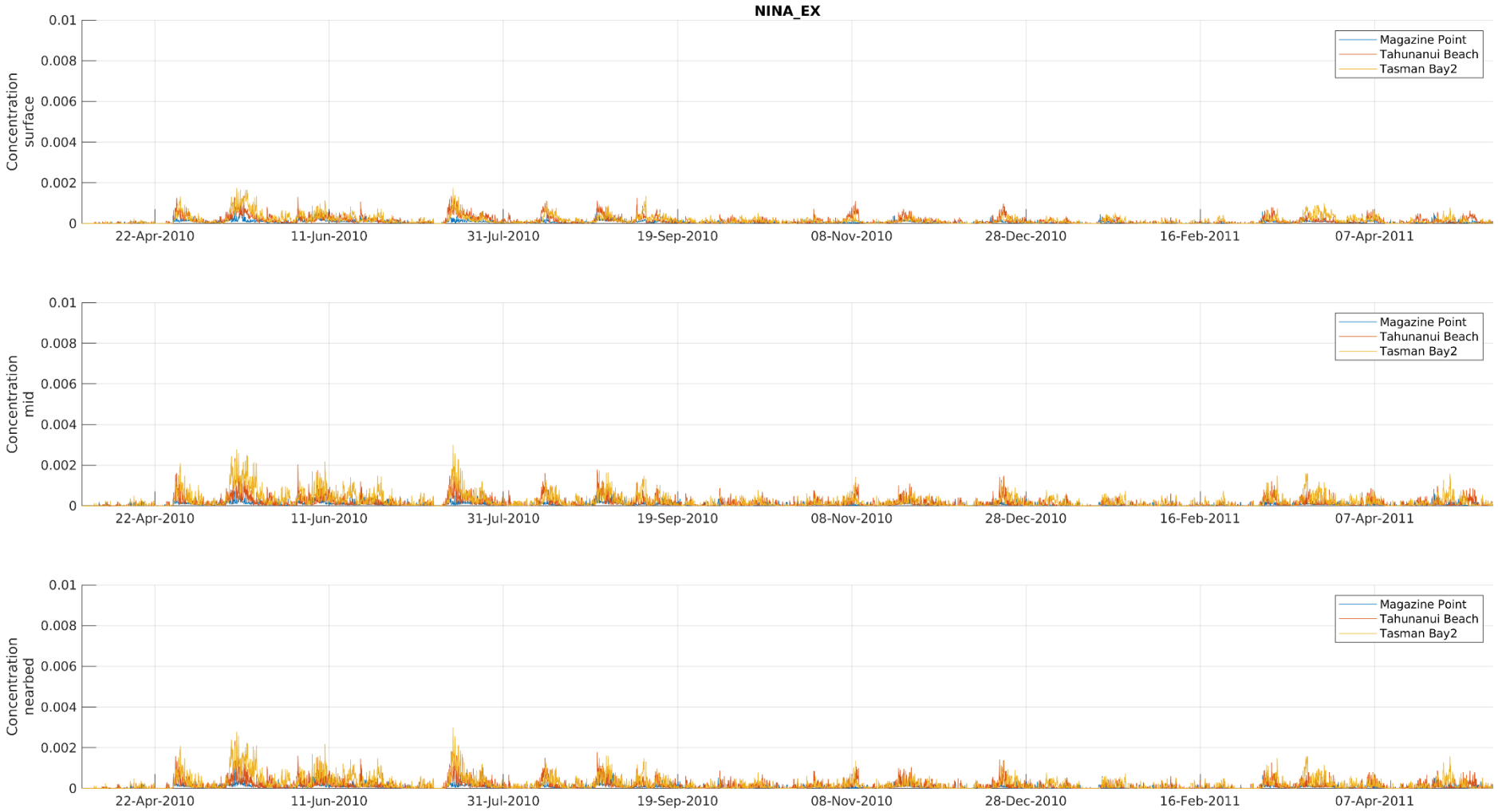

*Figure 3-11 Timeseries of contaminant concentration at sites (Figure 2-9), in surface, mid-water and nearbed levels, for **La Niña** annual period and **existing** discharge flows (**no inactivation**). The presented concentrations assume an initial undiluted concentration at the outfall of 1g.m^{-3}.*

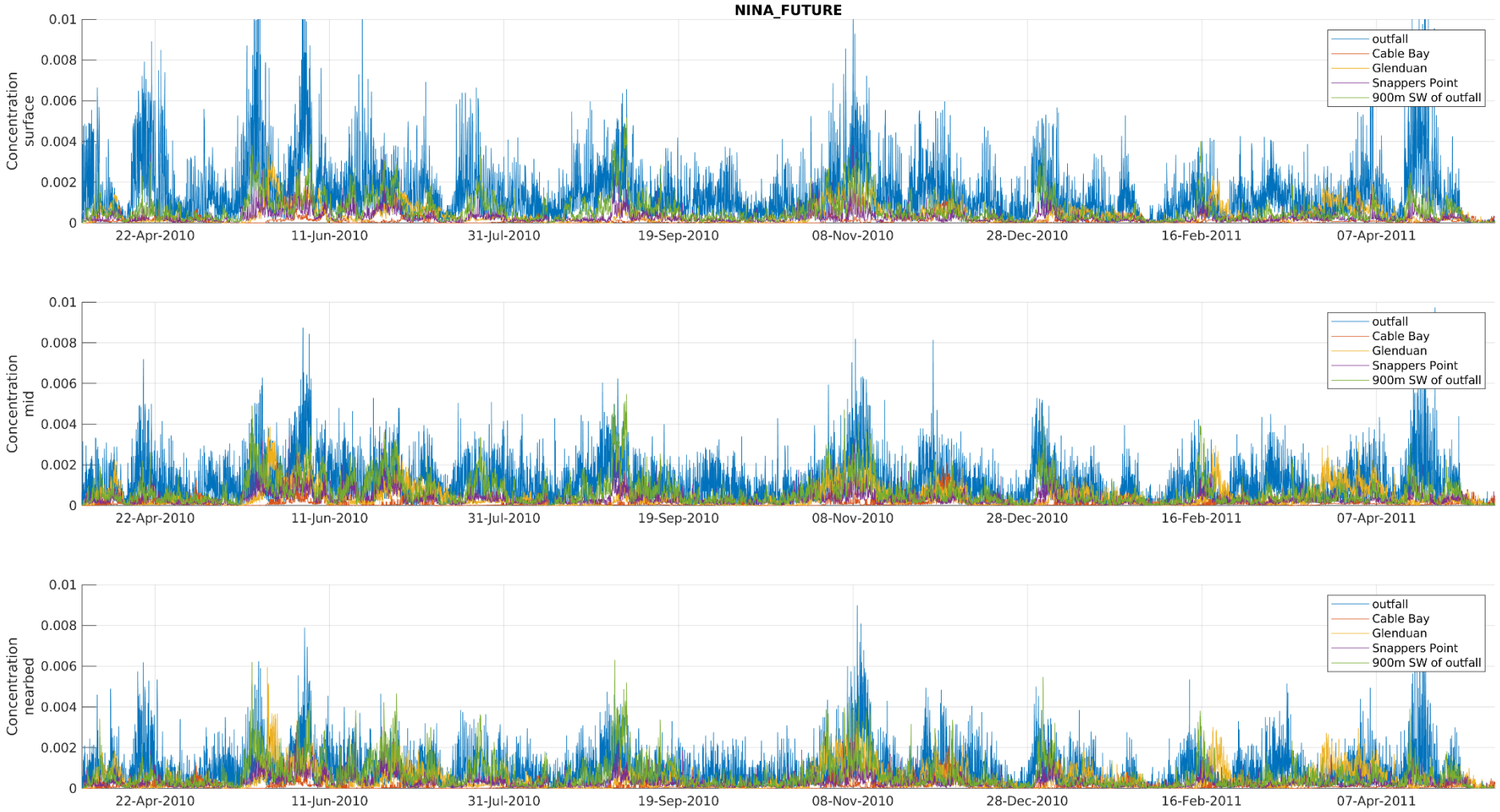
NINA_FUTURE
Concentration surface
Concentration mid
Concentration nearbed
0.01
0.008
0.006
0.004
0.002
0
22-Apr-2010
11-Jun-2010
31-Jul-2010
19-Sep-2010
08-Nov-2010
28-Dec-2010
16-Feb-2011
07-Apr-2011
outfall
Cable Bay
Glenduan
Snappers Point
900m SW of outfall

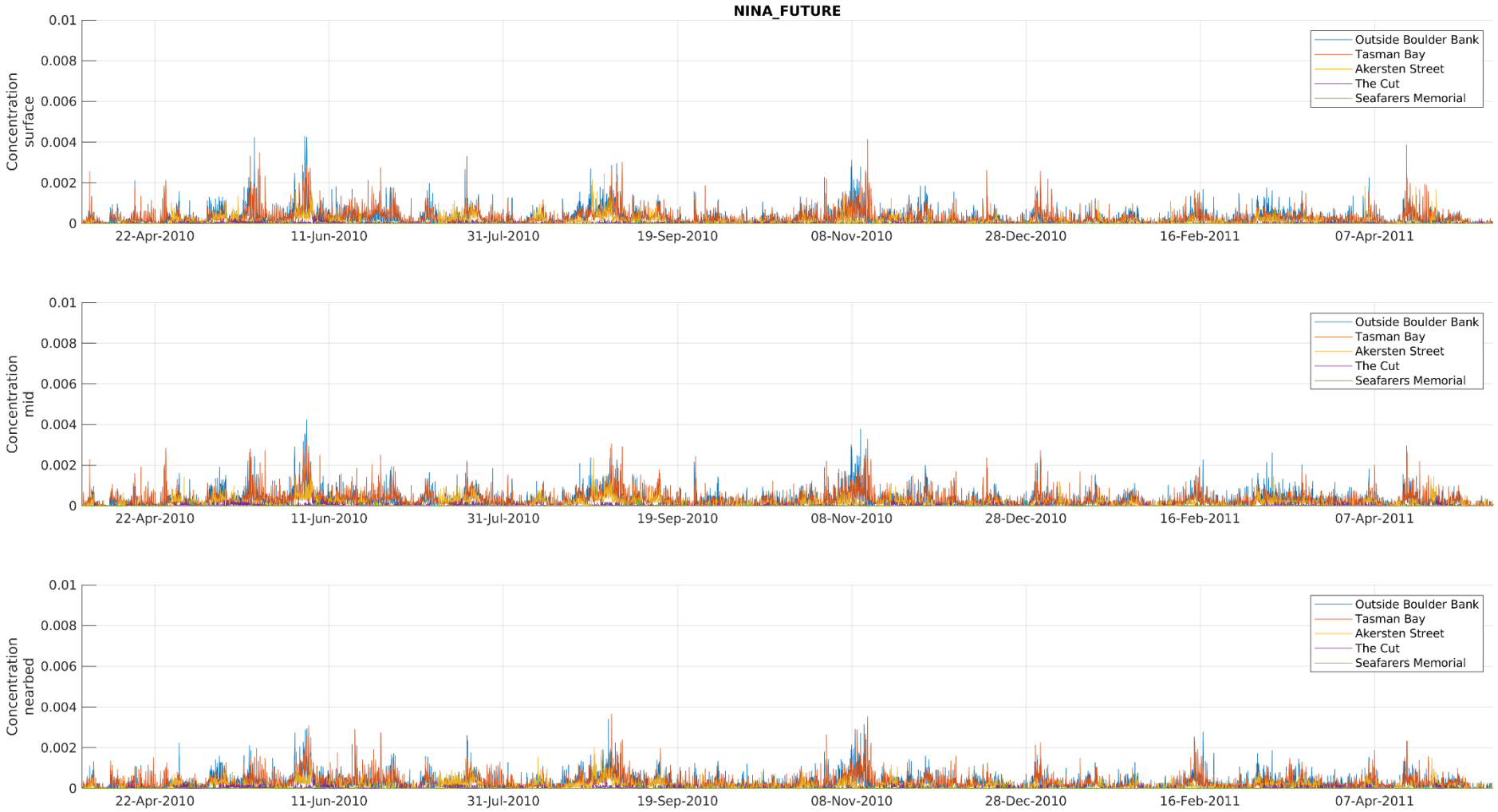
NINA_FUTURE
Concentration surface
Concentration mid
Concentration nearbed
0.01
0.008
0.006
0.004
0.002
0
22-Apr-2010
11-Jun-2010
31-Jul-2010
19-Sep-2010
08-Nov-2010
28-Dec-2010
16-Feb-2011
07-Apr-2011
Outside Boulder Bank
Tasman Bay
Akersten Street
The Cut
Seafarers Memorial

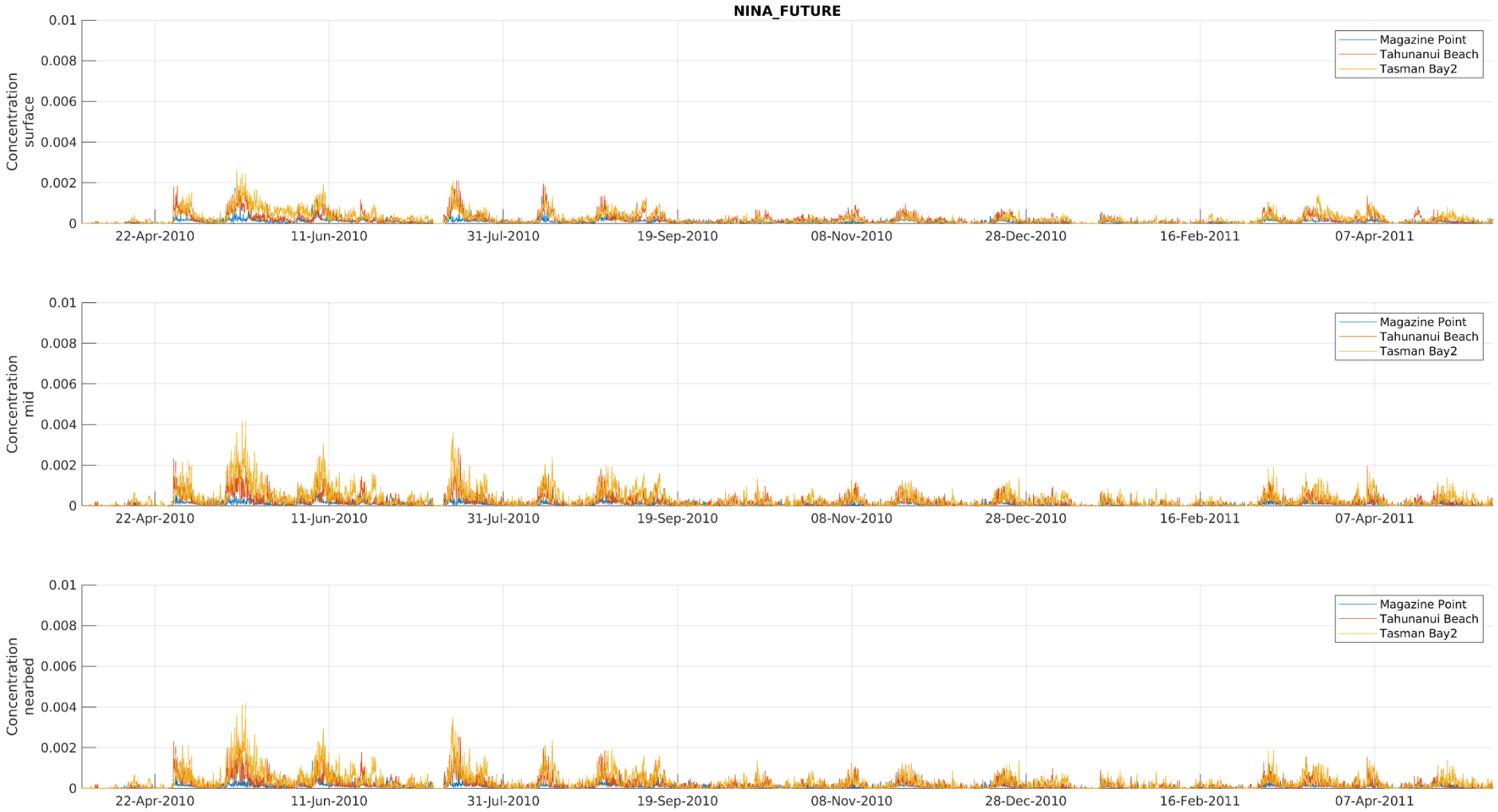

*Figure 3-12 Timeseries of contaminant concentration at sites (Figure 2-9), in surface, mid-water and nearbed levels, for **La Niña** annual period and **future** discharge flows (**no inactivation**). The presented concentrations assume an initial undiluted concentration at the outfall of 1g.m^{-3}.*

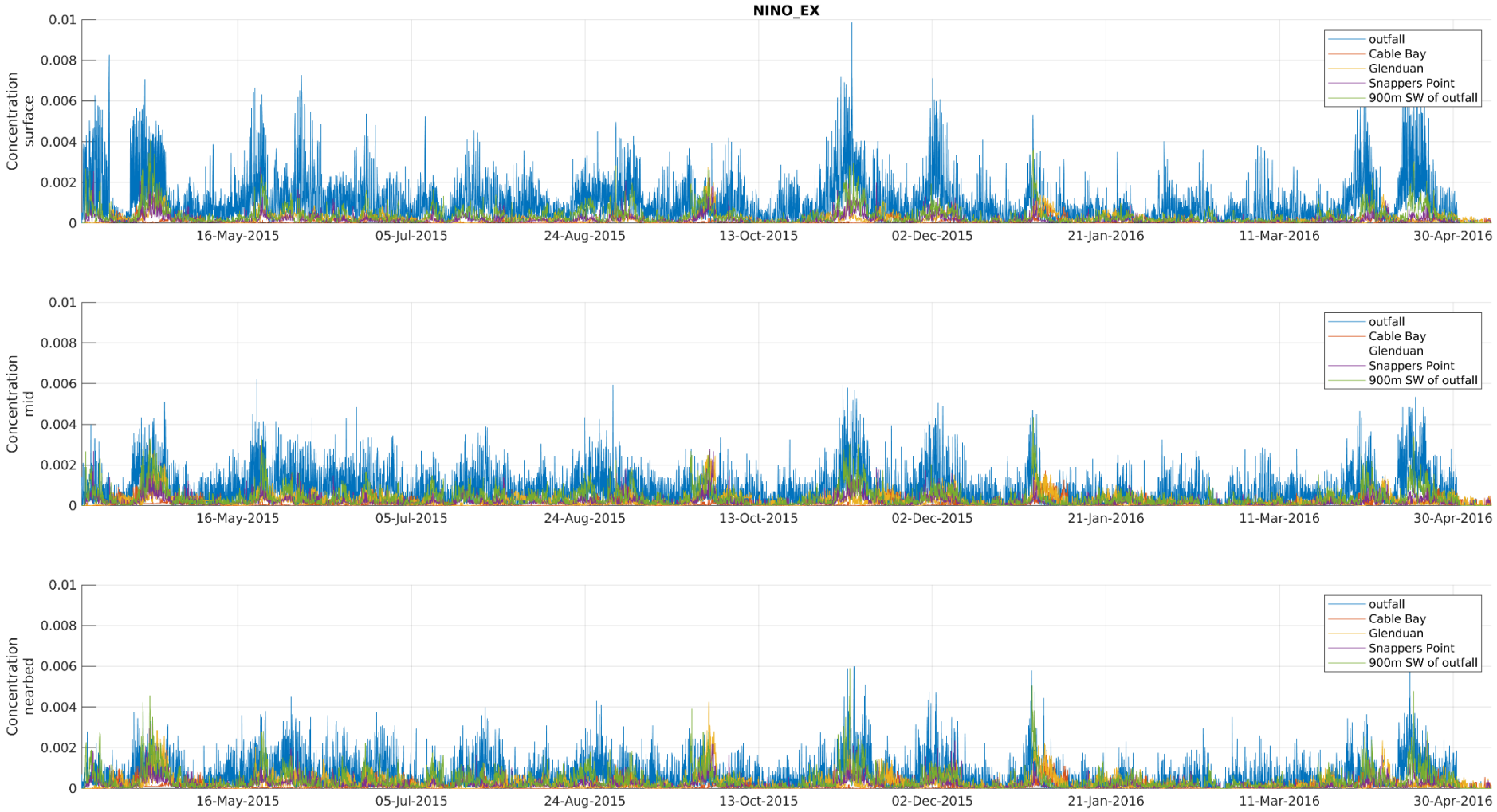
NINO_EX
Concentration surface
Concentration mid
Concentration nearbed
0.01
0.008
0.006
0.004
0.002
0
16-May-2015
05-Jul-2015
24-Aug-2015
13-Oct-2015
02-Dec-2015
21-Jan-2016
11-Mar-2016
30-Apr-2016
outfall
Cable Bay
Glenduan
Snappers Point
900m SW of outfall

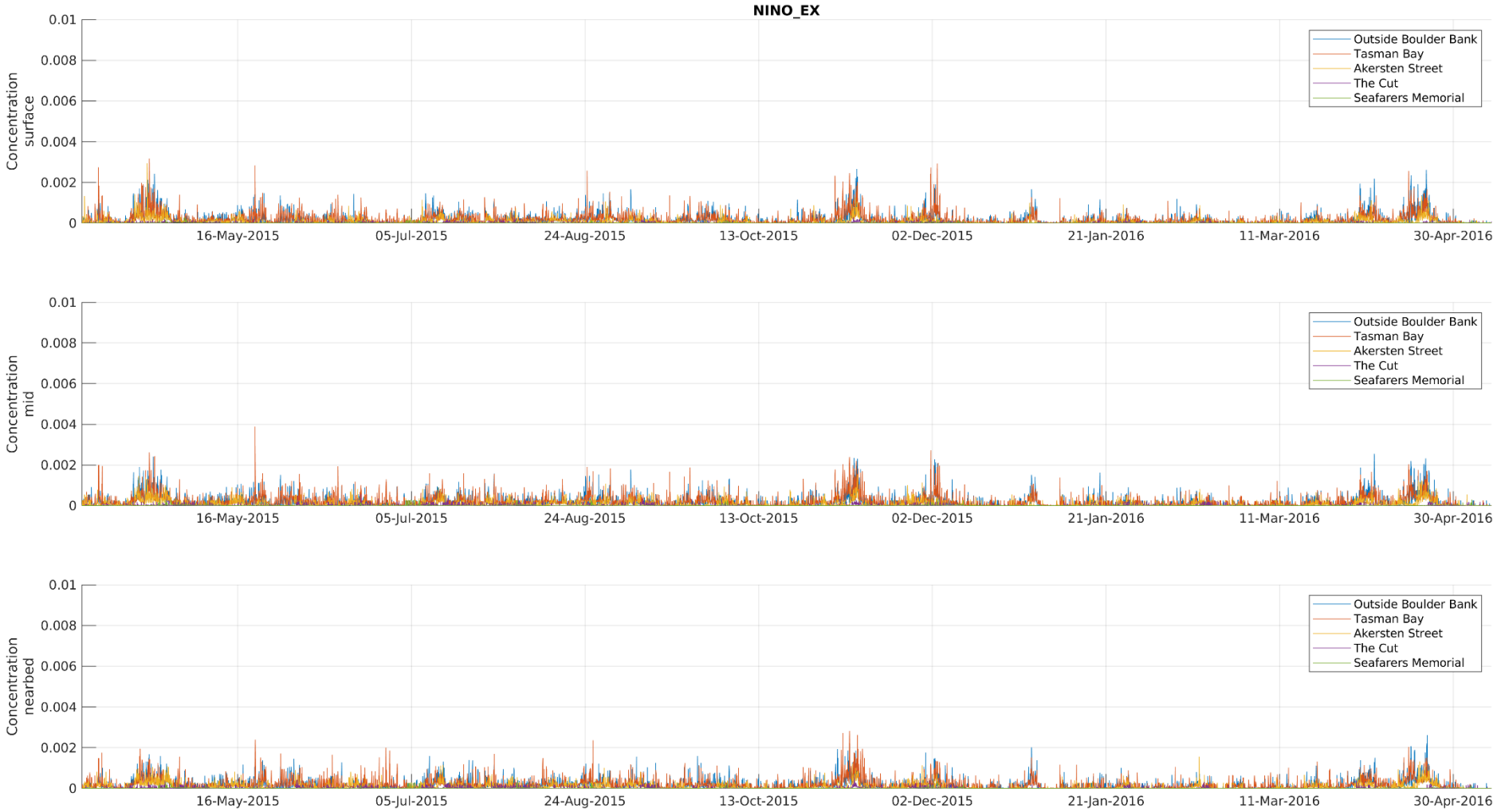
NINO_EX
Concentration surface
Concentration mid
Concentration nearbed
0.01
0.008
0.006
0.004
0.002
0
16-May-2015
05-Jul-2015
24-Aug-2015
13-Oct-2015
02-Dec-2015
21-Jan-2016
11-Mar-2016
30-Apr-2016
Outside Boulder Bank
Tasman Bay
Akersten Street
The Cut
Seafarers Memorial

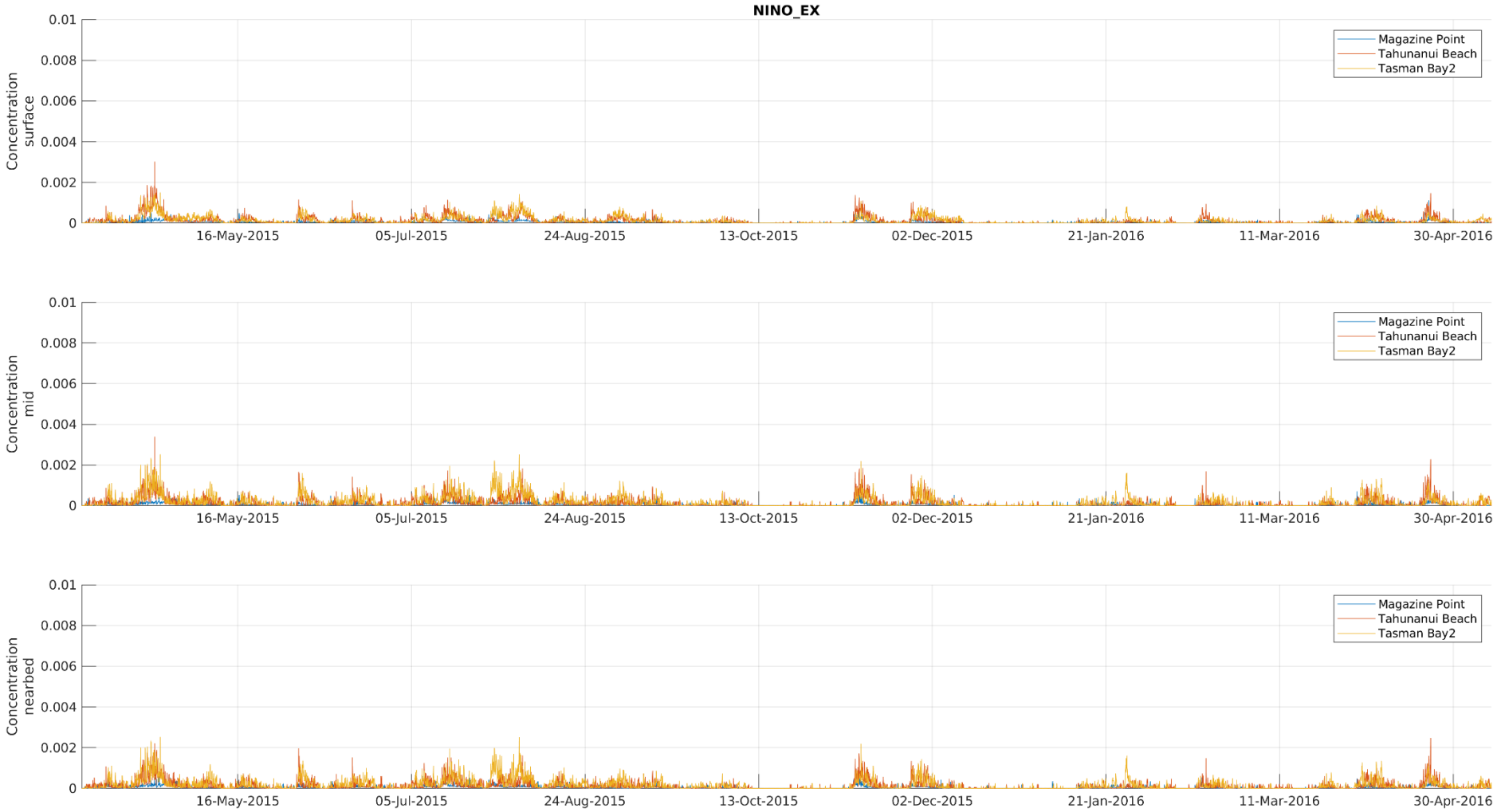

*Figure 3-13 Timeseries of contaminant concentration at sites (Figure 2-9), in surface, mid-water and nearbed levels, for **El Niño** annual period and **existing** discharge flows (**no inactivation**). The presented concentrations assume an initial undiluted concentration at the outfall of 1g.m^{-3}.*

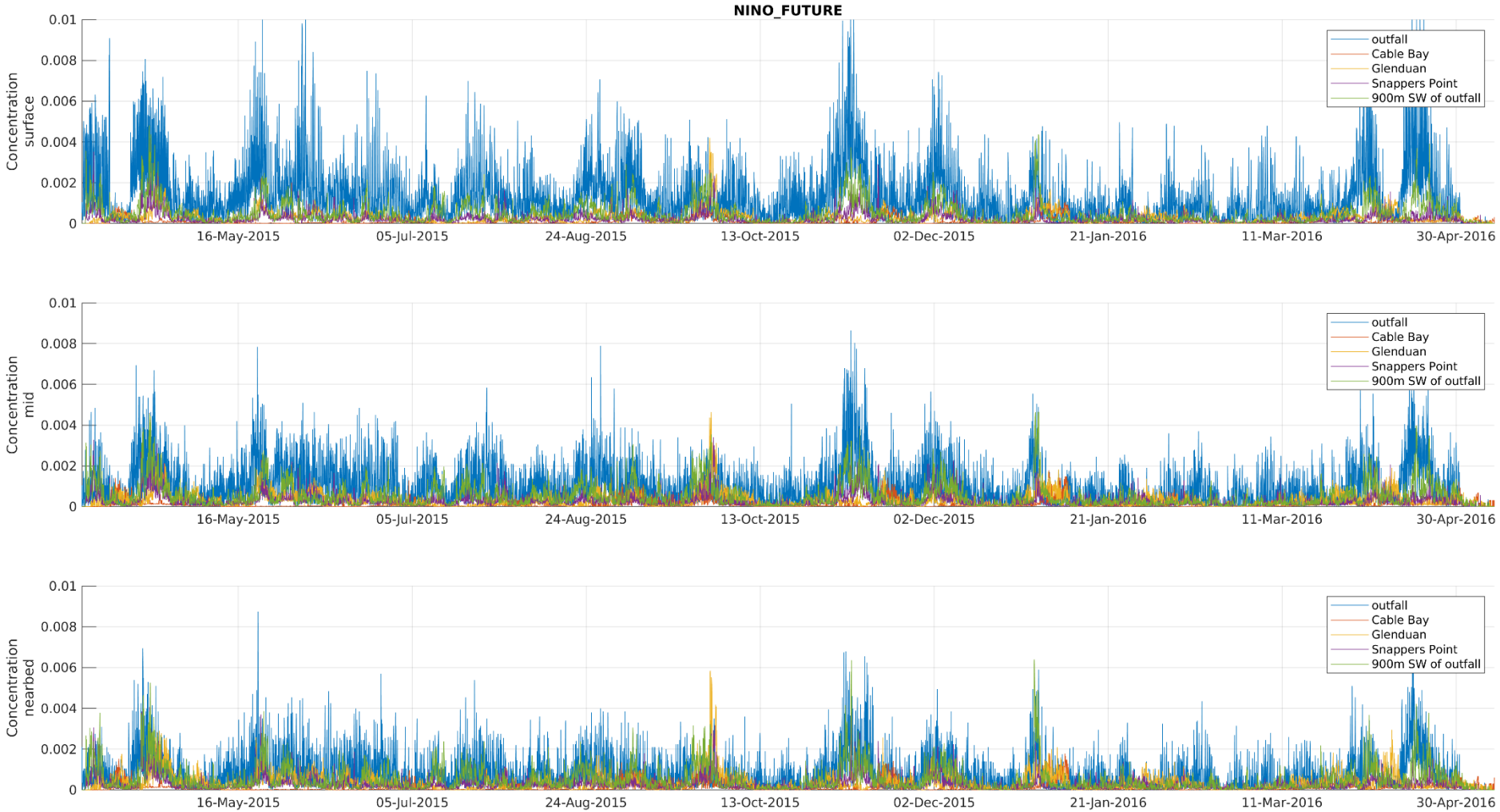
NINO_FUTURE
Concentration surface
Concentration mid
Concentration nearbed
0.01
0.008
0.006
0.004
0.002
0
16-May-2015
05-Jul-2015
24-Aug-2015
13-Oct-2015
02-Dec-2015
21-Jan-2016
11-Mar-2016
30-Apr-2016
outfall
Cable Bay
Glenduan
Snappers Point
900m SW of outfall

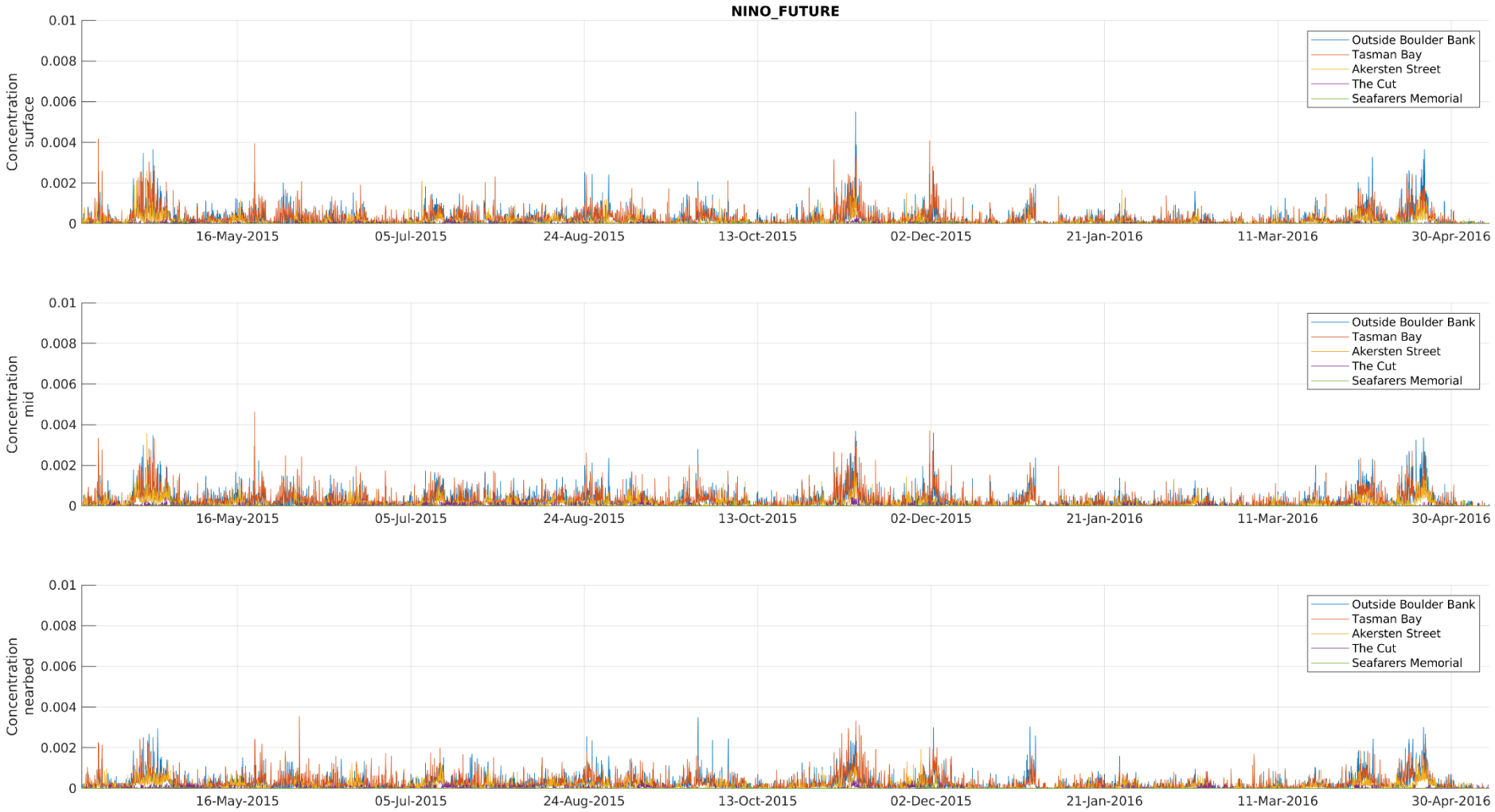
NINO_FUTURE
Concentration surface
Concentration mid
Concentration nearbed
0.01
0.008
0.006
0.004
0.002
0
16-May-2015
05-Jul-2015
24-Aug-2015
13-Oct-2015
02-Dec-2015
21-Jan-2016
11-Mar-2016
30-Apr-2016
Outside Boulder Bank
Tasman Bay
Akersten Street
The Cut
Seafarers Memorial

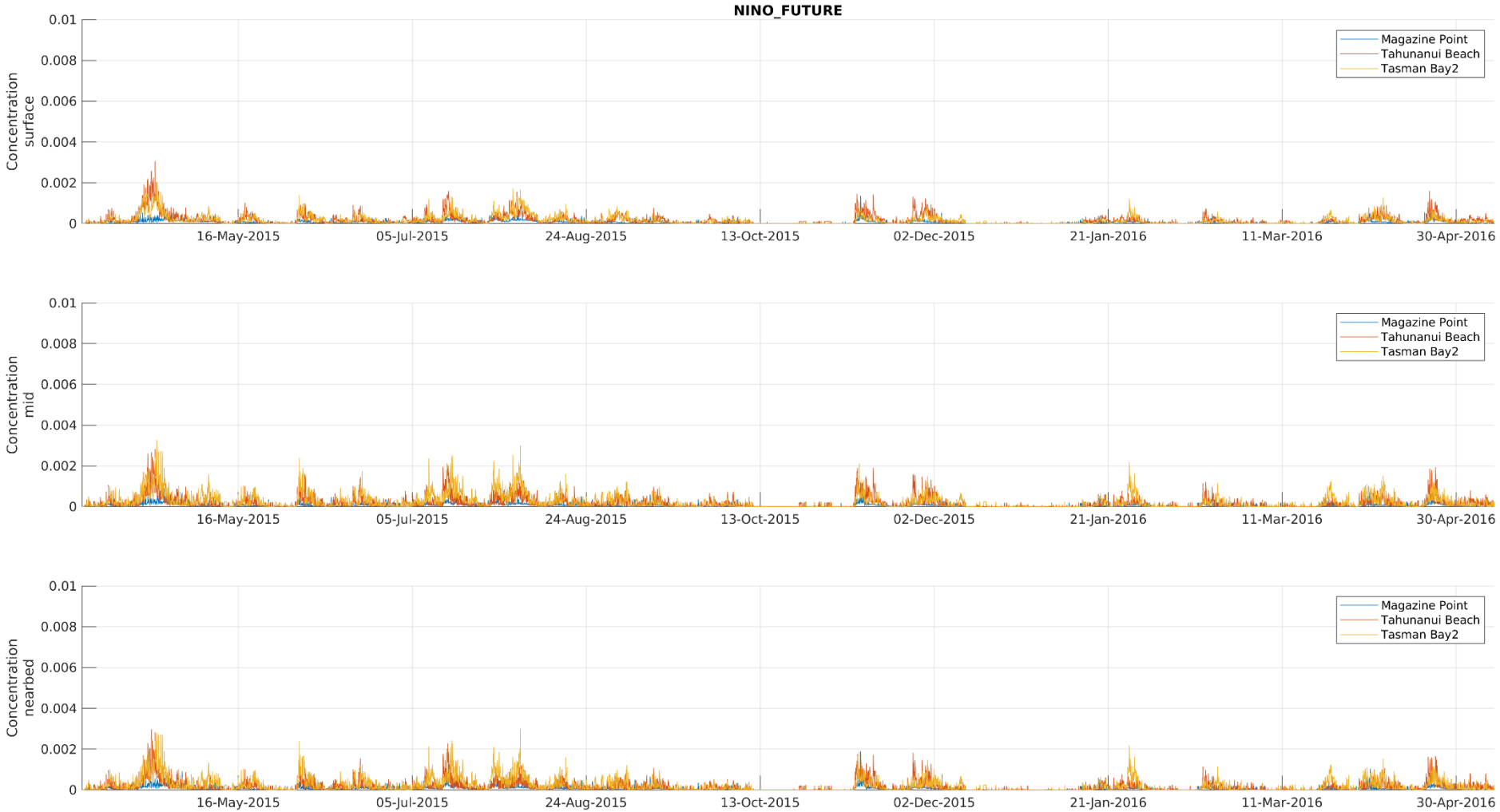

*Figure 3-14 Timeseries of contaminant concentration at sites (Figure 2-9), in surface, mid-water and nearbed levels, for **El Niño** annual period and **future** discharge flows (**no inactivation**). The presented concentrations assume an initial undiluted concentration at the outfall of 1g.m^{-3}.*

3.3. Additional analysis on the worst-case dilution characteristics in the current mixing zone

Additional analysis of model results was undertaken to supplement the original study, notably to quantify the existing dilution characteristics at the edges of the current mixing zone. The results are summarized in a technical note that addresses 3 items :

1) Assess few sites along the main plume axis to get a representative worst-case site (i.e., least dilution at the water surface):

2) 'Worst case' for the edges of current mixing zone and confirmation at what height in the water column that this occurs. The dilutions modelled at the edge of the mixing zone can then be used to determine an end of pipe discharge standard.

3) Assess near-field dilution with a new nominal modern diffuser design.

The technical note is included in Appendix B.

4.Summary

Nelson City Council (NCC) is interested in understanding the dilution and discharge characteristics of contaminant discharged from the Nelson North Wastewater Treatment Plant (NWWTP), and how the dilution characteristics may affect nearby beaches.

In order to quantify the hydrodynamics of the Tasman Bay, a calibrated and validated finite element model of the environs has been used. For this project, the model grid has been extended to cover a larger area around the outlet and resolution has been optimised to ensure the salient hydrodynamic processes are accurately captured. The hydrodynamic model was further validated using measured current velocity and water level data collected near to the discharge location. At the diffuser location the current direction pattern is bi-directional (southwest-northeast) and are aligned with the shoreline with typical velocities of the order 0.1-0.3 m/s.

A range of simulations were undertaken using CORMIX in order to estimate the near field plume characteristics for current year (2021) and predicted (2059) discharges. Results show that the dilution factor at the edge of the near field varies from 220.5 to 2871.4. Dilution tends to be higher in faster ambient current velocities although variations to this trend can occur depending on the ambient currents compared to the discharge velocity (i.e., the velocity the discharge exit the pipe), which depends on the flow rate simulated (i.e., p10, p50 and p90). In all scenarios, plume is wider in near stagnant water and extends downstream (flow direction) while reducing in extent in the across the flow direction under faster current flow. Plume does not contact the shoreline within the near-field zone for the conditions simulated in this study. The time when the plume transitions from near field to far field ranges from 3 minutes (p90, 0.4 m/s) to 77.8 minutes (1.3 hour, p10, 0.4 m/s).

The nearfield plume was included in the far-field model by releasing particles within time varying triangular footprints, describing the nearfield range NFR, and running 1 year-long simulations of wastewater discharges from the outfall location, within two contrasting historical contexts El Niño/La Niña episodes. The far-field dispersion footprints are elongated in the southwest-northeast axis which is driven by the local hydrodynamics. Dispersion patterns are very similar for La Niña and El Niño periods. The 1/5000 dilution contour footprint during La Niña year is slightly wider to the northeast of the outfall, and it also extends further south relative to the El Niño scenario. The increase of discharge flows (factor 1.3) due to the projected population increase results in similar footprint shapes but with larger spatial excursions.

The inclusion of contaminant deactivation has a significant impact on the spatial extents of the plume footprints. Maximum excursions of the 1/5000 dilution are of 2-3 km from outfall assuming a virus T90= 2 days, while it is ~ 7-8 km for a longer T90 = 32 days.

Timeseries of contaminant concentration were extracted at several sites throughout the study area to provide a basis for further assessment such as QMRA (Quantitative Microbial Risk Assessment).

5.References

Batchelor, G. K. (1952). Diffusion in a field of homogeneous turbulence. II. The relative motion of particles. *Cambridge Philosophical Society*, *48*, 345–362.

Bellasio, R., Bianconi,R, Mosca, S., & Zannetti, P. (2017). Formulation of the Lagrangian particle model LAPMOD and its evaluation against Kincaid SF6 and SO2 datasets. *Atmospheric Environment*, *163*, 87–98.

Boehm, A. B., Silverman, A. I., Schriewer, A., & Goodwin, K. (2019). Systematic review and meta-analysis of decay rates of waterborne mammalian viruses and coliphages in surface waters. *Water Research*, *164*, 114898. https://doi.org/10.1016/j.watres.2019.114898

Botev, Z. I, Grotowski, J. F, & Kroese, D.P. (2010). Kernel density estimation via diffusion. *Annals of Statistics*, *38*(5), 2916–2957.

Dagestad K.F, Röhrs J., Breivik O., & Ådlandsvik B. (2018). OpenDrift v1.0: A generic framework for trajectory modelling. *Geoscientfic Model Development*, *11*, 1405–1420.

Egbert, G. D., & Erofeeva, S. Y. (2002). Efficient inverse modelling of barotropic ocean tides. *Journal of Atmospheric and Oceanic Technology*, *19*(2), 183–204.

Eregno, Fasil Ejigu, Tryland, Ingun, Myrmel, Mette, Wennberg, Aina, Oliinyk, Anastasiia, Khatri, Mamata, Heistad, & Arve. (2018). Decay rate of virus and faecal indicator bacteria (FIB) in seawater and the concentration of FIBs in different wastewater systems. *Microbial Risk Analysis*, *8*, 14-21. https://doi.org/10.1016/j.mran.2018.01.001.

List, E., Gartrell, G., & Winant, C. (1990). Diffusion and dispersion in coastal waters. *Journal of Hydraulic Engineering., 116(10)*, 1158–1179.

Mellor, G. L. (1998). A Three Dimensional, Primitive Equation, Numerical Ocean Model (Users Guide). *Available on the Princeton Ocean Model Web Site:< Http://Www. Aos. Princeton. Edu/WWWPUBLIC/Htdocs. Pom*.

MetOcean Solutions. (2020). *Morphological model calibration* (v0.4).

MetOcean Solutions Ltd. (2017). *Bell Island discharge and dilution modelling* (P0332).

Okubo. (1974). Some speculations on oceanic diffusion diagrams. *Rapports et Procès-Verbaux Des Reunions Du Conseil Permanent International Pour l'Exploration de La Mer*.

Okubo, A. (1971). Oceanic diffusion diagrams. *Deep-Sea Research*, *18*, 789–802.

Richardson, L.F. (1962). Atmospheric diffusion shown on a distance neighbour graph. *Proc. R. Soc. London, Ser A,*(110), 709-737.

Röhrs et al. (2019). The effect of vertical mixing on the horizontal drift of oil spills. *Ocean Science*, *14*, 1581–1601.

Saha, S., Moorthi, S., Pan, H.-L., Wu, X., Wang, J., Nadiga, S., Tripp, P., Kistler, R., Woollen, J., Behringer, D., Liu, H., Stokes, D., Grumbine, R., Gayno, G., Wang, J., Hou, Y.-T., Chuang, H.-Y., Juang, H.-M. H., Sela, J., … Goldberg, M. (2010). The NCEP Climate Forecast System Reanalysis. *Bulletin of the American Meteorological Society*, *91*(8), 1015–1057. https://doi.org/10.1175/2010BAMS3001.1

Silverman, B. W. (1986). *Density Estimation for Statistics and Data Analysis* (Chapman and Hall Ltd.).

Stommel, H. (1949). Horizontal diffusion due to oceanic turbulence. *Journal of Marine Research*, *8*, 199–225.

Vitali, L., Monforti, F., Bellasio, R., Bianconi, R., Sachero, V., Mosca, S., & Zanini, G. (2006). Validation of a Lagrangian dispersion model implementing different kernel methods for density reconstruction. *Atmospheric Environment*, *40*, 8020–8033.

Zhang, Y. L., & Baptista, A. M. (2008). A semi-implicit Eulerian-Lagrangian finite element model for cross-scale ocean circulation. *Ocean Modelling*, *21*, 71–96.

Appendix A: CORMIX hydrodynamic classification

Flow Class MUIH

The discharge configuration is hydrodynamically "stable", that is the discharge strength (measured by its momentum flux) is weak in relation to the layer depth and in relation to the stabilizing effect of the discharge buoyancy (measured by its buoyancy flux). The buoyancy effect is very strong in the present case.

The following flow zones exist:

1) Weakly deflected plane jet in crossflow: The flow issuing from the equivalent slot diffuser is initially dominated by the wastewater momentum (jet-like) and is weakly deflected by the ambient current.
2) Strongly deflected plane plume: After some distance the discharge buoyancy becomes the dominating factor (plume-like). The plume is deflected by the effect of the strong ambient current.
3) Surface layer approach: The bent-over submerged jet/plume approaches the terminal level. Within a short distance the concentration distribution becomes relatively uniform across the plume width and thickness. or
3) Density current along diffuser line: The plume develops along the diffuser line due to continuous inflow of mixed buoyant water. The plume spreads laterally along the layer boundary (surface or pycnocline) which it is being advected by the ambient current. The mixing rate is relatively small. This zone extends from beginning to end of the diffuser line.

The zones listed above constitute the NEAR-FIELD REGION in which strong initial mixing takes place. ***

4) Buoyant spreading at layer boundary: The plume spreads laterally along the layer boundary (surface or pycnocline) while it is being advected by the ambient current. The plume thickness may decrease during this phase. The mixing rate is relatively small. The plume may interact with a nearby bank or shoreline.
5) Passive ambient mixing: After some distance the background turbulence in the ambient shear flow becomes the dominating mixing mechanism. The passive plume is growing in depth and in width. The plume may interact with the channel bottom and/or banks.

Flow Class MUIV

The discharge configuration is hydrodynamically "stable", that is the discharge strength (measured by its momentum flux) is weak in relation to the layer depth and in relation to the stabilizing effect of the discharge buoyancy (measured by its buoyancy flux). The buoyancy effect is very strong in the present case.

The following flow zones exist:

1) Weakly deflected plane jet in crossflow: The flow issuing from the equivalent slot diffuser is initially dominated by the wastewater momentum (jet-like) and is weakly deflected by the ambient current.
2) Weakly deflected plane plume: After some distance the discharge buoyancy becomes the dominating factor (plume-like). The plume deflection by the ambient current is still weak.
3) Layer boundary impingement / upstream spreading: The weakly bent jet/plume impinges on the layer boundary (water surface or pycnocline) at a near-vertical angle. After impingement the flow spreads in all directions (more or less radially) along the layer boundary. In particular, the flow spreads some distance upstream against the ambient flow, and laterally across the ambient flow. This spreading is dominated by the strong buoyancy of the discharge.

*** The zones listed above constitute the NEAR-FIELD REGION in which strong initial mixing takes place. ***

4) Buoyant spreading at layer boundary: The plume spreads laterally along the layer boundary (surface or pycnocline) while it is being advected by the ambient current. The plume thickness may decrease during this phase. The mixing rate is relatively small. The plume may interact with a nearby bank or shoreline.
5) Passive ambient mixing: After some distance the background turbulence in the ambient shear flow becomes the dominating mixing mechanism. The passive plume is growing in depth and in width. The plume may interact with the channel bottom and/or banks.

SPECIAL CASE: If the ambient is stagnant, then advection and diffusion by the ambient flow (zones 4 and 5) cannot be considered. the mixing is limited to the near-field region (zones 1 to 3) and the predictions will be terminated at this stage.

Such stagnant water predictions may be a useful initial mixing indicator for a given site and discharge design. For practical final predictions, however, the advection and diffusion of the ambient flow – no matter how small in magnitude - should be considered.

Flow Class MU8

An alternating multiport diffuser with predominantly perpendicular alignment is discharging into an ambient flow. For this diffuser configuration the net horizontal momentum flux is zero so that no significant diffuser-induced currents are produced in the water body. However, the local effect of the discharge momentum flux is strong in relation to the layer depth and in relation to the stabilizing effect of the discharge buoyancy, so that the discharge configuration is hydrodynamically "unstable".

The following flow zones exist:

1) Alternating perpendicular diffuser with unstable near-field zone: The destabilizing effect of the discharge jets produces an unstable nearfield zone. For stagnant or weak cross-flow conditions, a vertical recirculation zone is being produced leading to mixing over the full layer depth: however, the flow tends to re-stratify outside this zone that extends a few layer depths around the diffuser line. For strong cross-flow, additional destratification and mixing are produced.

or, alternatively, a second possibility exists for strongly buoyant discharges :

1) Near-vertical surface impingement, upstream spreading, vertical mixing, and buoyant restratification: The destabilizing effect of the discharge jets produces an unstable nearfield zone. For stagnant or weak cross-flow conditions, a vertical recirculation zone is being produced leading to mixing over the full layer depth: however, the flow tends to restratify outside this zone that extends a few layer depths around the diffuser line. In particular, upstream spreading will occur due to the strong buoyancy of the discharge.

*** The zones listed above constitute the NEAR-FIELD REGION in which strong initial mixing takes place. ***

2) Buoyant spreading at layer boundary: The plume spreads laterally along the layer boundary (surface or pycnocline) while it is being advected by the ambient current. The plume thickness may decrease during this phase. The mixing rate is relatively small. The plume may interact with a nearby bank or shoreline.

3) Passive ambient mixing: After some distance the background turbulence in the ambient shear flow becomes the dominating mixing mechanism. The passive plume is growing in depth and in width. The plume may interact with the channel bottom and/or banks.

SPECIAL CASE: If the ambient is stagnant, then advection and diffusion by the ambient flow (zones 2 and 3) cannot be considered. The mixing is limited to the near-field region (zone 1) and the predictions will be terminated at this stage.

Appendix B: Technical note on dilution near the outfall

Nelson North Wastewater Treatment Plant (NWWTP) dispersion modelling

Technical note on dilution near the outfall

Report prepared for Nelson City Council

March 2023

MetOcean SOLUTIONS

Document History

Versions

Version	Revision Date	Summary	Reviewed by
0.0	23/03/2023	Draft for internal review	Weppe
0.1	24/03/2023	Draft for client review	Berthot
0.2	28/07/2023	Draft for client review	Weppe/Cussioli

Distribution

Version	Date	Distribution
1.0		

Document ID: P0526

Contents

List of Figures

List of Tables

1.Introduction

This technical note covers an additional scope following the Nelson North Wastewater Treatment Plant dispersion modelling study (MetOcean Solutions, 2022).

The model results from the previous modelling (MetOcean Solutions, 2022) study were re-analysed with a focus on the nearfield plume footprint to address 3 items:

1) Assess few sites along the main plume axis to get a representative worst-case site (i.e. least dilution at the water surface):
2) 'Worst case' for the edges of current mixing zone and confirmation at what height in the water column that this occurs. The dilutions modelled at the edge of the mixing zone can then be used to determine an end of pipe discharge standard.
3) Assess near field dilution with a new nominal modern diffuser design

Note the results are provided for the existing and future El Niño and La Niña scenarios with no contaminant die-off. The same processing approach as used (MetOcean Solutions, 2022) is following to generate the dilutions timeseries.

Consistent with MetOcean Solutions (2022), conservative estimates of contaminant concentrations at sites of interest was obtained, by taking the maximum of predicted concentrations with the kernel or 2D histogram techniques at each timestep.

2.Item 1

The objective of the item is to assess surface dilution at a few sites along the main plume axis to get a representative worst-case site (i.e. least dilution at the water surface).

Surface dilutions were extracted at several sites along the primary plume axis, including the outfall location. Extraction sites are shown in Figure 2-1, and locations are provided in Table 2-1. They include the outfall location and sites located on either side along the axis of the plume, first at 50m from the outfall, then every 100m. Some additional sites were added within areas of relatively elevated concentrations following concentration patterns (i.e. smaller dilutions).

Percentile statistics of the dilutions extracted at all sites are shown in Figure 2-2 to Figure 2-13. For the El Nino scenario, with existing discharge, at the surface level, the lowest dilutions are observed at the outfall site and closest sites to the northeast (N50) and southwest (S50). Dilution levels experienced 1% of the time (P1) are 290, 198, 206 at sites N50, outfall, and S50 respectively. Corresponding median (P50) dilutions (i.e. exceeded 50% of the time) levels are 2109, 1667, 2063. Lower dilutions in the close vicinity of the outfall are expected given the importance of oscillating tides (southwest-northeast axis) in the overall hydrodynamic regime. This results in longer residence time around the release location, and therefore larger concentration/ lower dilutions in that area.

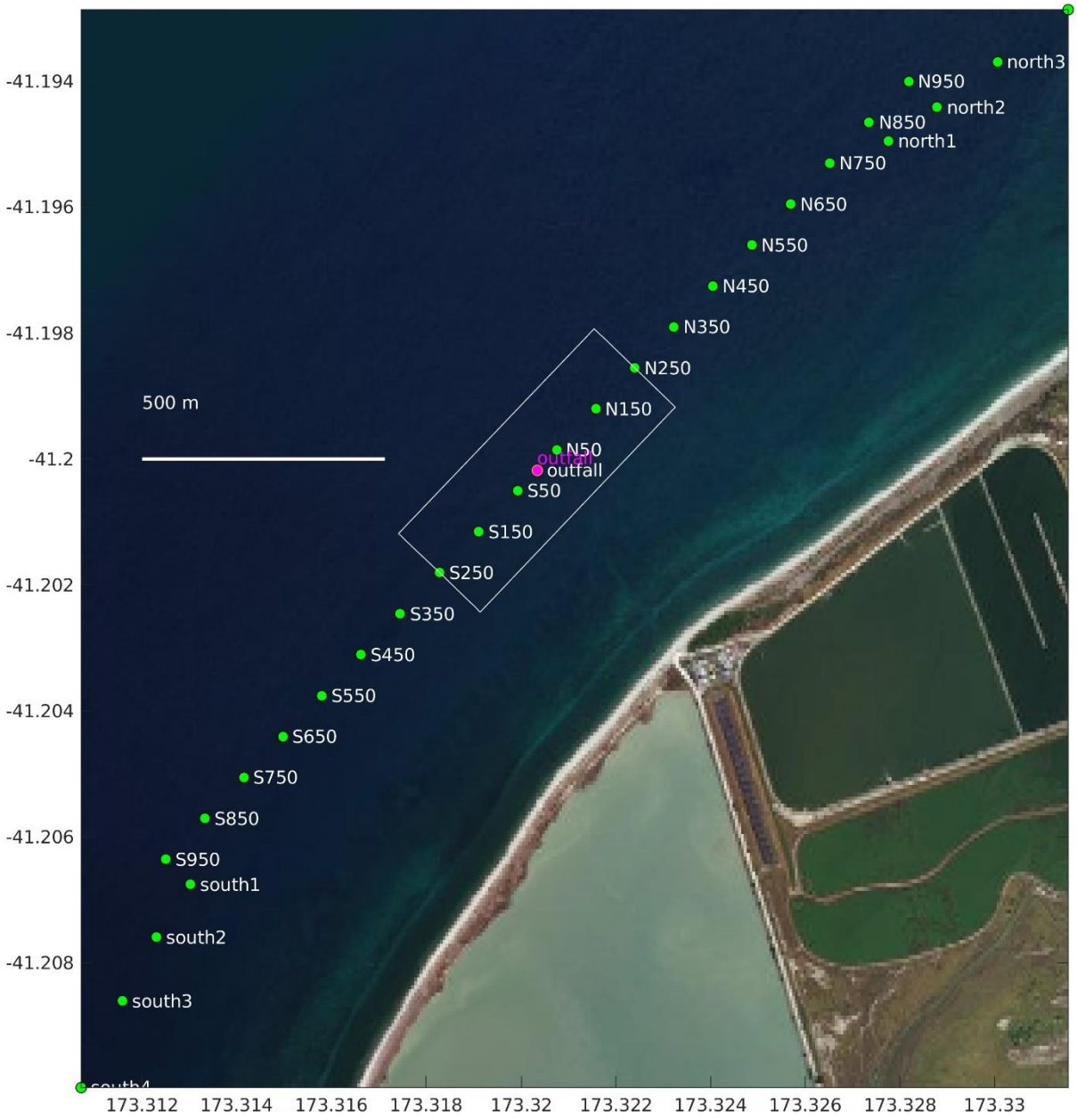

Figure 2-1 Extraction sites along the primary plume axis. They include the outfall location and sites located on either side along the axis of the plume, first at 50m, then every100m.

Table 2-1 Extraction sites along the primary plume axis (WGS84).

Site name	Lon	Lat
'S950'	173.312498	-41.206357
'S850'	173.313323	-41.205707
'S750'	173.314149	-41.205057
'S650'	173.314974	-41.204407
'S550'	173.315800	-41.203756
'S450'	173.316625	-41.203106
'S350'	173.317450	-41.202456
'S250'	173.318276	-41.201806
'S150'	173.319101	-41.201155
'S50'	173.319926	-41.200505
'outfall'	173.320339	-41.200180
'N50'	173.320752	-41.199855
'N150'	173.321577	-41.199205
'N250'	173.322402	-41.198554
'N350'	173.323228	-41.197904
'N450'	173.324053	-41.197254
'N550'	173.324878	-41.196603
'N650'	173.325703	-41.195953
'N750'	173.326528	-41.195303
'N850'	173.327354	-41.194652
'N950'	173.328179	-41.194002
'south1'	173.313013	-41.206758
'south2'	173.312300	-41.207593
'south3'	173.311587	-41.208607
'south4'	173.310715	-41.209979
'north1'	173.327757	-41.194949
'north2'	173.328787	-41.194412
'north3'	173.330056	-41.193697
'north4'	173.331562	-41.192862

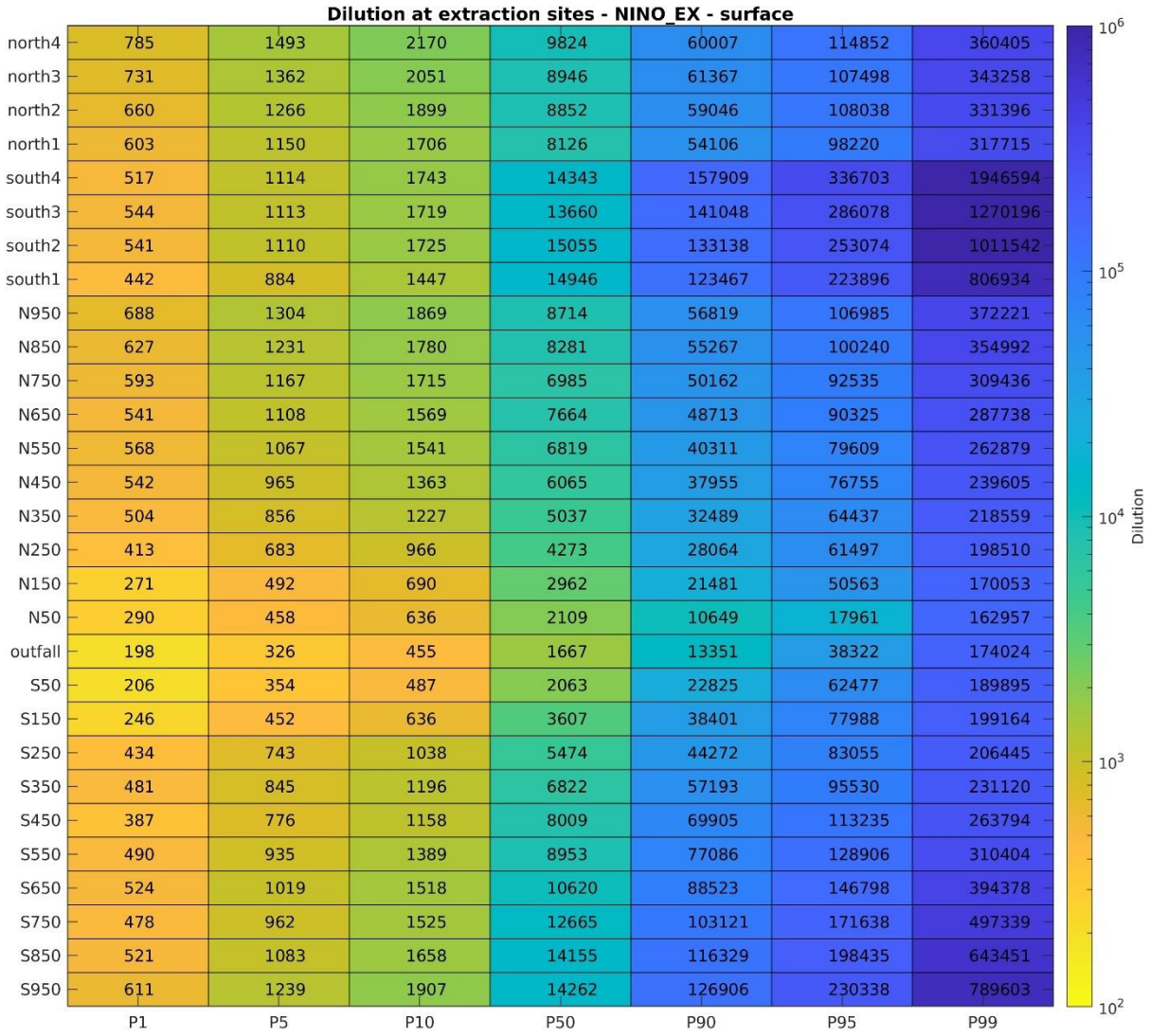

Figure 2-2 Dilution percentile at extraction site shown in Figure 2-1 for the El Niño scenario with existing discharge, at the surface level. Note the colour scale is logarithmic.

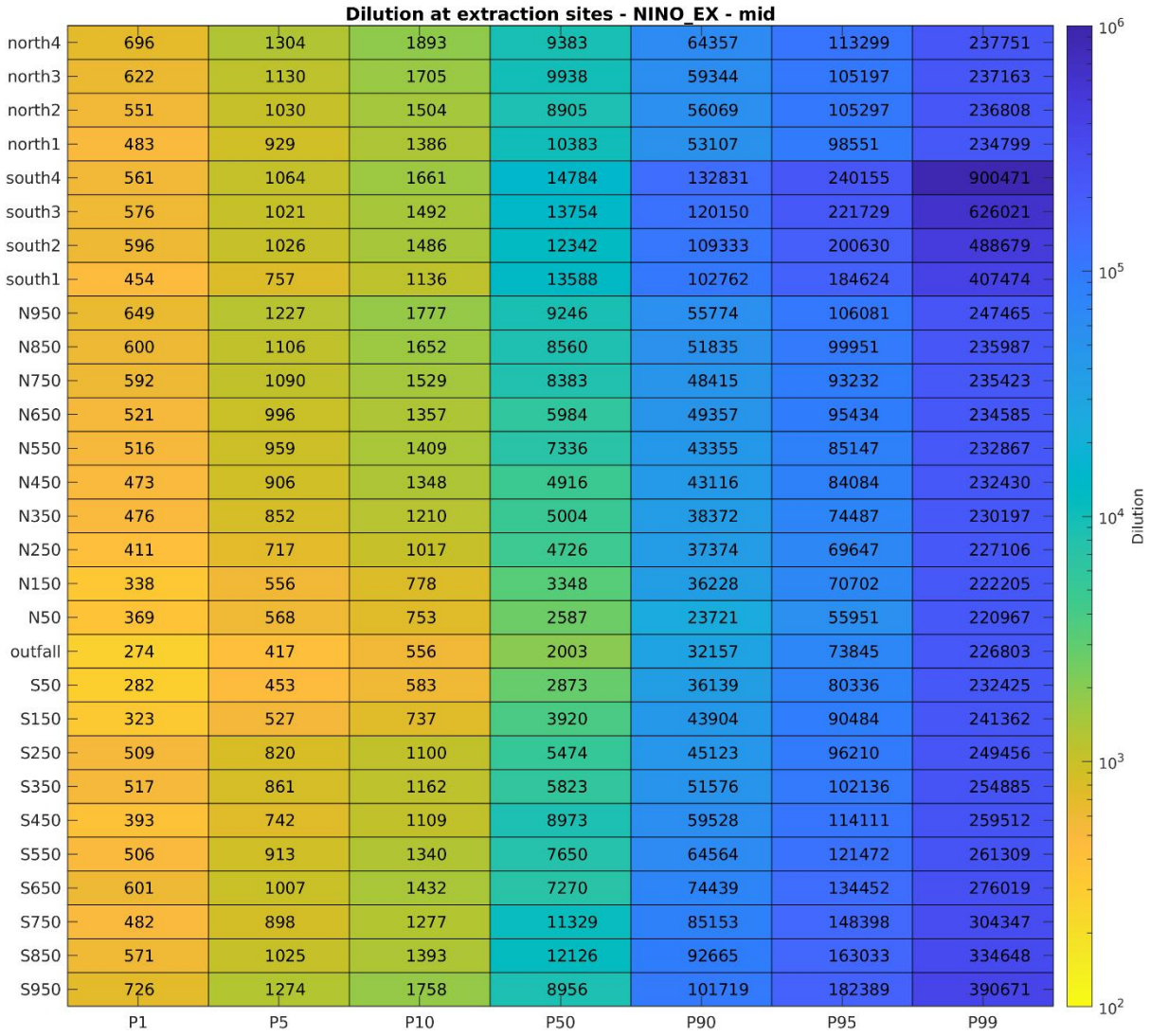

Figure 2-3 Dilution percentile at extraction site shown in Figure 2-1 for the El Niño scenario with existing discharge, at the mid-depth level. Note the colour scale is logarithmic.

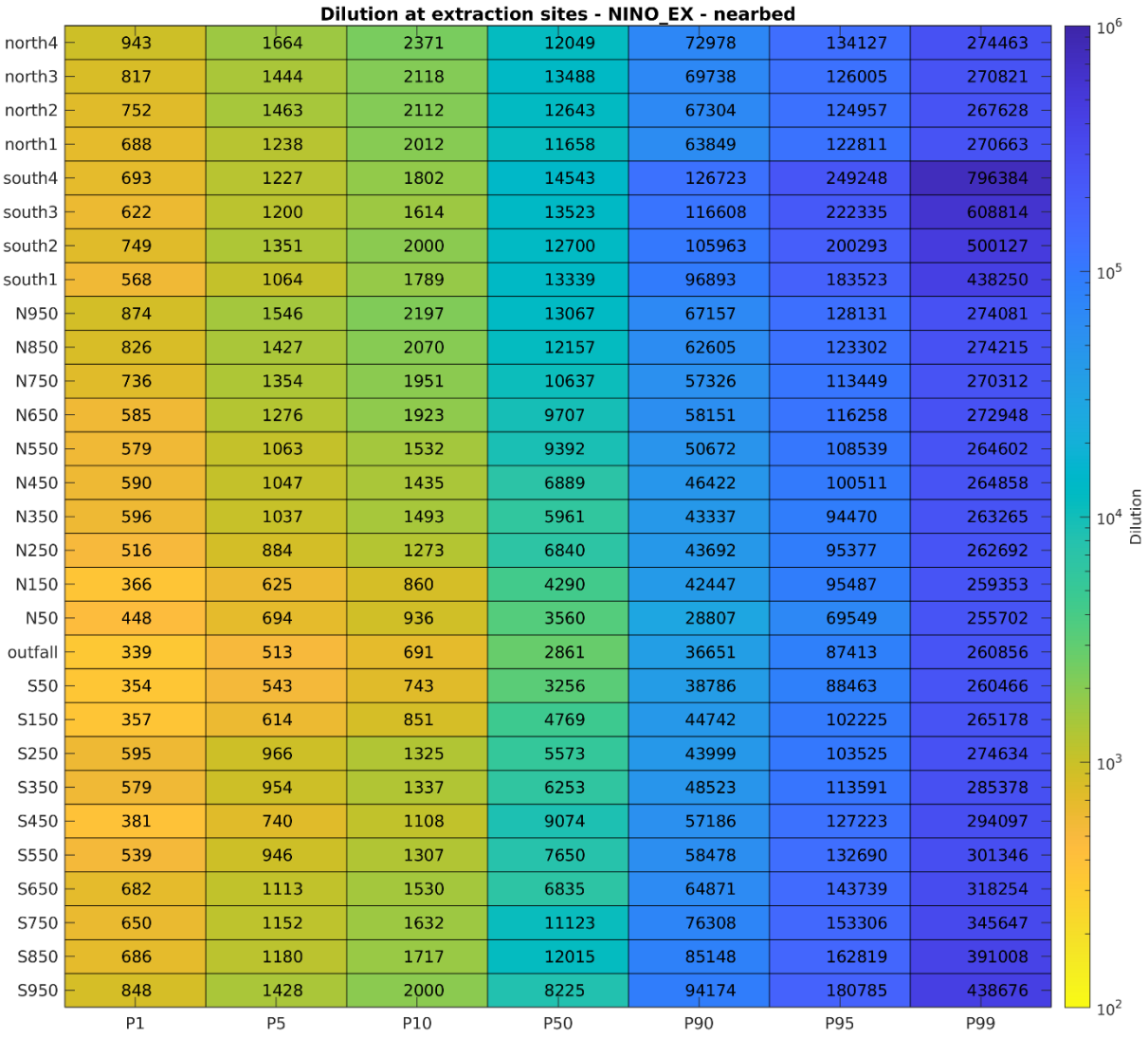

Figure 2-4 Dilution percentile at extraction site shown in Figure 2-1 for the El Niño scenario with existing discharge, at the nearbed level. Note the colour scale is logarithmic.

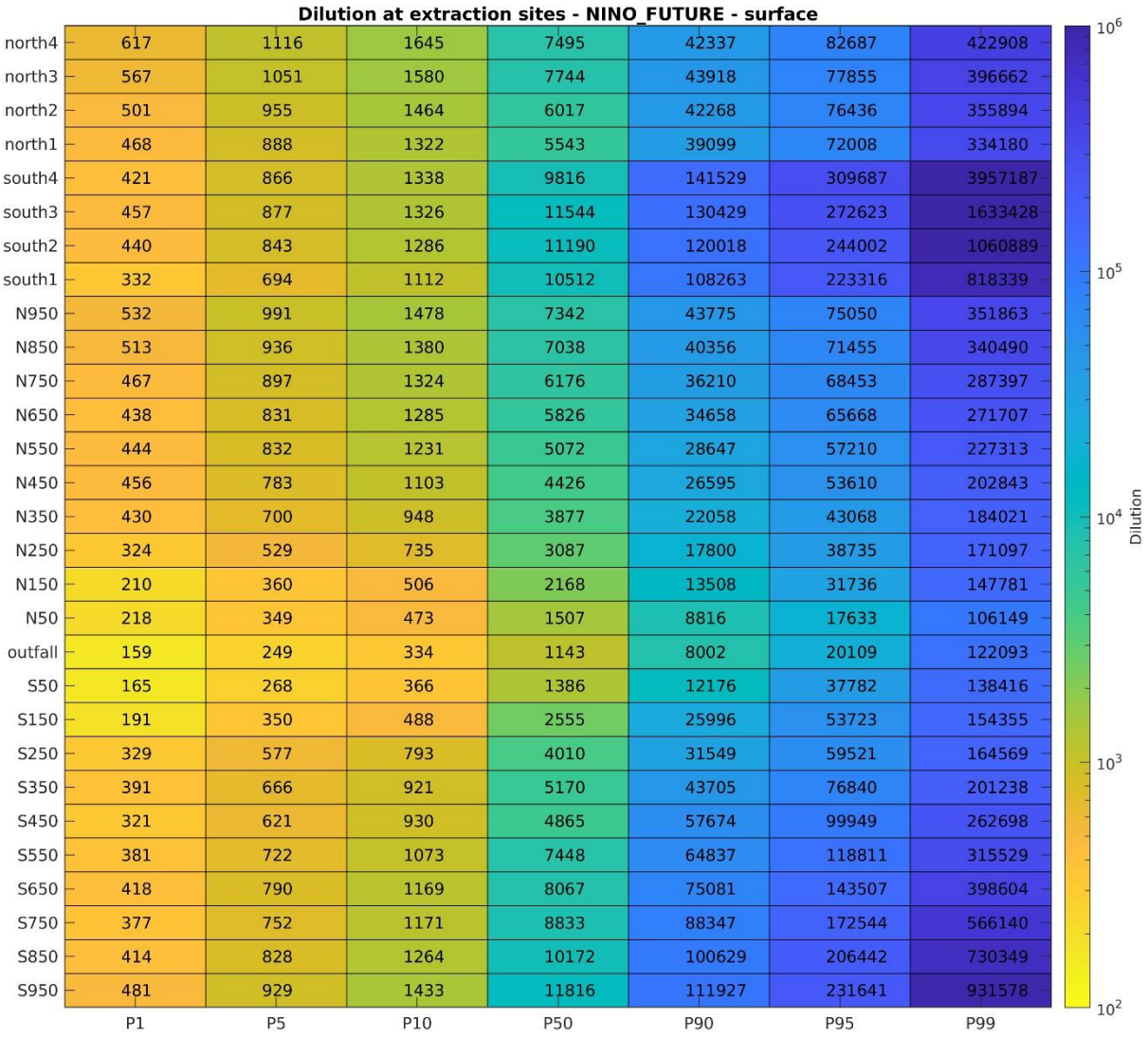

Figure 2-5 Dilution percentile at extraction sites shown in Figure 2-1 for the El Niño scenario with future discharge at the surface level. Note the colour scale is logarithmic.

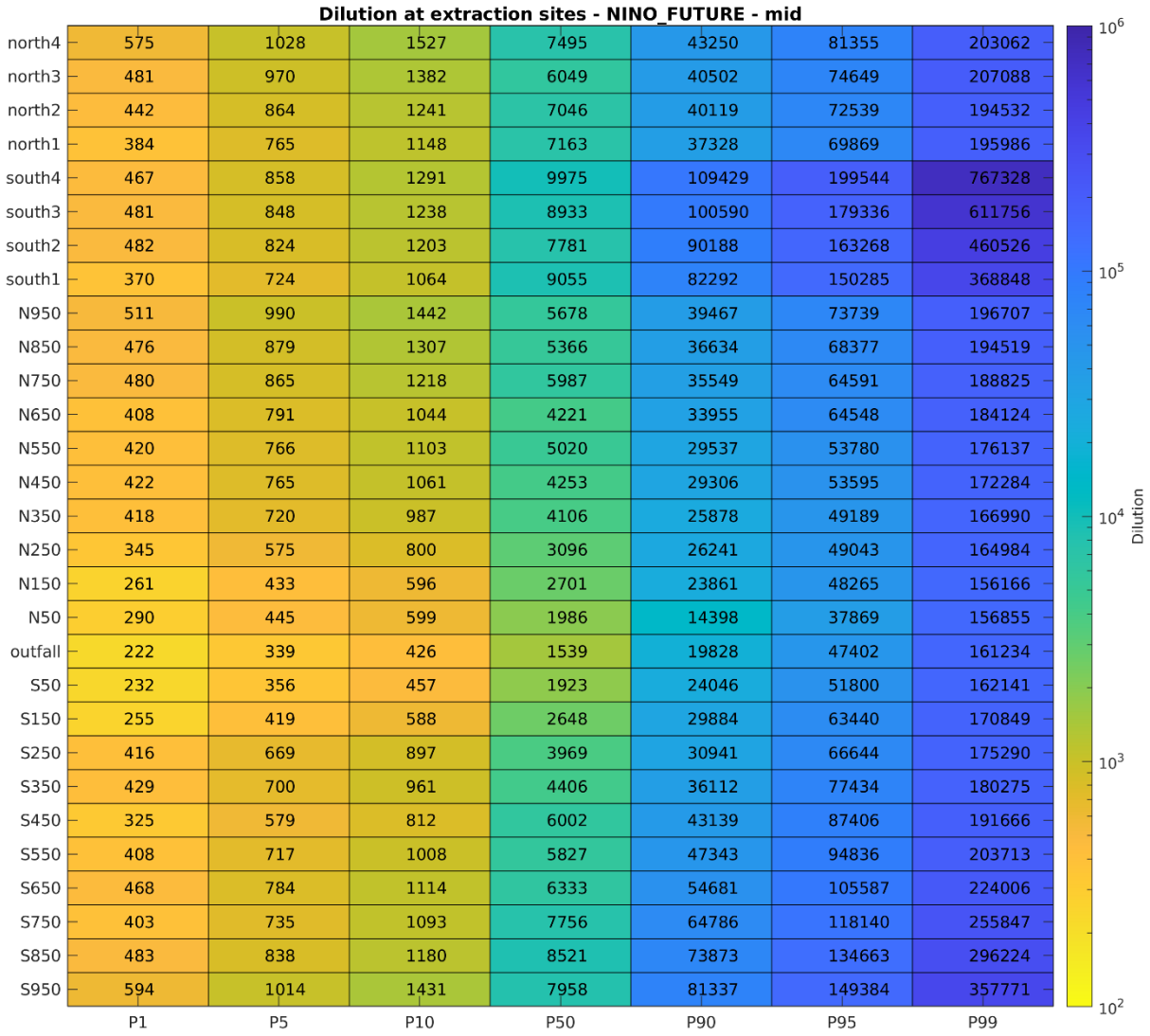

Figure 2-6 Dilution percentile at extraction sites shown in Figure 2-1 for the El Niño scenario with future discharge at the mid-depth level. Note the colour scale is logarithmic.

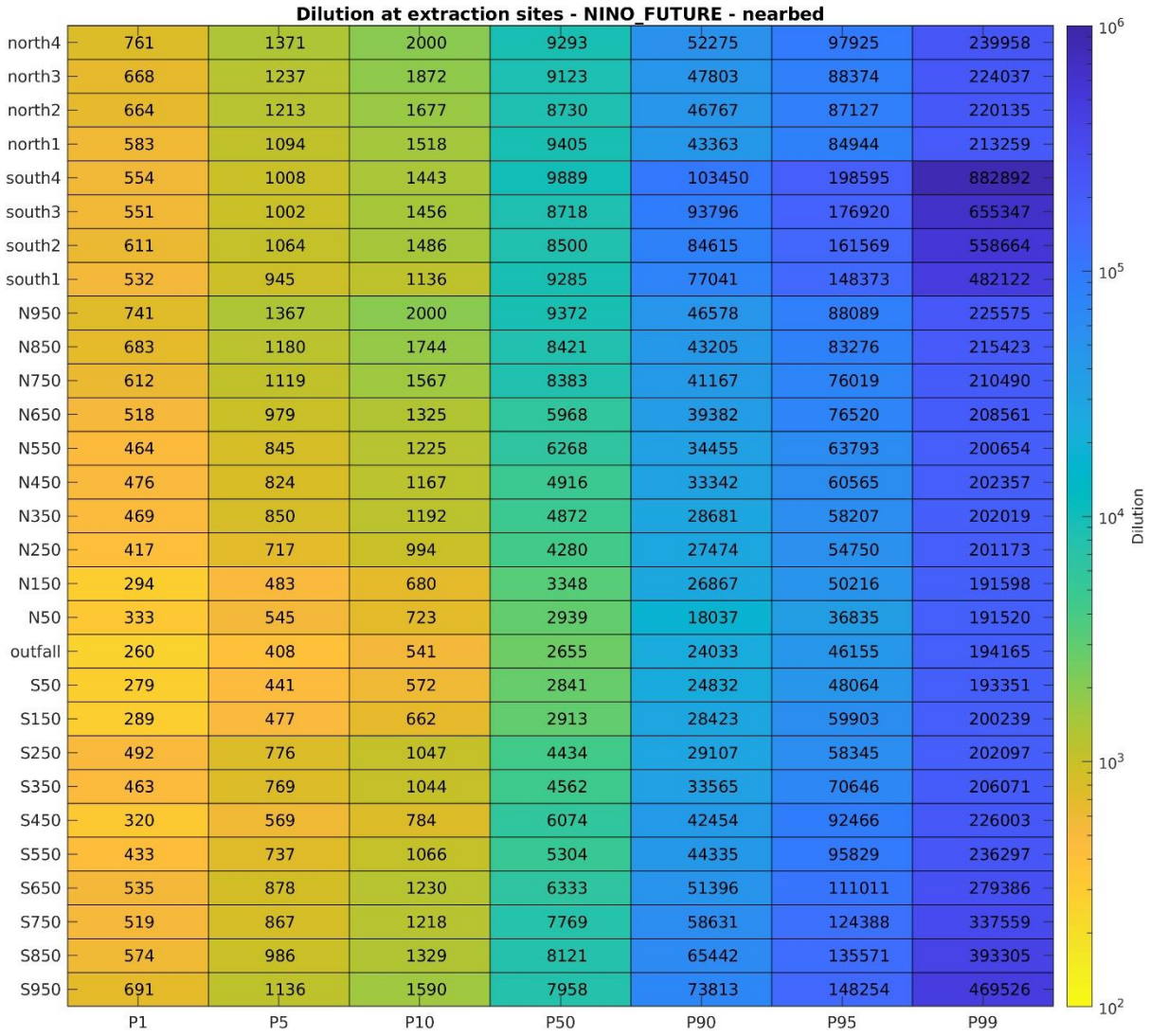

Figure 2-7 Dilution percentile at extraction sites shown in Figure 2-1 for the El Niño scenario with future discharge at the nearbed level. Note the colour scale is logarithmic.

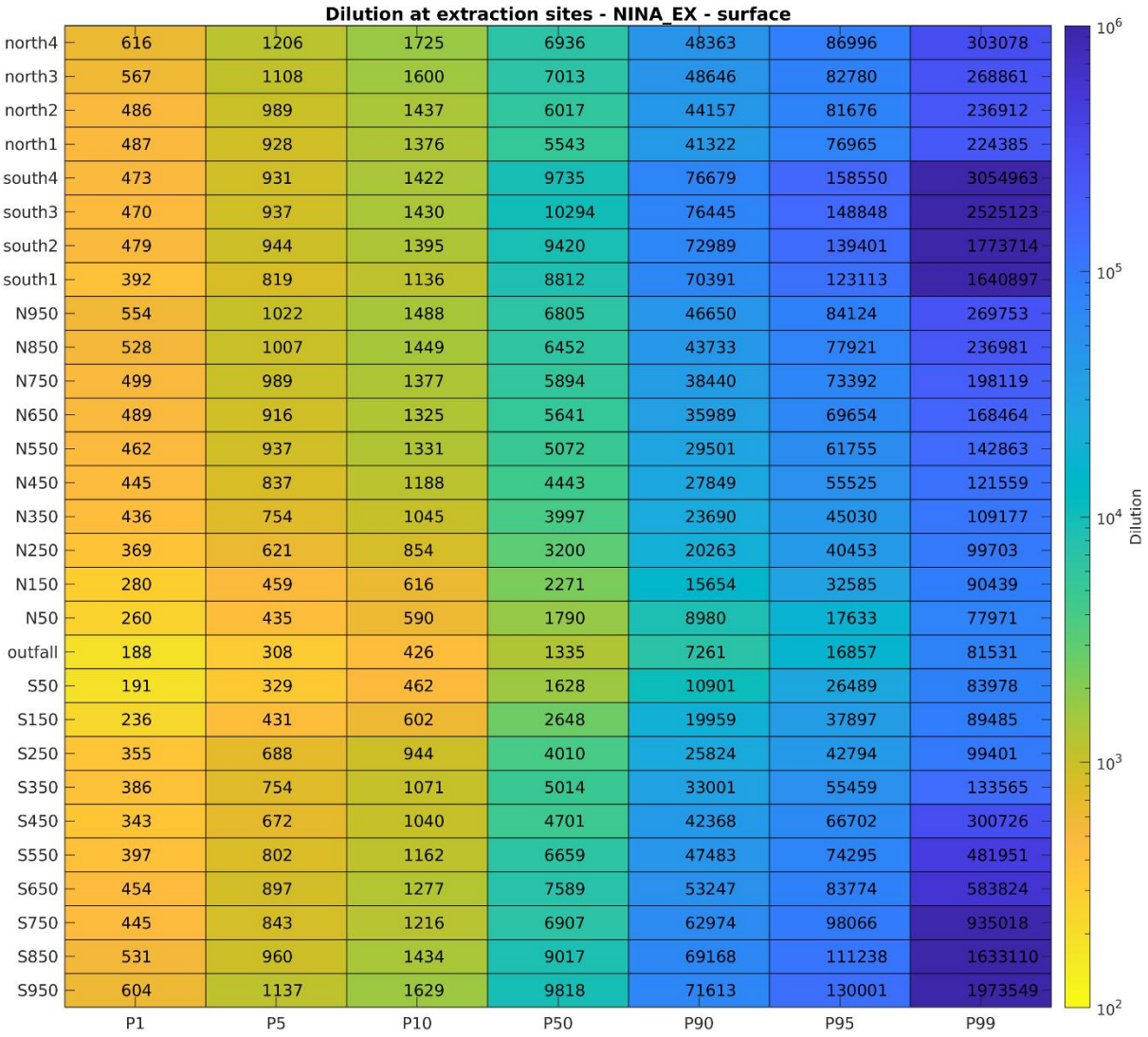

Figure 2-8 Dilution percentile at extraction sites shown in Figure 2-1 for the La Niña scenario with existing discharge at the surface level. Note the colour scale is logarithmic.

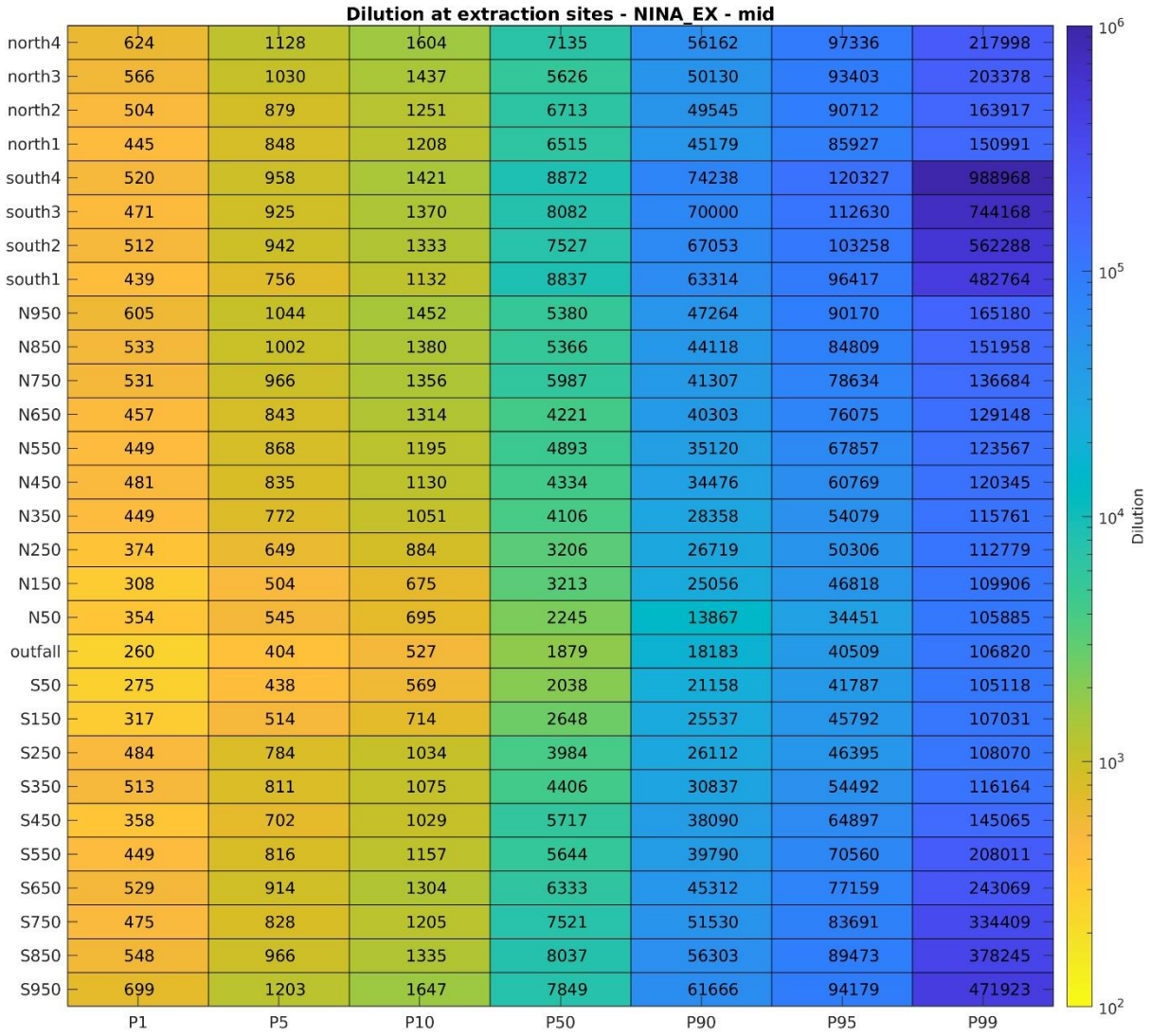

Figure 2-9 Dilution percentile at extraction sites shown in Figure 2-1 for the La Niña scenario with existing discharge at the middepth level. Note the colour scale is logarithmic.

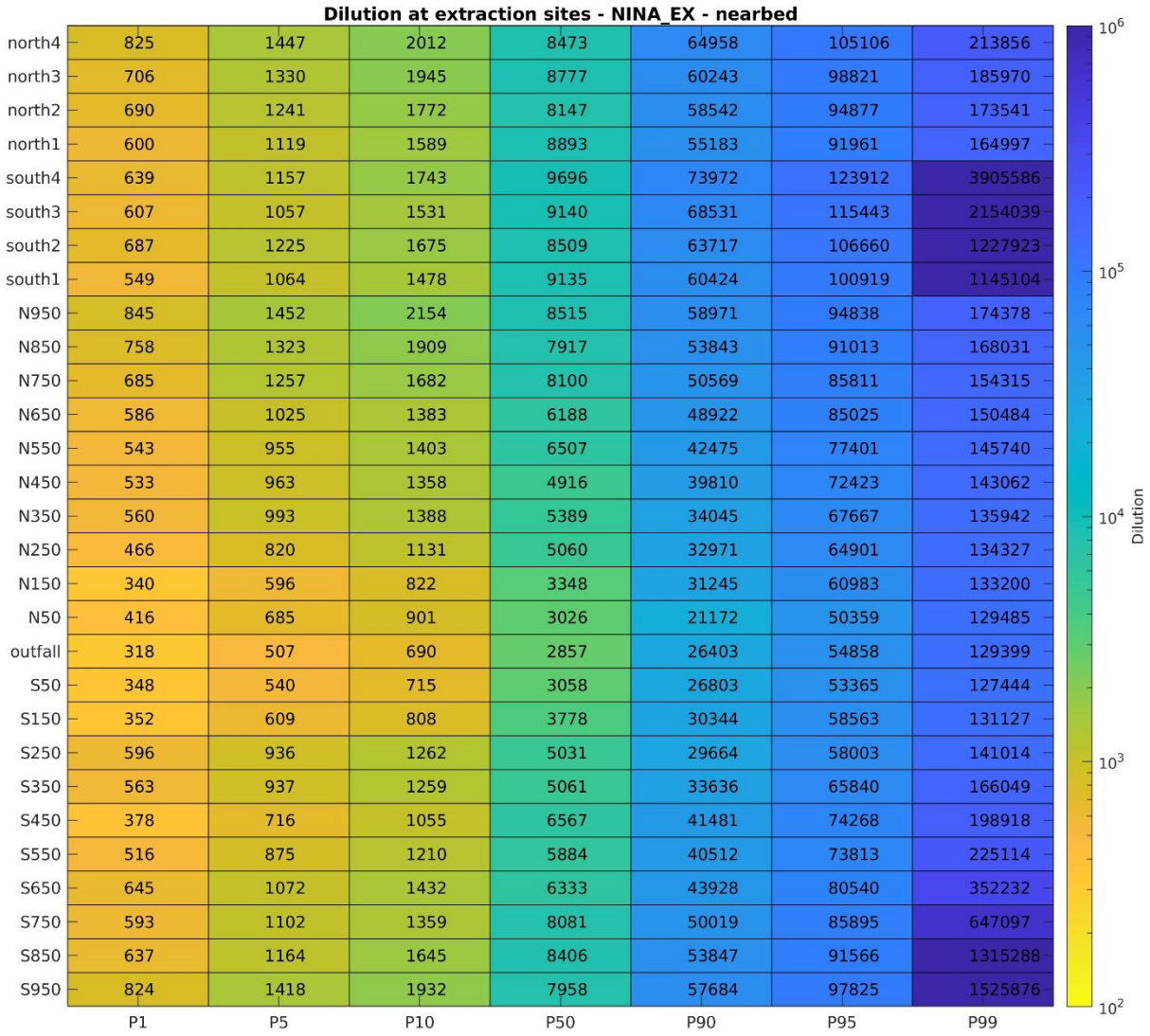

Figure 2-10 Dilution percentile at extraction sites shown in Figure 2-1 for the La Niña scenario with existing discharge at the nearbed level. Note the colour scale is logarithmic.

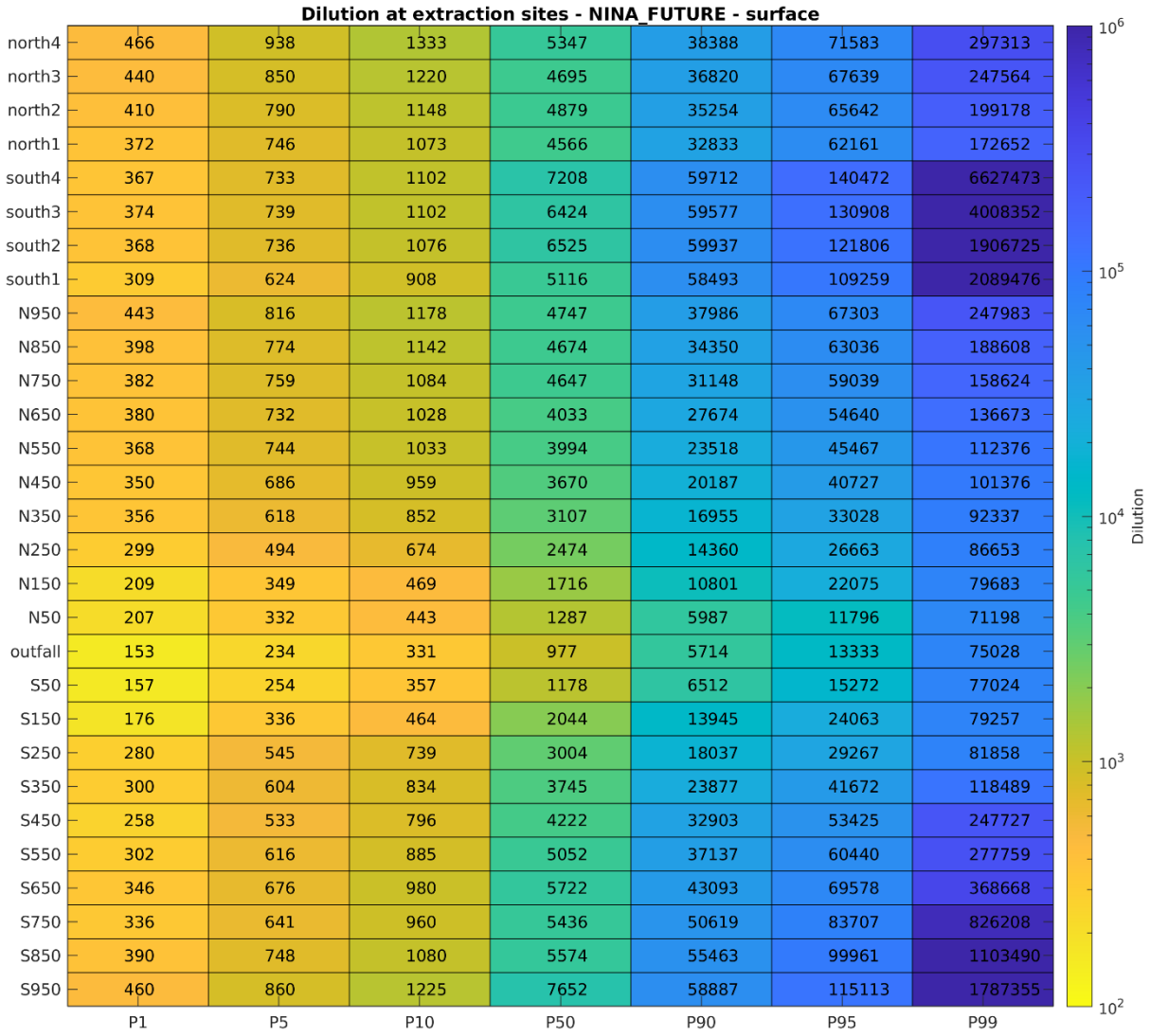

Figure 2-11 Dilution percentile at extraction sites shown in Figure 2-1 for the La Niña scenario with future discharge at the surface level. Note the colour scale is logarithmic.

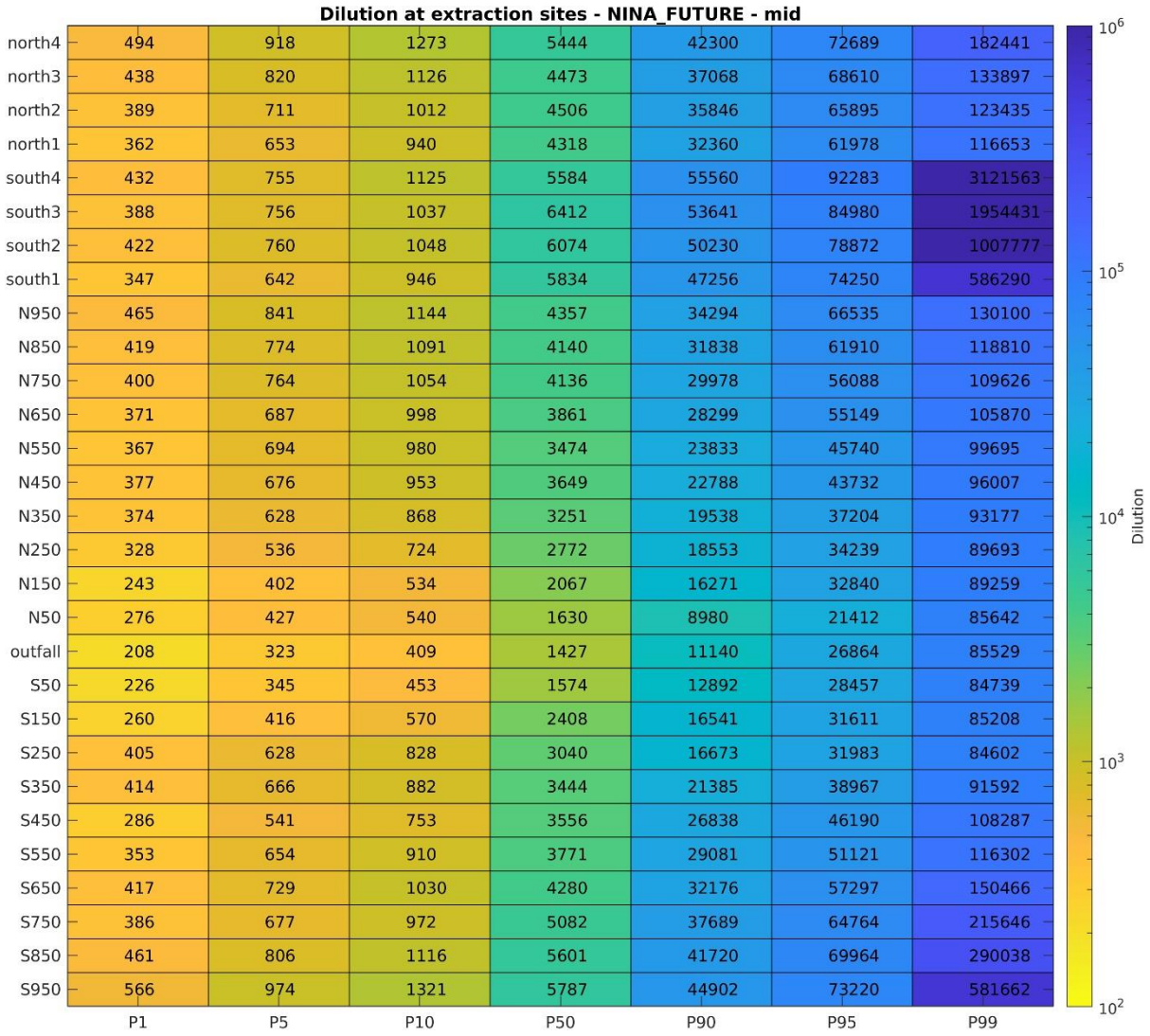

Figure 2-12 Dilution percentile at extraction sites shown in Figure 2-1 for the La Niña scenario with future discharge at the mid-depth level. Note the colour scale is logarithmic.

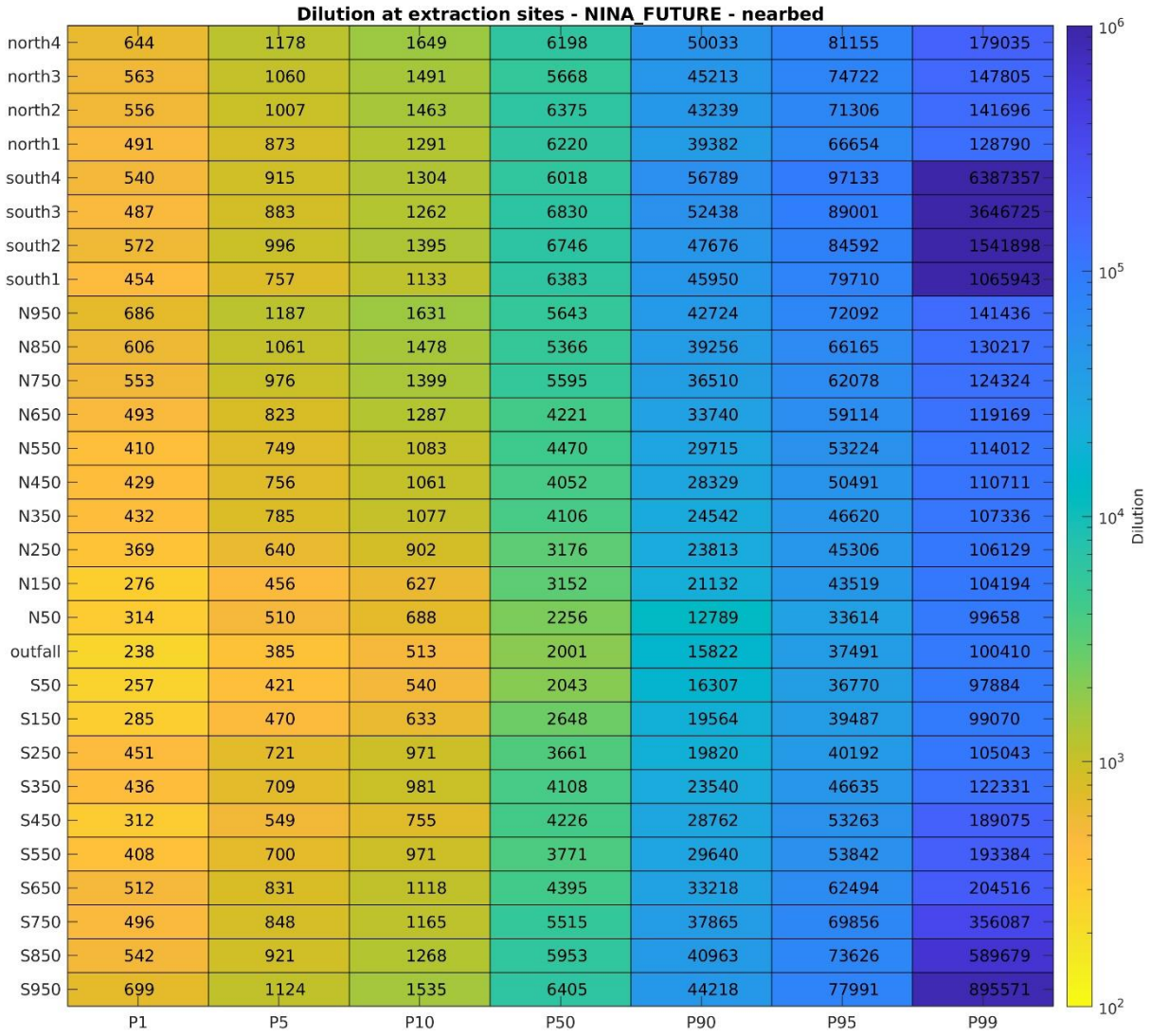

Figure 2-13 Dilution percentile at extraction sites shown in Figure 2-1 for the La Niña scenario with future discharge at the nearbed level. Note the colour scale is logarithmic.

3.Item 2

The nearfield dynamics are incorporated in the far-field model using nearfield length, width, and thickness at each time step (see Figure 3-1). These metrics are interpolated from the look-up table produced by the CORMIX [1] model, according to ambient hydrodynamic flow velocity, and wastewater discharge flow (see MetOcean Solutions, 2022). The orientation of the release cone is adjusted at each release time according to ambient hydrodynamic flow direction.

General statistics on the nearfield plume metrics are provided in Table 3-1 to inform on general plume dimensions. Median nearfield length, half width, and surface thickness are 248.0 m , 21.0 m and 11.1 m respectively. Note some values are identical for some different percentiles (e.g. P1, P5, P10 for the nearfield length. This is because we use nearest neighbour extrapolation for the hydrodynamic and discharge flow conditions that fall outside of the range covered by the lookup table events.

Successive release footprints over the duration of the particle-tracking simulations were combined to map the possible extents of the plume after the initial nearfield dynamics, and before it gets advected by ambient current in the far-field model. The nearfield plume map is shown in Figure 3-2. The colour indicates the probability of wastewater to end up in a given area after the nearfield dynamics, over the annual period considered. Yellow zones are zones where the wastewater ends up more regularly after the nearfield dynamics, whereas blue areas are areas where the wastewater can end up at time, but less frequently. The extraction sites considered in item 1 can be used to inform on dilution along the nearfield plume main axis.

A 3D view of the nearfield plume is shown in Figure 3-3. We see that the plume has larger extents in the shallower levels and becomes more compact near its deeper extremity (at ~14 m below surface) (see also Table 3-1). Vertical slices are shown in Figure 3-4. As in previous plots, the colour informs on the probability for the wastewater to end up in a particular area. On the horizontal, largest probabilities are typically found within 200m of the outfall with two hotspots on either side of the outfall (to the northeast and south-west). On the vertical, most frequent depth range is [0-4m] below surface. The plume footprint then goes down the water column to ~ 10-12m below the surface, within 200-

[1] www.cormix.info

500m of the outfall, but with reduced probability. Deeper excursions (~14m) are possible though less frequent, and typically only up to ~125 m either side of the outfall.

Timeseries of dilutions were extracted around the edge of the current mixing zone, which is a rectangular box centred on the outfall with its main axis along the nearfield plume footprint (NCC, pers. comm., 2023) (Figure 3-5).

Dilution percentiles are presented in Figure 3-6 to Figure 3-17 for the different scenarios. Minimum dilution percentiles (i.e. worst-case) experienced around the mixing zone are tabulated in Table 3-2. For example, the minimum P1 dilution for El Nino scenario under the current discharge, at the surface, is 413. Corresponding dilution level for La Nina scenario is 355. Minimum dilutions are generally observed at the sites mix17-N250, or mix3-S250 which are aligned with the nearfield plume footprint.

Minimum dilution levels are consistently smaller for La Nina scenario compared to El Nino, though they general remain within a similar order of magnitude. The lower La Nina dilutions can be attributed to weaker hydrodynamic flows in the vicinity of the outfall during La Nina scenario, which are therefore less efficient in dispersing the released contaminant, relative to El Nino scenario (see current roses at outfall location in Figure 3-18 and Figure 3-19 reproduced from MetOcean Solutions, 2022).

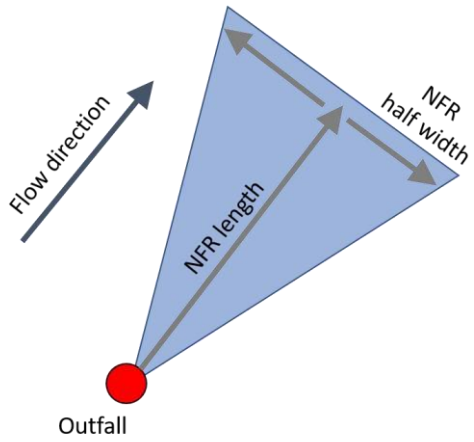

Figure 3-1 Sketch showing the triangular release footprint defined from the nearfield dynamics metrics NFR length and mid width. Particles were released on the surface layer within a thickness defined by the NFR thickness.

Table 3-1 Nearfield plume length, half-width, and thickness percentiles.

	P1	P5	P10	P25	P50	P75	P90	P95	P99
NFR length	104.6	104.6	104.6	139.3	248.0	460.4	738.0	938.0	1466.7
NFR half-width	18.7	19.6	19.9	20.5	21.0	24.7	90.0	92.4	185.9
NFR thickness	2.2	3.5	5.7	10.0	11.1	12.2	13.5	13.5	13.5

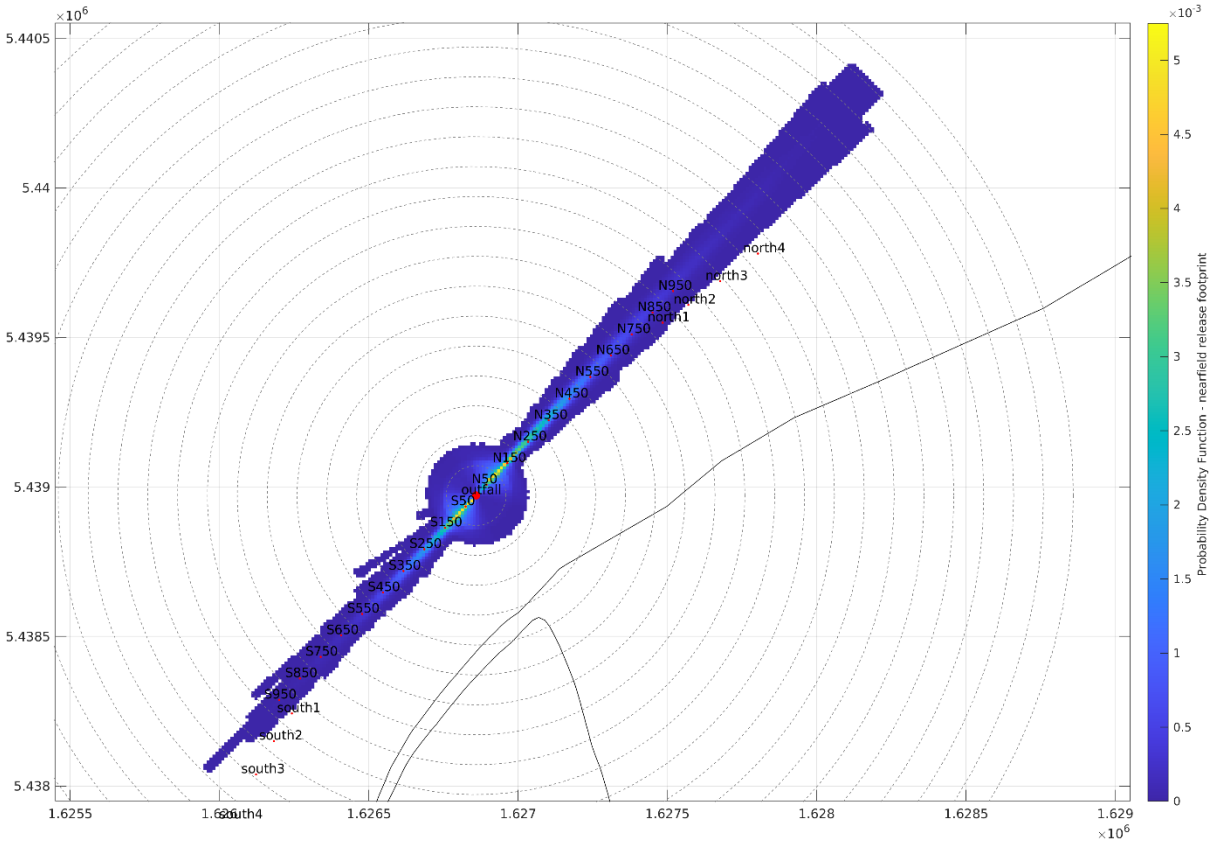

Figure 3-2 Plan view of the release footprint after initial nearfield dynamics. The colour indicates the probability of wastewater to end up in a given area after the nearfield dynamics, over the annual period considered. Sum of all probabilities is 1. Yellow zones are zones where the wastewater ends up more regularly after the nearfield dynamics, whereas blue areas are areas where the wastewater can end up at time, but with a lower probability. The outfall location and extraction sites are shown as red dots. Concentric circles are added every 100m from the outfall for scale.

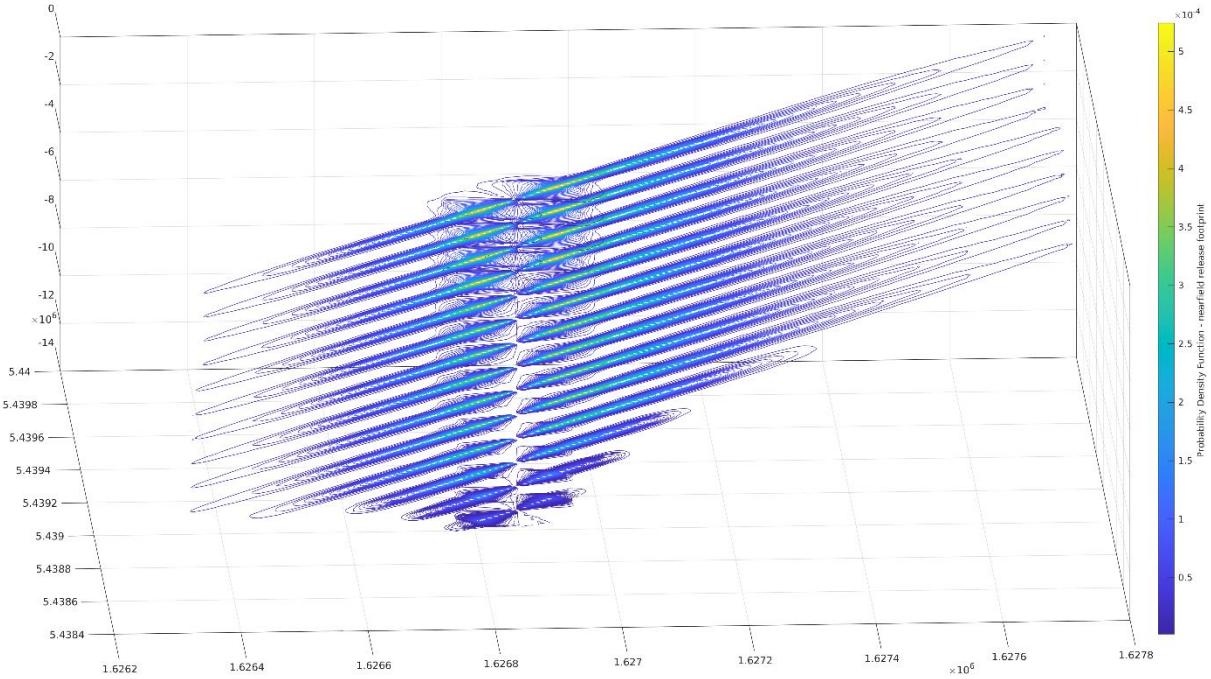

Figure 3-3 3D view of the release footprint after initial nearfield dynamics. The colour indicates the probability of wastewater to end up in a given area after the nearfield dynamics, over the annual period considered. The vertical axis is the water column height where 0 is the sea surface; sum of all probabilities is 1. Yellow zones are zones where the wastewater ends up more regularly after the nearfield dynamics, whereas blue areas are areas where the wastewater can end up at time, but with a lower probability.

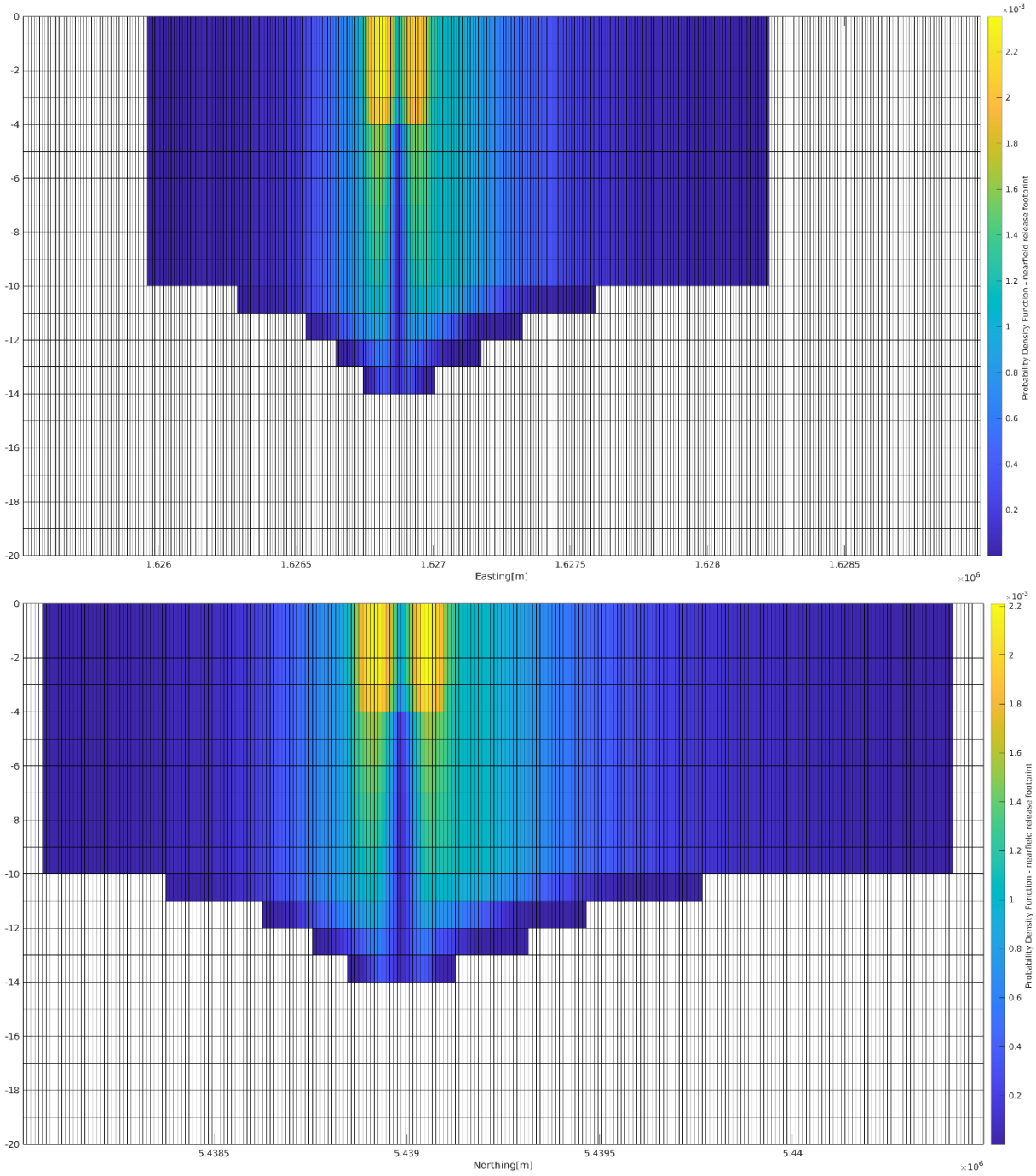

Figure 3-4 Vertical slices of the 3D nearfield release footprint, along the x and y axes. The colour indicates the probability of wastewater to end up in a given area after the nearfield dynamics, over the annual period considered. Sum of all probabilities is 1. Yellow zones are zones where the wastewater ends up more regularly after the nearfield dynamics, whereas blue areas are areas where the wastewater can end up at time, but with a lower probability.

Figure 3-5 Extraction sites around the edges of the mixing zone.

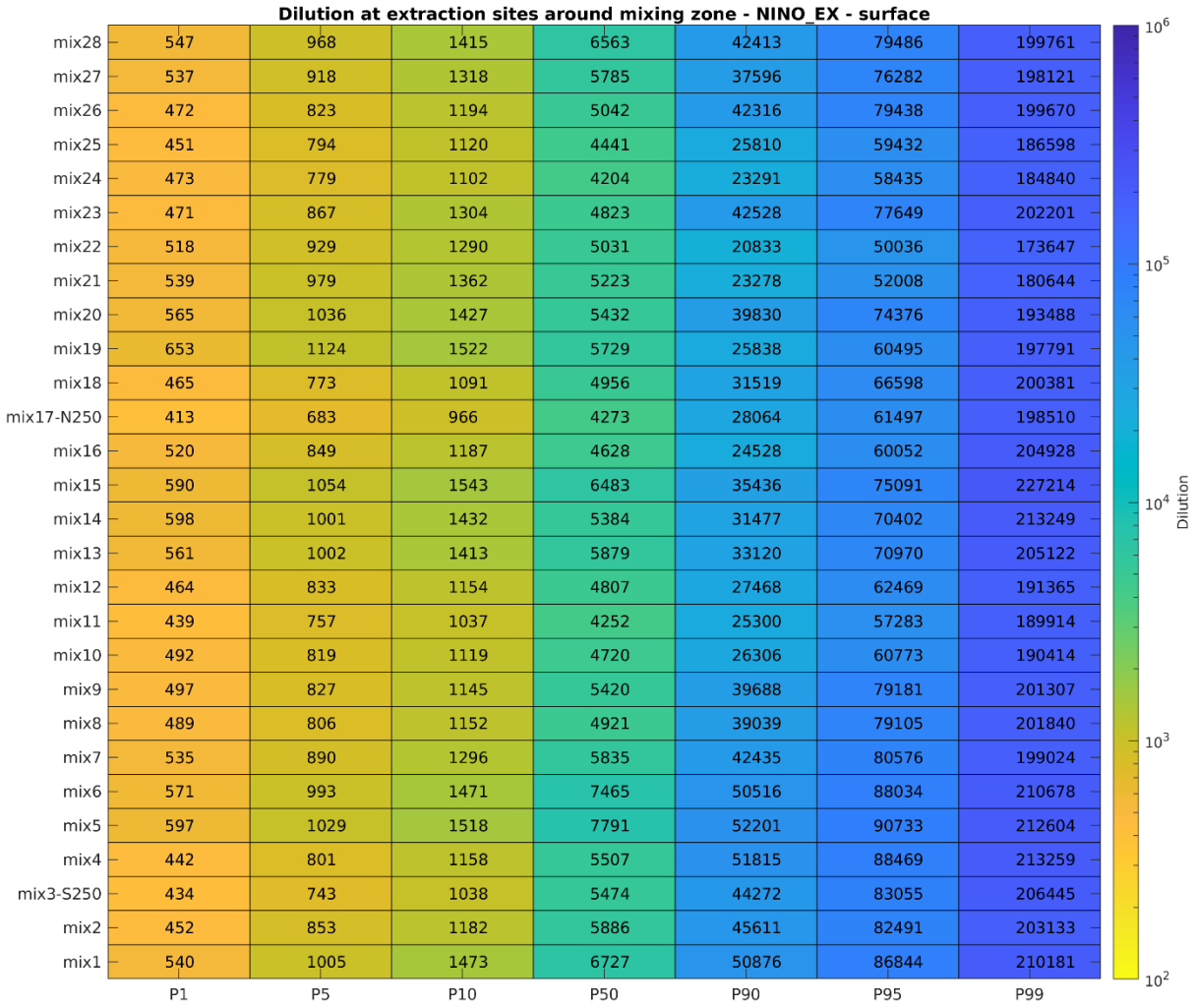

Figure 3-6 Dilution percentile at extraction sites around the mixing zone edges (Figure 3-5) for the El Niño scenario with existing discharge at the surface level. Note the colour scale is logarithmic.

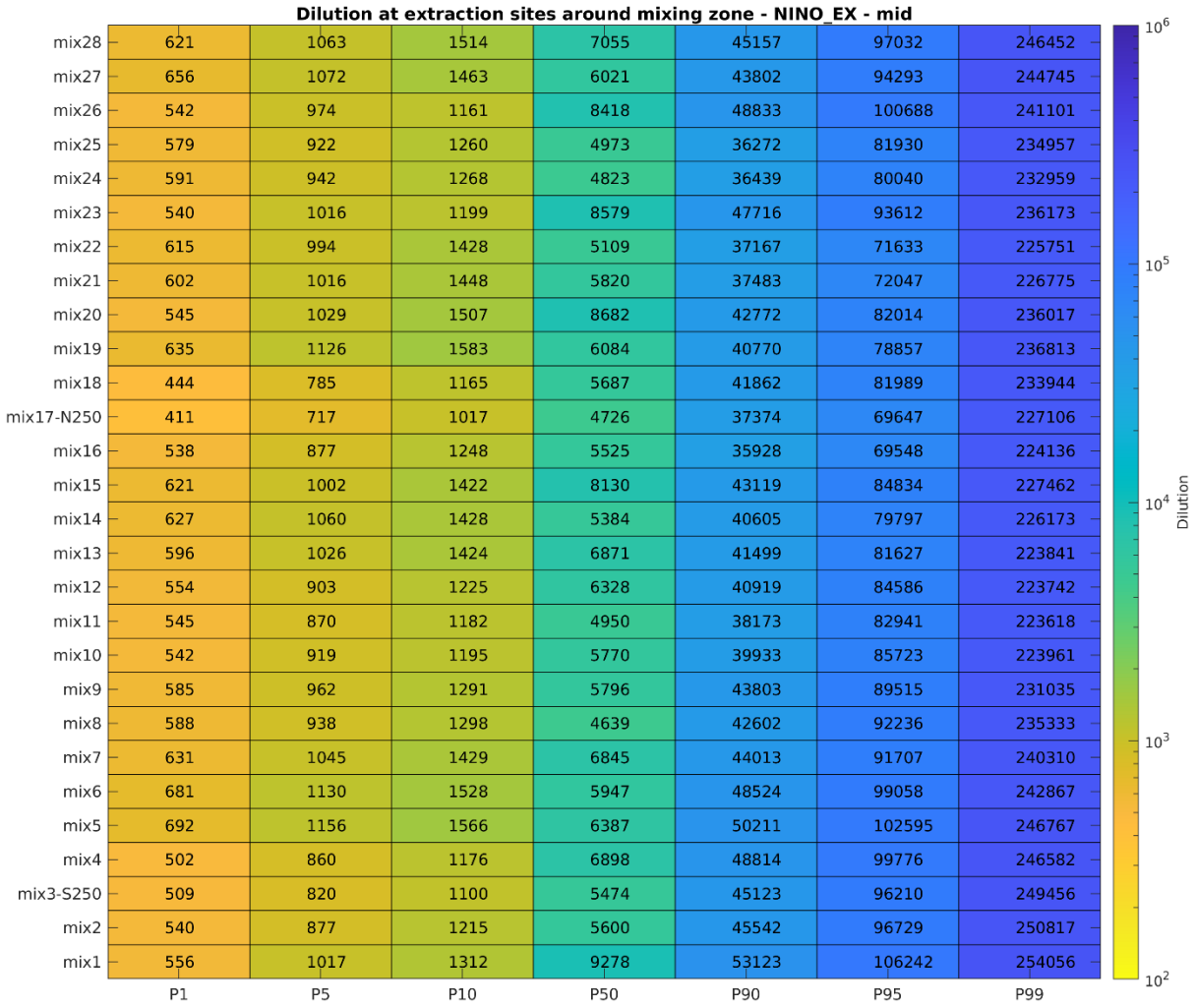

Figure 3-7 Dilution percentile at extraction sites around the mixing zone edges (Figure 3-5) for the El Niño scenario with existing discharge at the mid-depth level. Note the colour scale is logarithmic.

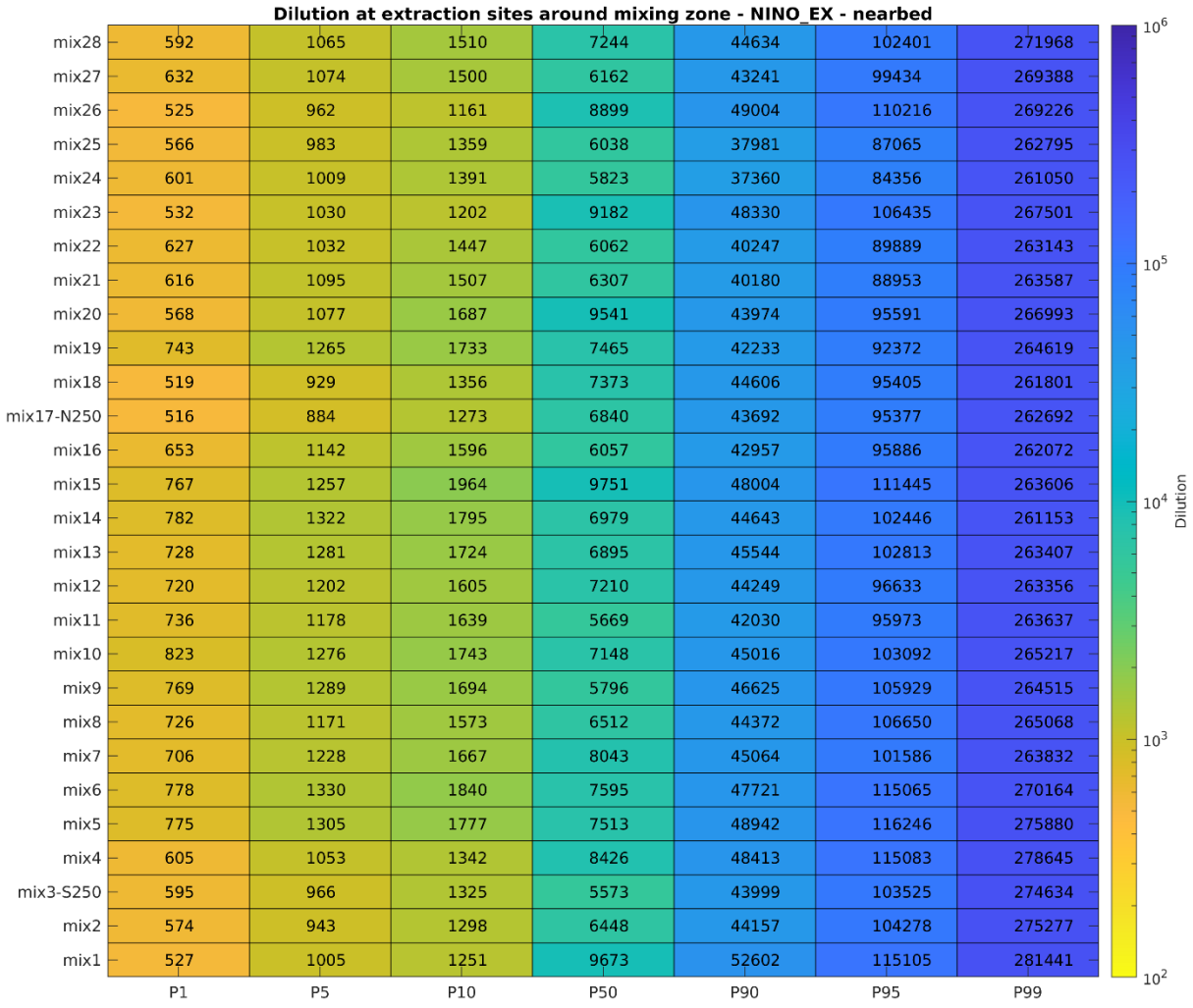

Figure 3-8 Dilution percentile at extraction sites around the mixing zone edges (Figure 3-5) for the El Niño scenario with existing discharge at the nearbed level. Note the colour scale is logarithmic.

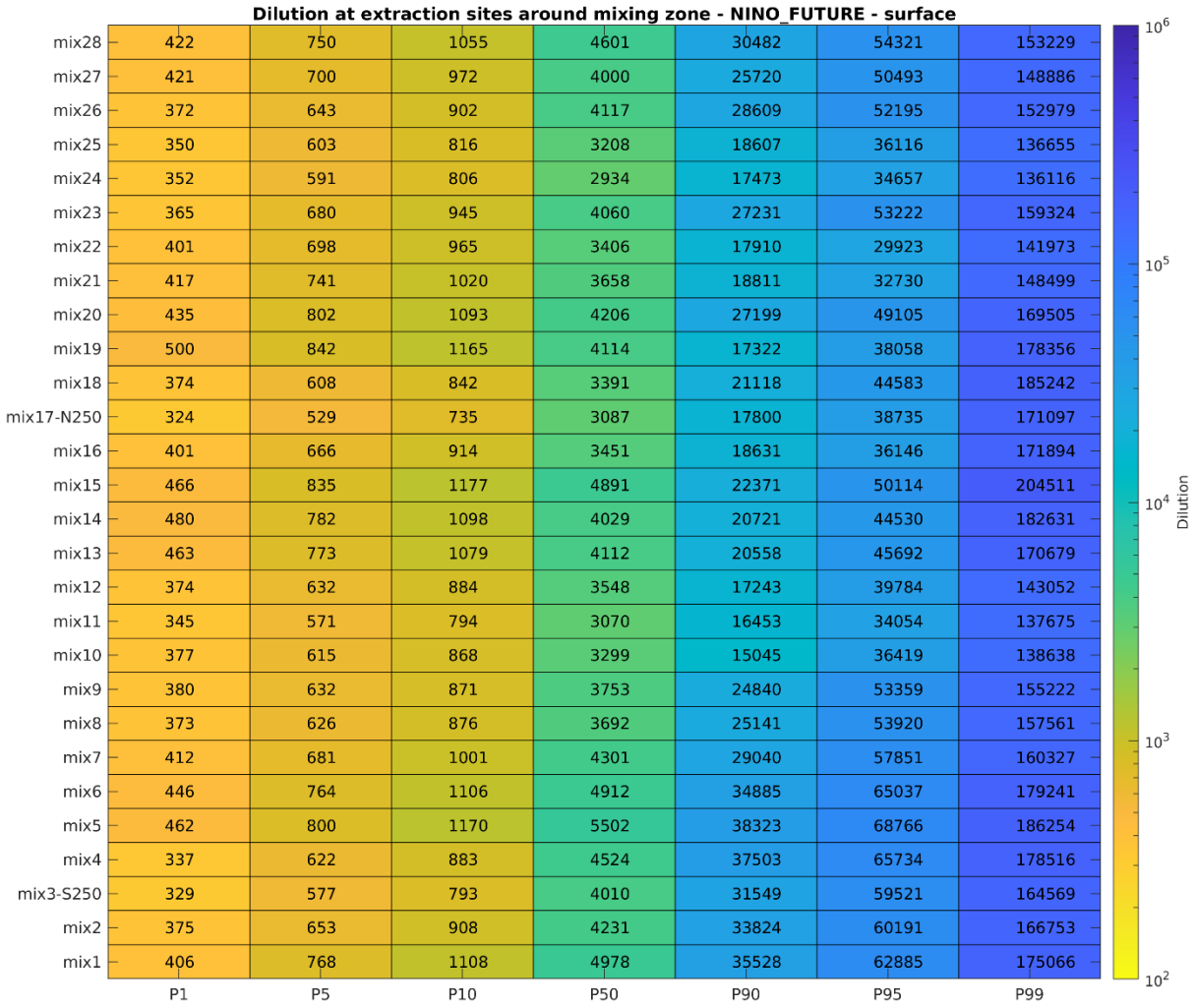

Figure 3-9 Dilution percentile at extraction sites around the mixing zone edges (Figure 3-5) for the El Niño scenario with future discharge at the surface level. Note the colour scale is logarithmic.

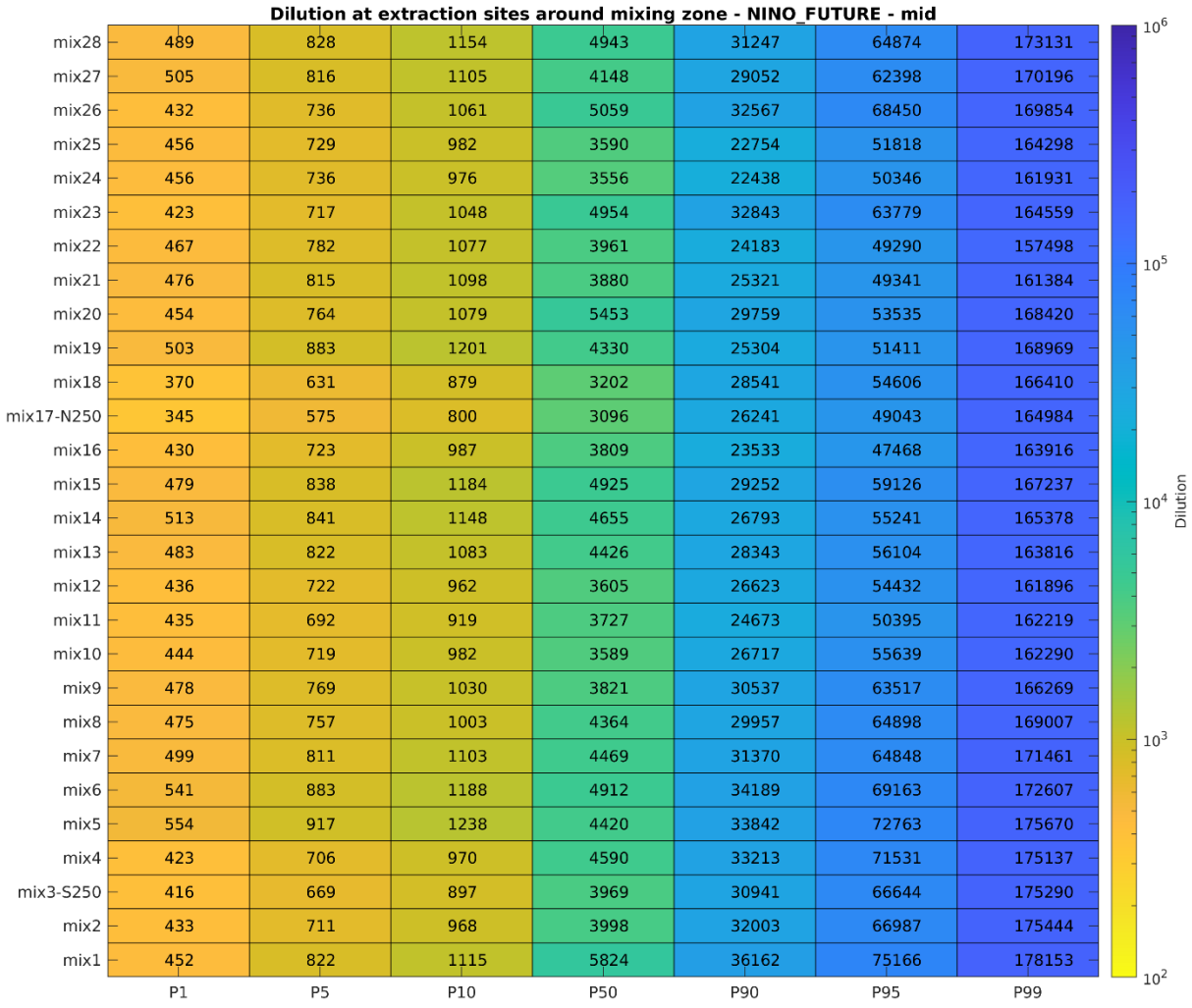

Figure 3-10 Dilution percentile at extraction sites around the mixing zone edges (Figure 3-5) for the El Niño scenario with future discharge at the mid-depth level. Note the colour scale is logarithmic.

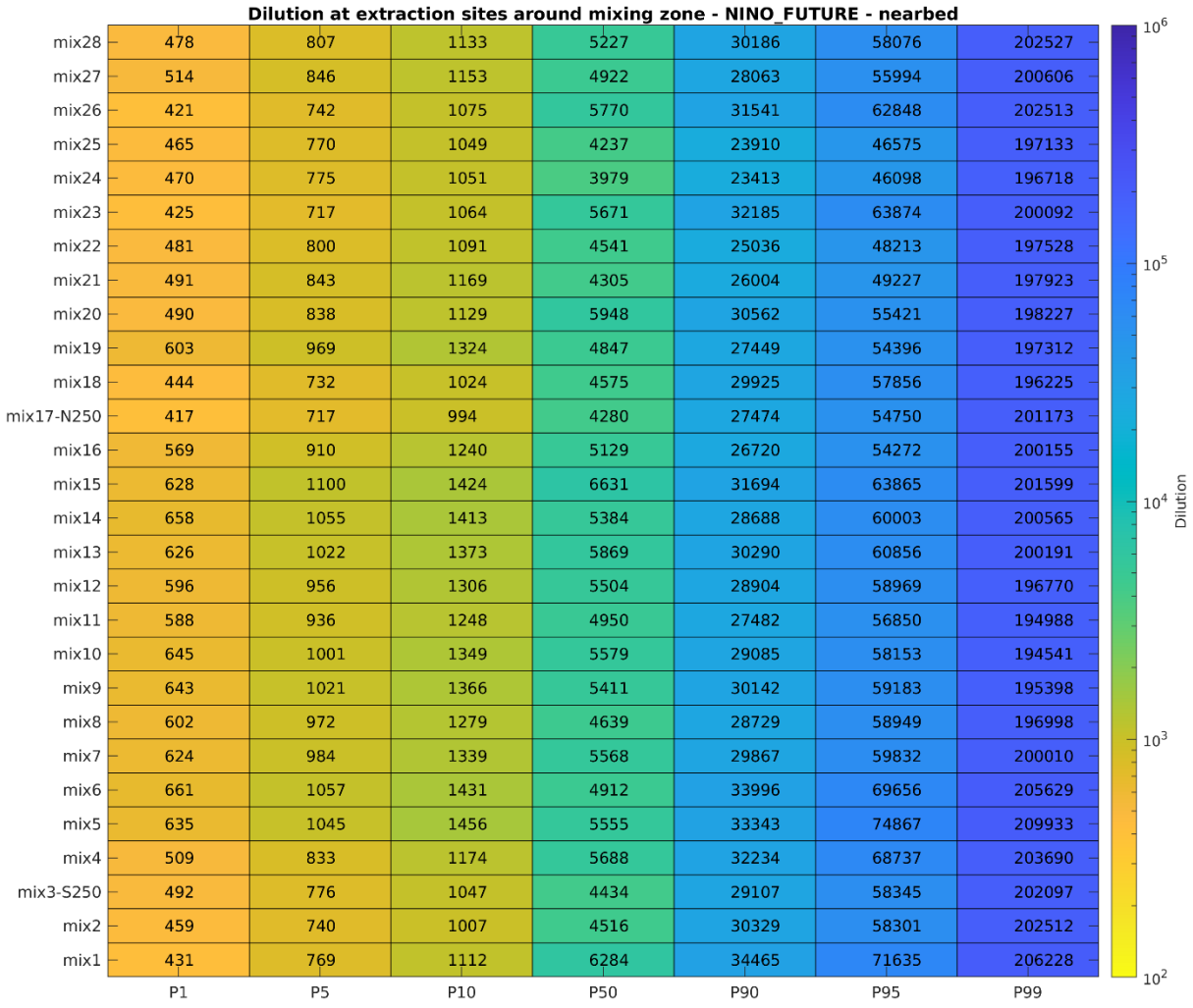

Figure 3-11 Dilution percentile at extraction sites around the mixing zone edges (Figure 3-5) for the El Niño scenario with future discharge at the nearbed level. Note the colour scale is logarithmic.

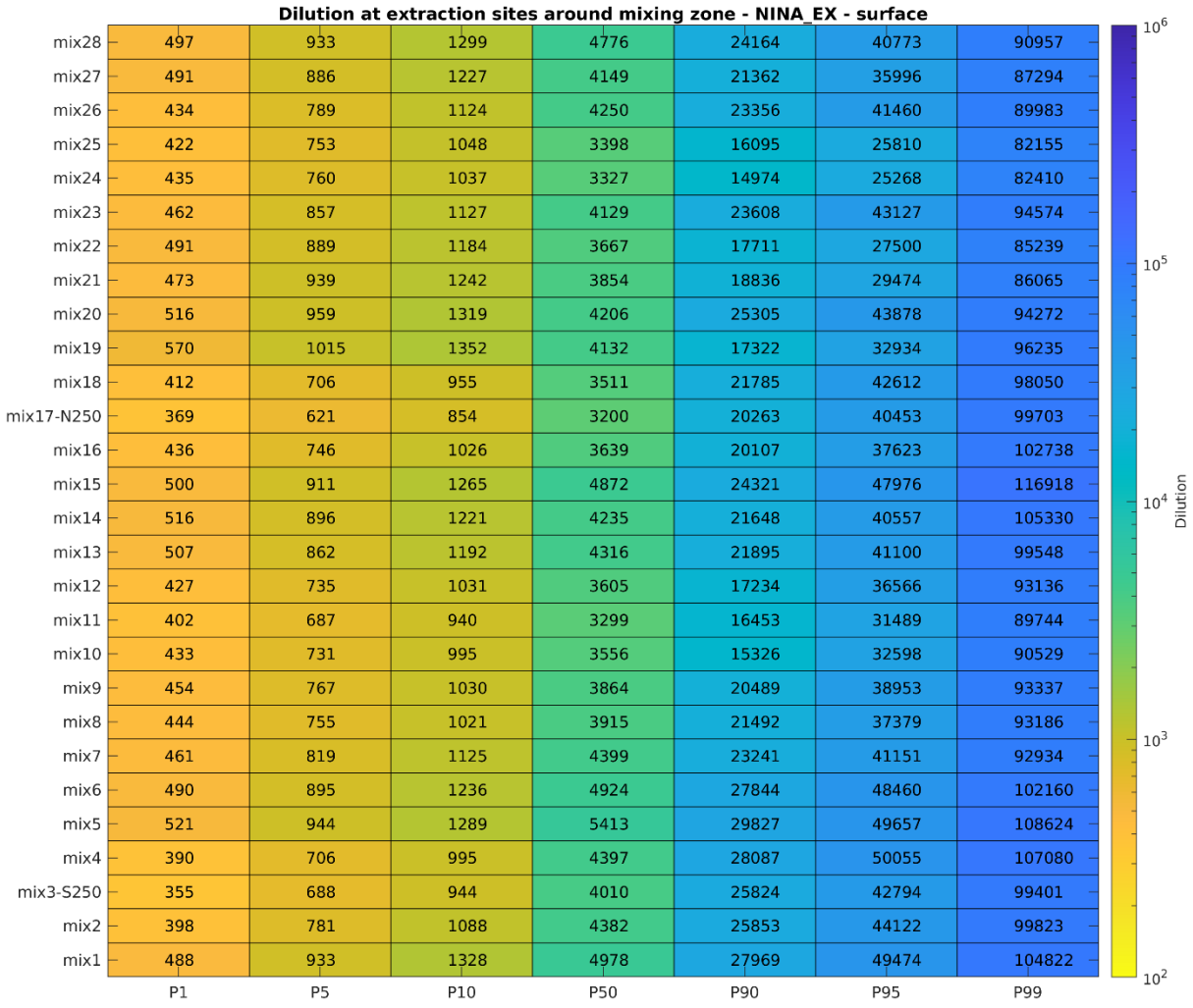

Figure 3-12 Dilution percentile at extraction sites around the mixing zone edges (Figure 3-5) for the La Niña scenario with existing discharge at the surface level. Note the colour scale is logarithmic.

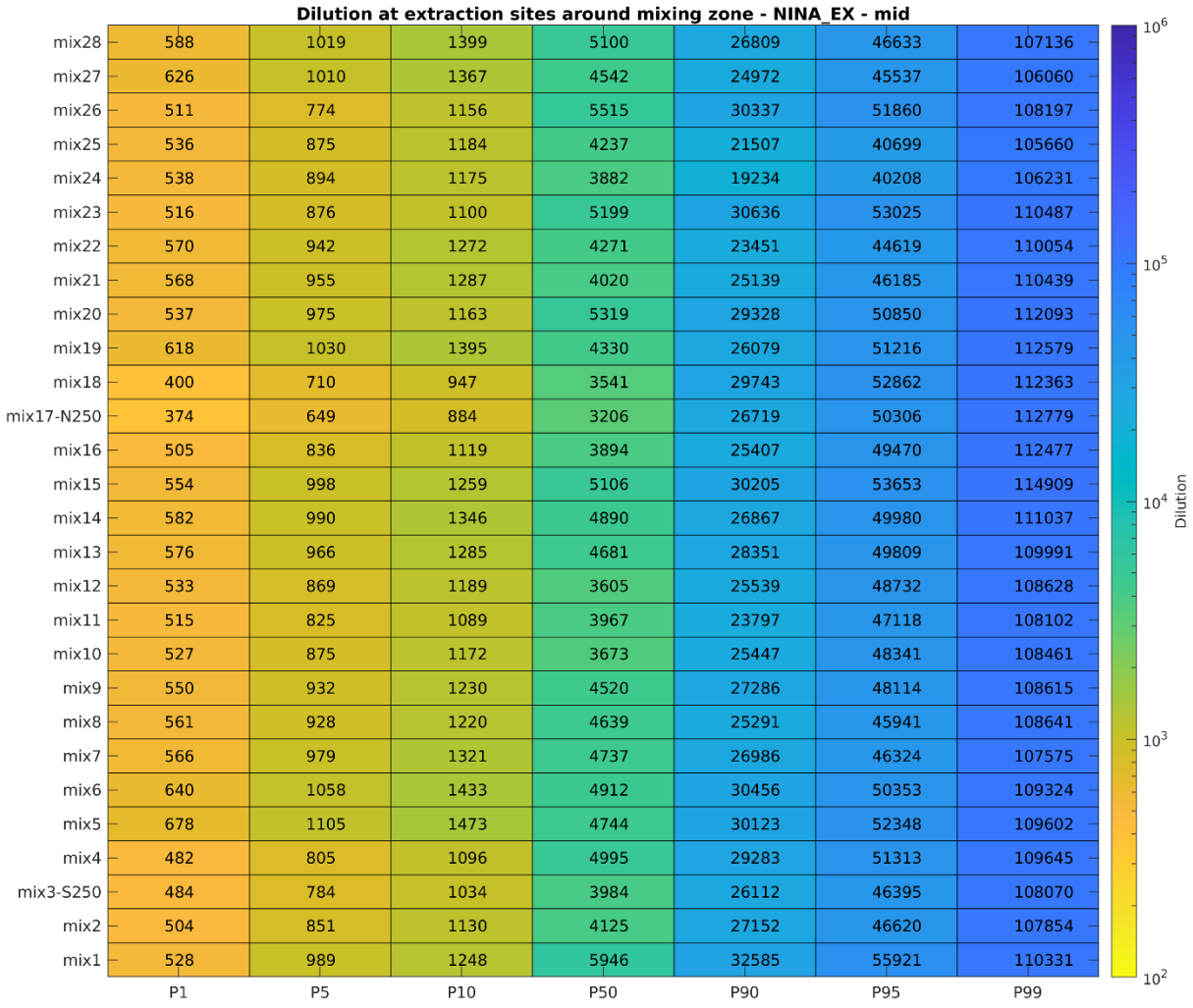

Figure 3-13 Dilution percentile at extraction sites around the mixing zone edges (Figure 3-5) for the La Niña scenario with existing discharge at the mid-depth level. Note the colour scale is logarithmic.

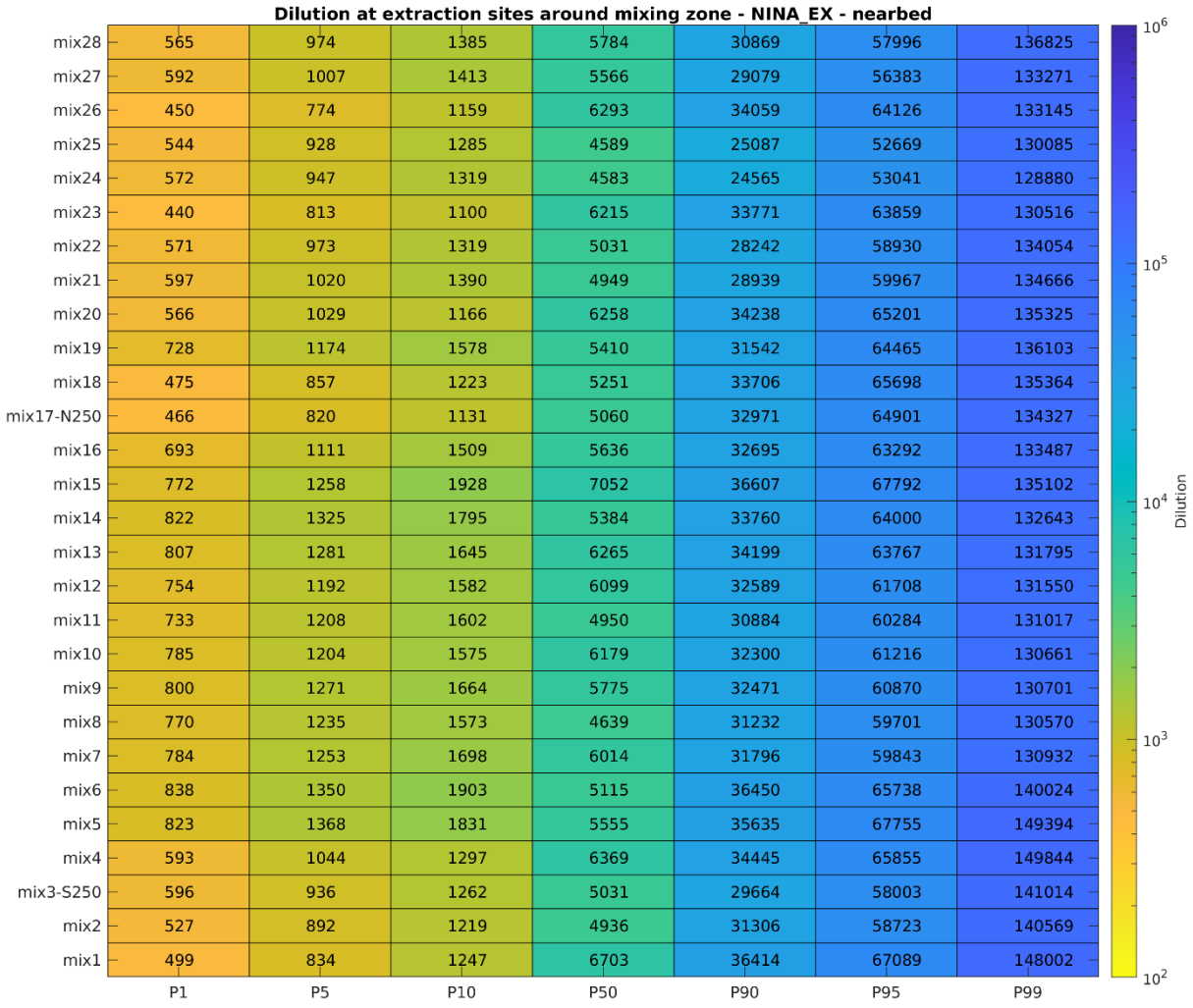

Figure 3-14 Dilution percentile at extraction sites around the mixing zone edges (Figure 3-5) for the La Niña scenario with existing discharge at the nearbed level. Note the colour scale is logarithmic.

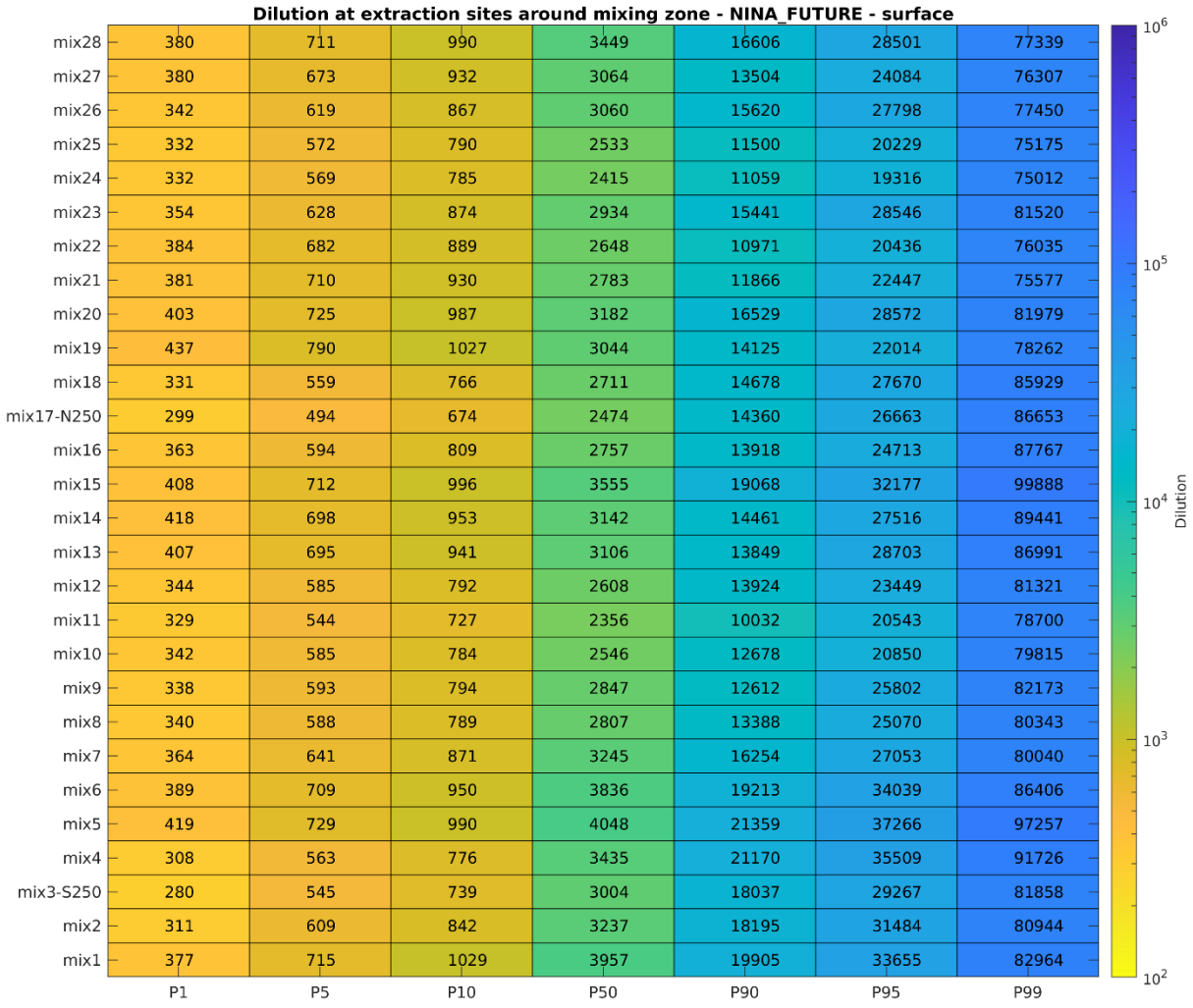

Figure 3-15 Dilution percentile at extraction sites around the mixing zone edges (Figure 3-5) for the La Niña scenario with future discharge at the surface level. Note the colour scale is logarithmic.

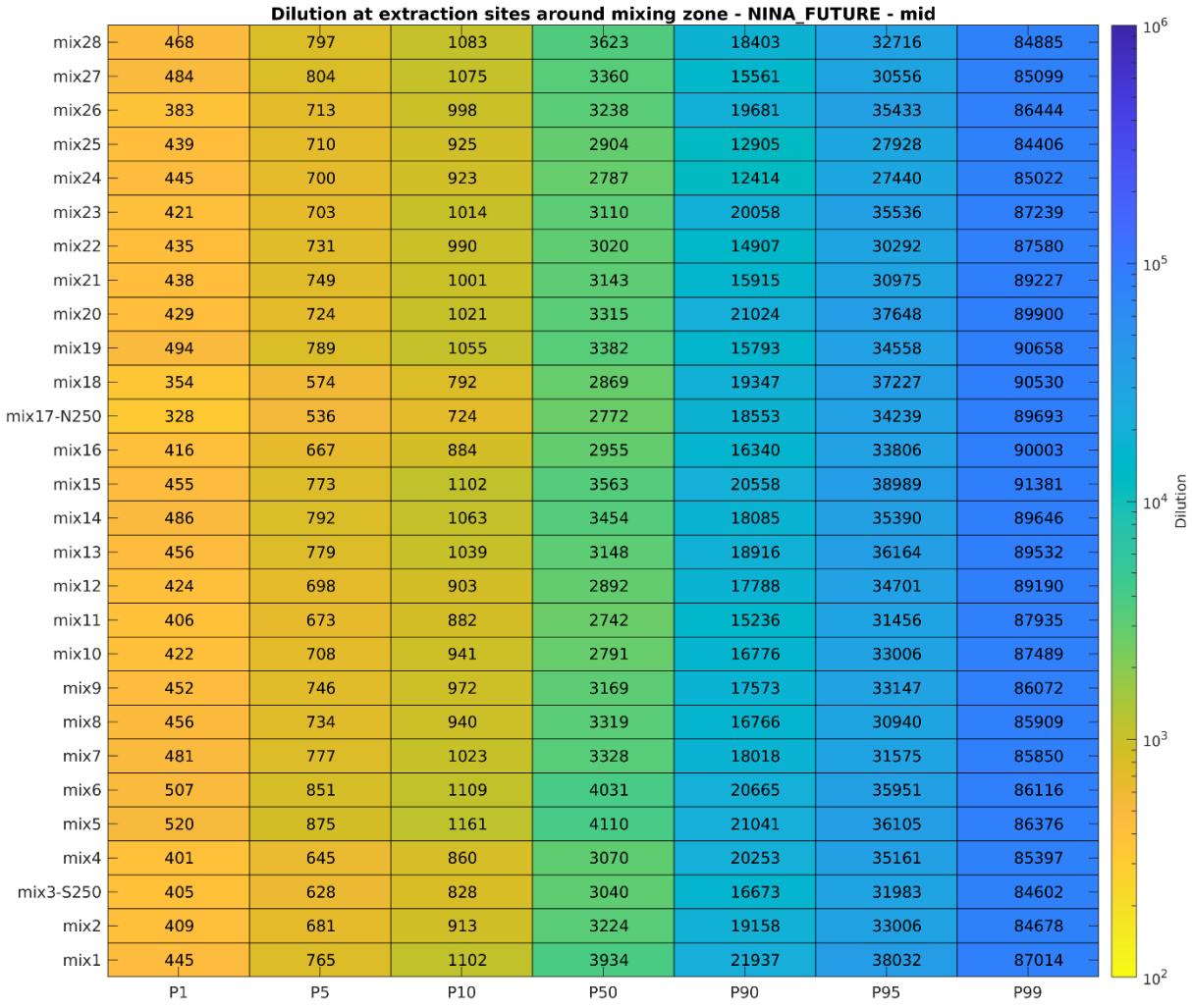

Figure 3-16 Dilution percentile at extraction sites around the mixing zone edges (Figure 3-5) for the La Niña scenario with future discharge at the mid-depth level. Note the colour scale is logarithmic.

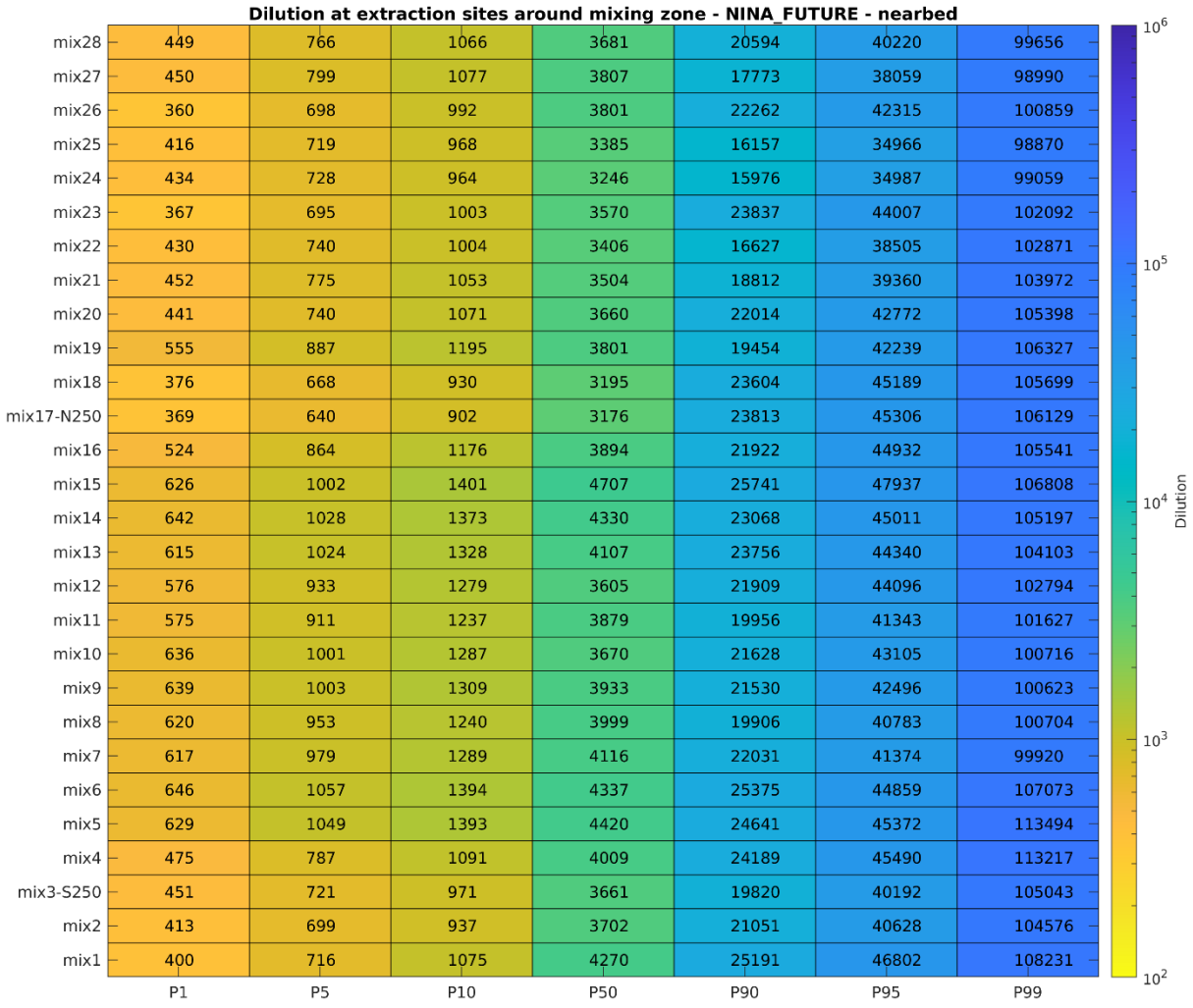

Figure 3-17 Dilution percentile at extraction sites around the mixing zone edges (Figure 3-5) for the La Niña scenario with future discharge at the nearbed level. Note the colour scale is logarithmic.

Table 3-2 Minimum dilutions around the edges of the mixing zone for the different scenarios.

NINO_EXISTING	P1	P5	P10	P50	P90	P95	P99
surface	413	683	966	4204	20833	50036	173647
mid	411	717	1017	4639	35928	69548	223618
nearbed	516	884	1161	5573	37360	84356	261050
NINO_FUTURE							
surface	324	529	735	2934	15045	29923	136116
mid	345	575	800	3096	22438	47468	157498
nearbed	417	717	994	3979	23413	46098	194541
NINA_EXISTING							
surface	355	621	854	3200	14974	25268	82155
mid	374	649	884	3206	19234	40208	105660
nearbed	440	774	1100	4583	24565	52669	128880
NINA_FUTURE							
surface	280	494	674	2356	10032	19316	75012
mid	328	536	724	2742	12414	27440	84406
nearbed	360	640	902	3176	15976	34966	98870

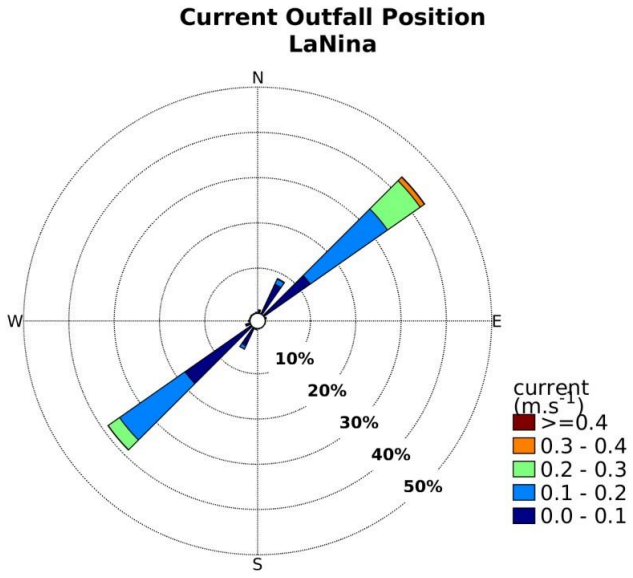

Figure 3-18 Rose of depth-averaged current at the outfall location during La Nina annual period.

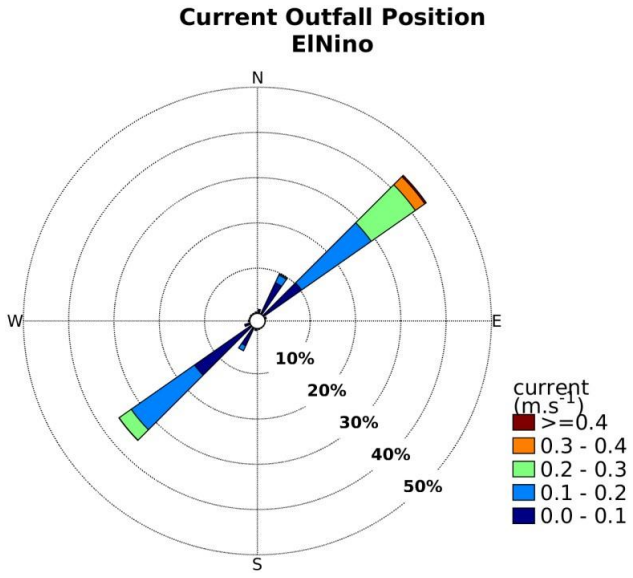

Figure 3-19 Rose of depth-averaged current at the outfall location during El Nino annual period.

4.Item 3

Nelson City Council considered an upgrade of the current outfall diffuser to improve mixing of the wastewater at the outfall. The current diffuser design is considerably different from the proposed upgrade (Figure 4-1 and Figure 4-2, respectively) and therefore a rerun of the near-field model was necessary to assess changes in the near field. Near-field modelling of the initial turbulent mixing was undertaken using CORMIX (see section 2.2 in MetOcean Solutions, 2022).

The proposed upgrade design is a 2-arm diffuser, extending 100 m each at an angle of 30 degrees to the centreline, 60 degrees between the two arms (Figure 4-2). The pipe that connects the diffusers to the treatment plant is perpendicular to the shoreline and is approximately 430 m long. There are a total of 40 ports in each arm, with openings approximately 2.5 m apart and on alternate sides. The ports are fitted with a duckbill valve. The initial height of the diffuser port centreline is at 0.5 m above seabed.

Due to limitations in the model setup, the following factors have to be considered in order to represent the proposed design:

- The model setup did not include the duckbill fitted on the ports. We used a port opening diameter of 75 mm (informed by Nelson City Council).
- The model can only have one arm per simulation. Therefore, we simulated each arm separately, and half of the discharge flow in each arm.

The model output provided the geometry of the nearfield (length and width) as well as the dilution at the edge of the nearfield that can be used as input in far-field particle tracking modelling (not carried out at this stage for the proposed design). In this subsequent stage (far-field modelling), the nearfield results for both arms can be combined, accounting for the distance between the arms (see the "V" shape design) and assess the different dilutions for the QMRA analysis.

Simulations

Ambient and wastewater characteristics (temperature and salinity) were setup as previously for the current diffuser simulations (see MetOcean Solutions, 2022). Wastewater is buoyant (has a lower density) in relation to the ambient (receiving) water. A total of 15 CORMIX near-field simulations where undertaken. We used half of the flow that have been previously simulated to account for a single arm, and simulated the discharge flow under 5 different ambient current velocities: 0.05, 0.10, 0.20, 0.30, 0.40 m/s (Table 4-1)

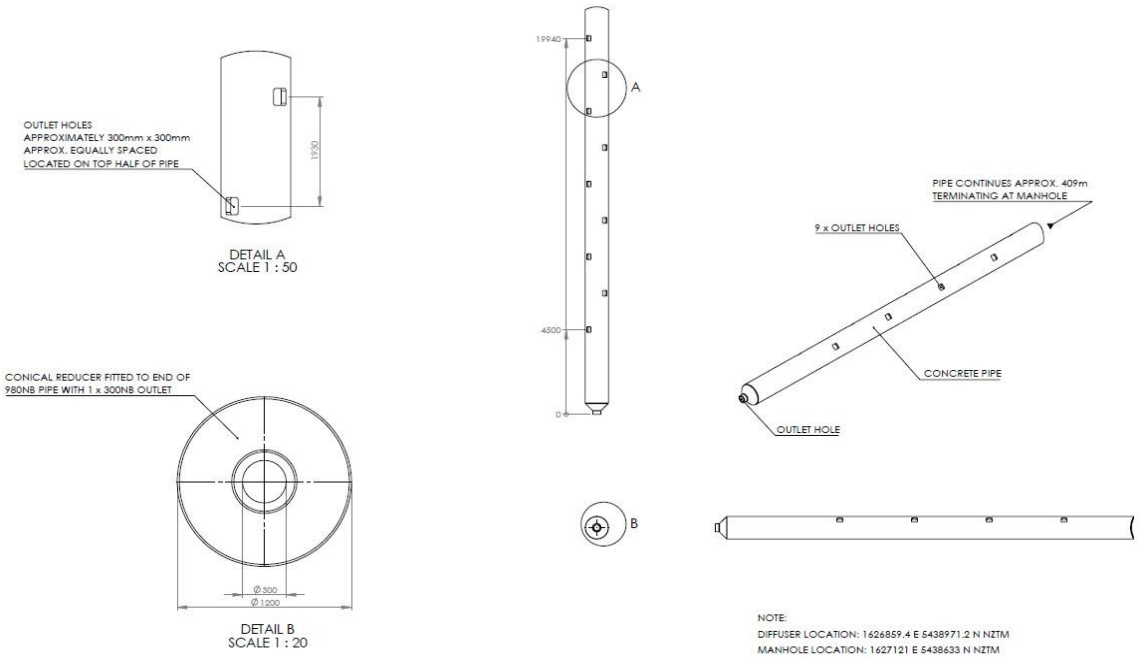

Figure 4-1 Current diffuser design and dimensions (Source: Nelson City Council).

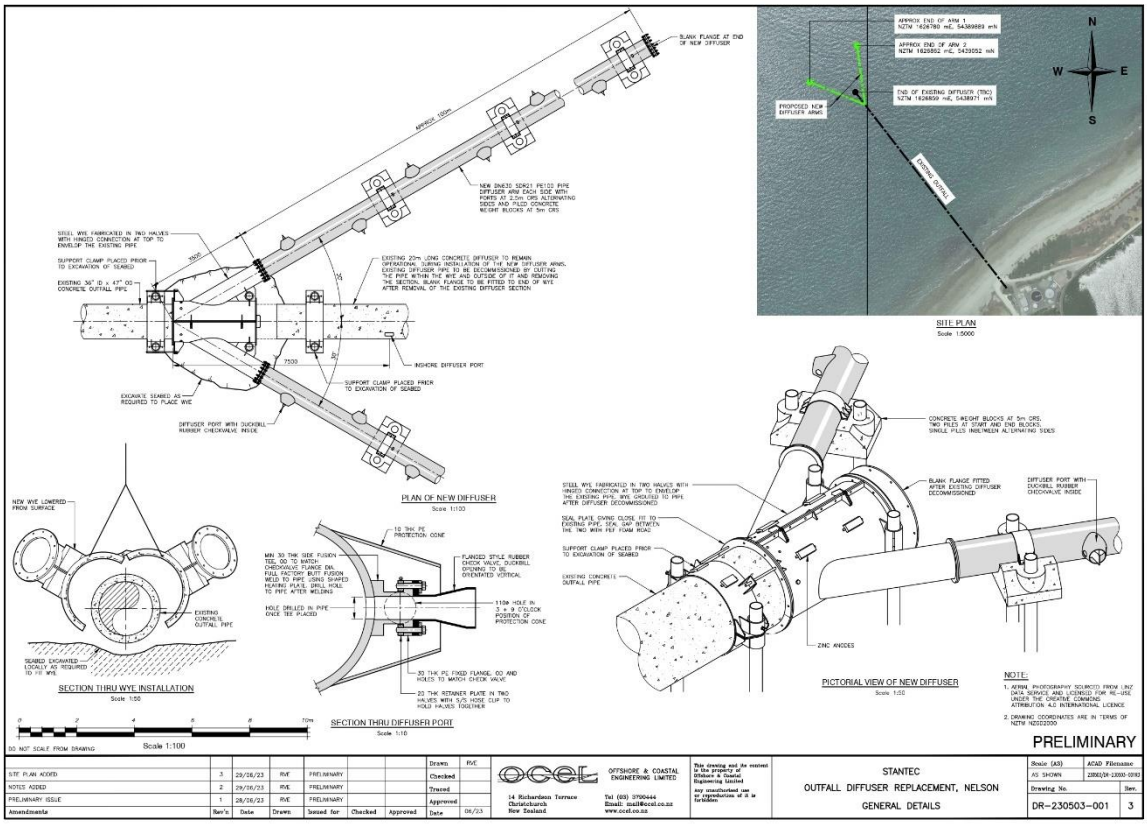

Figure 4-2 Proposed diffuser upgrade design and dimensions (Source: Nelson City Council).

Table 4-1 CORMIX near-field list of simulations.

Scenarios	Ambient current (m/s)	Total Flow rate (m^3/s)	Flow rate – EACH ARM (m^3/s)
p10	0.05	0.048	0.024
	0.10		
	0.20		
	0.30		
	0.40		
p50	0.05	0.094	0.047
	0.10		
	0.20		
	0.30		
	0.40		
p90	0.05	0.185	0.0925
	0.10		
	0.20		
	0.30		
	0.40		

Results

A range of simulations were undertaken in order to estimate the nearfield plume characteristics. It is noted that the proposed design is a 2-arm diffuser and, due to model setup limitations, the simulations considered one arm only and half of the flow, so results should be interpreted accordingly. The intention was to use these nearfield results at each arm for the particle release in the far-field modelling (which was finally not undertaken).

The nearfield region (NFR) describes the zone of strong initial mixing where the so-called nearfield processes occur (i.e., the initial jet characteristic of momentum flux, buoyancy flux and outfall geometry influence the jet trajectory and mixing of a wastewater discharge). It is the region of the receiving water where outfall design conditions are most likely to have an impact on in-stream concentrations. Beyond that is the far field region where physical mixing mechanisms are dominating with spreading motions and passive diffusion controlling the trajectory and dilution of the wastewater discharge plume.

Results show that in general, the dilution at the edge of the nearfield region (for one-arm) is significantly higher for the proposed upgrade (Table 4-2 vs Table 4-3). Dilution with the proposed design varies from 913.3 to 21,205.2 (Table 4-3). We note that, in reality, there would be a superimposition of the modelled plume with the plume released from the other arm. However, the large dilution difference predicted for the existing vs proposed design suggest that the mixing would still be improved for the 2-arm setup . Dilution tends to be higher in faster ambient current velocities (for the same flow rate). Variations to this trend across different flow rates can occur depending on the ambient currents compared to the discharge velocity (i.e., the velocity the discharge flow exits the pipe).

In all scenarios, the nearfield region is expected to be shorter (NFR length) and wider (NFR width) in near stagnant water while, under faster current flow, this region lengthens in the flow direction (Table 4-3).

The transition between nearfield and far-field dynamics (the edge of the nearfield) occurred between 4.2 minutes to 35.1 minutes, for the different conditions simulated and does not reach the shoreline.

*Table 4-2 Results for near-field simulations for the **EXISTING** diffuser. NFR = Near-field region.*

Scenarios	Ambient current (m/s)	Flow rate (m^3/s)	Discharge velocity (m/s)	NFR length (m)	NFR half-width (m)	NFR thickness (m)	Concentration at NFR edge (%)	Dilution at NFR edge	Cumulative travel time (minutes)	CORMIX Hydrodynamic Classification
p10	0.05	**0.048**	0.07	104.6	24.7	13.5	0.144	693.4	18.5	MU1H
	0.10		0.07	220.1	21.1	11.8	0.096	1037.4	29.3	MU1H
	0.20		0.07	613.7	20.2	10.1	0.059	1702.5	48.7	MU1H
	0.30		0.07	1182.4	19.3	9.6	0.043	2308.5	63.6	MU1H
	0.40		0.07	1907.3	18.7	9.2	0.035	2871.4	77.8	MU1H
p50	0.05	**0.094**	0.13	121.7	92.4	3.5	0.292	342.6	24.8	MU1V
	0.10		0.13	167.5	21.1	12.9	0.173	577.4	20.0	MU1H
	0.20		0.13	433.3	20.6	10.5	0.108	922.6	33.2	MU1H
	0.30		0.13	825.0	19.8	9.9	0.081	1242.3	44.4	MU1H
	0.40		0.13	1333.9	19.1	9.5	0.065	1535.4	54.3	MU1H
p90	0.05	**0.185**	0.26	154.7	185.9	2.2	0.454	220.5	37.0	MU1V
	0.10		0.26	131.7	22.2	13.5	0.309	324.1	13.8	MU1H
	0.20		0.26	310.6	21.0	11.1	0.199	502.7	22.5	MU1H
	0.30		0.26	33.75	8.9	13.5	0.256	390.2	3.7	MU8
	0.40		0.26	33.75	8.8	13.5	0.194	514.5	2.8	MU8

*Table 4-3 Results for near-field simulations for the **PROPOSED** upgrade diffuser. NFR = Near-field region.*

Scenarios	Ambient current (m/s)	Flow rate – ONE ARM (m^3/s)	Discharge velocity (m/s)	NFR length (m)	NFR half-width (m)	NFR thickness (m)	Concentration at NFR edge (%)	Dilution at NFR edge	Cumulative travel time (minutes)	CORMIX Hydrodynamic Classification
p10	0.05	**0.024**	0.14	47.63	56.81	13.50	0.0313	3195.3	12.0	MU1H
	0.10		0.14	114.04	52.43	13.50	0.0170	5898.3	17.7	MU1H
	0.20		0.14	305.41	51.19	12.91	0.0091	11015.4	25.2	MU1H
	0.30		0.14	555.34	51.00	12.61	0.0062	16079.8	30.6	MU1H
	0.40		0.14	853.67	50.93	12.49	0.0047	21205.2	35.1	MU1H
p50	0.05	**0.047**	0.27	37.53	59.31	13.50	0.0587	1703.7	8.5	MU1H
	0.10		0.27	84.72	53.87	13.50	0.0323	3094.7	12.5	MU1H
	0.20		0.27	58.75	43.72	13.50	0.0199	5022.8	11.2	MU8
	0.30		0.27	58.75	43.49	13.50	0.0133	7494.5	7.5	MU8
	0.40		0.27	58.75	43.41	13.50	0.0100	9974.1	5.6	MU8
p90	0.05	**0.0925**	0.52	29.89	62.58	13.50	0.1095	913.3	6.1	MU1H
	0.10		0.52	26.18	50.54	12.55	0.0729	1371.5	4.2	MU8
	0.20		0.52	58.75	43.95	13.50	0.0390	2565.9	11.1	MU8
	0.30		0.52	58.75	43.59	13.50	0.0262	3817.3	7.5	MU8
	0.40		0.52	58.75	43.47	13.50	0.0197	5074.9	5.6	MU8

5. References

MetOcean Solutions. (2022). *Nelson North Wastewater Treatment Plant (NWWTP) dispersion modelling* (No. P0526; p. 117). MetOcean Solutions.